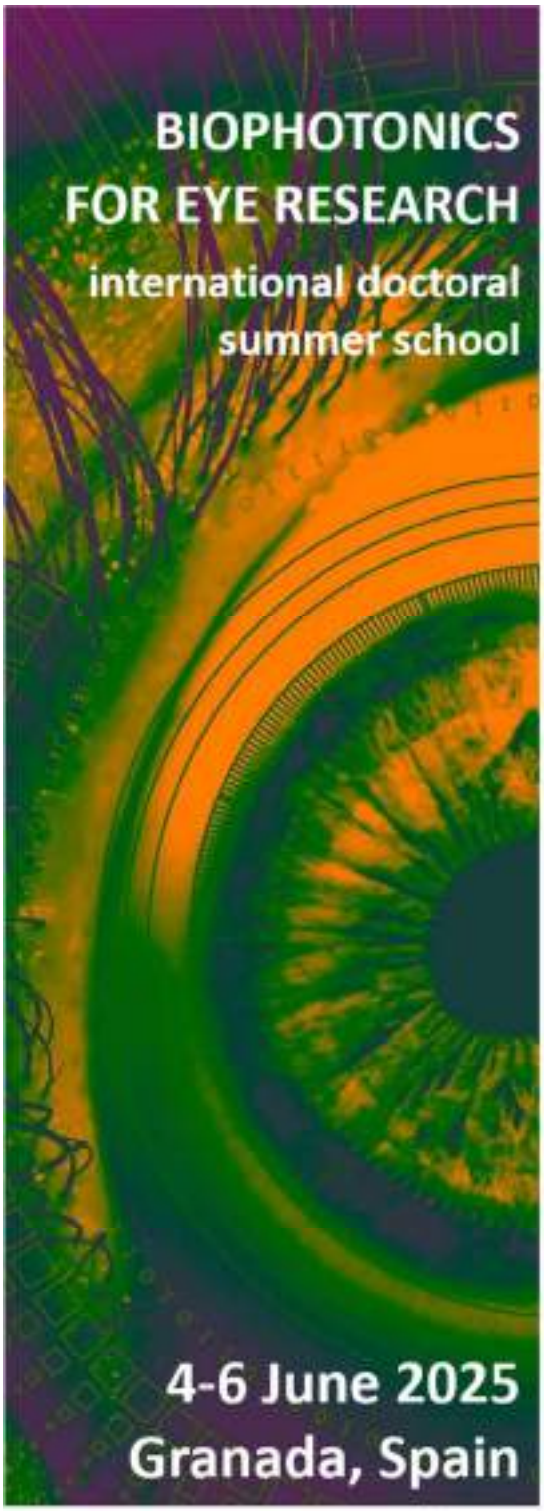

Biophotonics for Eye Research

BER2025GRANADA

The Biophotonics for Eye Research international doctoral summer school is a scientific meeting dealing with aspects of the Physics and Engineering of the human eye.

This meeting aims to follow on from the summer schools organized previously by the Visual Sciences committee of the Spanish Optical Society (SEDOPTICA). In this meeting, we shall focus on new results and techniques in imaging technology and optics of vision.

The format of the meeting is a series of classes, invited lectures with ample time for discussion and interaction, and scientific contributions presentations. The interaction of basic science and cutting edge technology to develop future solutions for better vision will be at the center of the workshop.

Young researchers and doctoral students will present their research in dedicated sessions.

The meeting will be hosted by the University of Granada in the summer of 2025.

ORGANIZING & SCIENTIFIC COMMITTEE

María Viñas	Institute of Optics-CSIC (Spain)
Mikel Aldaba	Technical University of Catalonia-UPC (Spain)
Clara Mestre	Technical University of Catalonia-UPC (Spain)
Alba Paniagua	University of Castilla La Mancha (Spain)
José Juan Castro	University of Granada (Spain)
Justo Arines	University of Santiago de Compostela-USC (Spain)
María S. Millán	Technical University of Catalonia-UPC (Spain)
E Josua Fernández	University of Murcia (Spain)
Juanma Bueno	University of Murcia (Spain)
Pablo Artal	University of Murcia & VOPTICA (Spain)
Aixa Alarcón	Johnson & Johnson Vision (The Netherlands)
Susana Marcos	University of Rochester (USA)
Carlos Dorronsoro	Institute of Optics-CSIC & 2EyesVision (Spain)
Jaume Pujol	Technical University of Catalonia-UPC (Spain)
Brian Vohnsen	University College Dublin (Ireland)
Christina Schwarz	University of Tübingen (Germany)
Katarzyna Komar	Int. Centre for Translational Eye Research (Poland)
Linda Lundström	KTH Royal Institute of Technology (Sweden)
Walter Furlan	University of Valencia (Spain)
Laura Remon	University of Zaragoza (Spain)
Jose M. Meijome	University of Minho (Portugal)

LOCAL COMMITTEE

José Juan Castro;
Sonia Ortiz;
Miriam Casares;
José Ramón Jiménez;
Rosario González;
Francesco Martino;
Pilar Granados;
Luis J. del Barco

ISBN	978-84-09-73079-7
Publisher	Sociedad Española de Óptica
Tittle:	Proceedings of the Biophotonics for eye research summer school 2025 of the Spanish Optical Society
Peer reviewed by	Sociedad Española de Óptica
Conference	Biophotonics for eye research summer school 2025 of the Spanish Optical Society nº 2, Granada 2025
Format	Digital: descarga Detalle Formato: Formato fijo ; PDF
Collection	Proceedings of the Biophotonics for eye research summer school of the Spanish Optical Society
Nr. / Edition Nr.	1/1
Language	Inglés
Publishing date	01/08/2025
Place of publication	España
Main Topic Thema	TTB : Óptica aplicada
	4G : Para currículos y exámenes internacionales
Topic Thema	PHJ : Física óptica
Main Topic IBIC	TTB : Óptica aplicada

GOLD SPONSORS

servilens fit&cover™ a contact lens company

INDO

UNIVERSIDAD DE GRANADA

Escuela Internacional de Posgrado

Facultad de Ciencias

OPTICA
Advancing Optics and Photonics Worldwide

SILVER SPONSORS

Johnson&Johnson

phaseform

WOOPTIX

NKT Photonics LASING

tobii

fotónica21
Plataforma Tecnológica Española de Fotónica

2EyesVision

COLLABORATORS

essilor

iberOptics sistemas ópticos

SmarThings4Vision

imagine eyes

slack Join BER2025 **SLACK** channel!!
https://shorturl.at/7Jvgo

BER2025 will gather students, researchers, and renowned scholars in an international forum on Biophotonics for eye research, with a series of classes, invited lectures with ample time for discussion and interaction, and scientific contributions presentations. The interaction of basic science and cutting-edge technology for eye research will be at the center of the workshop.

TECHNICAL PROGRAM

	4 June-Wednesday	*5 June-Thursday*	*6 June-Friday*
		BREAKFAST WITH THE EXPERTS	
		KEYNOTE TALK	
Morning		***SESSION I*** Optics and vision	***SESSION IV*** New horizons in refractive, cataract and eye surgery
		SESSION II Structural & Functional disruptions of the eye	***SESSION V*** Visual Function, Smart Glasses and Diagnostics tools
Afternoon	***SOCIAL EVENT*** Networking poster session sponsored by OPTICA Ambassador program	***SESSION III*** Microscopy, retina and beyond	***POSTER SESSION***
	BIOPHOTONICS: INDUSTRIAL APPLICATIONS	***YOUNG RESEARCHERS ORAL SESSION***	***KEYNOTE TALK, AWARDS CEREMONY & CLOSING REMARKS***
Evening	***KEYNOTE TALK***	***SOCIAL EVENT*** Carmen de la Victoria	***VISIT TO LA ALHAMBRA***
	WELCOME RECEPTION		

The **ORAL SESSIONS** will be held in the Aula Magna of the Faculty of Sciences (University of Granada).

POSTER SESSIONS, **COFFEE BREAKS** and **COMMERCIAL EXHIBITORS** will be located in the hall of the Faculty of Sciences, near the Aula Magna.

		WEDNESDAY	
	15:00-18:00	**SOCIAL EVENT. *Networking poster session* sponsored by OPTICA Ambassador program**	
	16:30-17:00	**Coffe Break**	
	18:00-19:00	**BIOPHOTONICS: INDUSTRIAL APPLICATIONS**	
4 JUNE	**18:00 - 18:15**	**Patrick Kolsch** Head of Global Market Development for Life Science and Biomedical. NKT Photonics	*Advancing Ophthalmic Imaging and Surgery with Fiber Lasers: Innovations in Retinal Diagnostics and Corneal Procedures*
	18:15 - 18:30	**Lucie Sawides** Scientist & former Industry. *Spanish National Research Council (CSIC) & 2EyesVision*	*Simultaneous vision simulators: bridging research & industry applications in eye care*
	18:30 - 18:45	**Vanessa Morcillo** VP of Business Development Camera. *Wooptix*	*SEBI RT1000 - TEYEDE: Wavefront Sensing - From Industrial Precision to Ophthalmic Innovation*
		Discussion	*Moderator: Antonio Castelo (EPIC)*
	19:00-20:00	**KEYNOTE TALK**	
		Prof. Susana Marcos University of Rochester (US)	*Visual Optics: An eye into the future*
	20:00-22:00	**WELCOME RECEPTION**	

		THURSDAY	
	8:00-9:00	***BREAKFAST WITH THE EXPERTS***	
	9:00-09:45	**KEYNOTE TALK**	
		Prof. Kate Grieve Institut de la Vision Paris (France)	*Live imaging of retinal cell dynamics with full field optical coherence tomography*
	09:45-11:15	**SESSION I. Optics and vision**	
	09:45-09:50	**María Viñas Peña** Institute of Optics-CSIC (Spain)	*Vision: ocular optics, brain and beyond*
	09:50-10:10	**Alberto de Castro** Institute of Optics-CSIC (Spain)	*Eye Physiology, accommodation and crystalline lens*
	10:10-10:30	**Prof. J.M. Bueno** University of Murcia (Spain)	*Retinal Structure Analysis through Two-Photon Imaging Microscopy*
	10:30-10:50	**Prof. Eva Acosta** University of Santiago de Compostela (Spain)	*Computational approaches for eye research*
	10:50-11:15	**Discussion**	*Moderator: Justo Arines (USC)*
	11:15-11:30	**Break**	
	11:30-13:30	**SESSION II. Structural & Functional disruptions of the eye**	
5 JUNE	**11:30-11:50**	**Prof. J.M. González-Méijome** Universidade do Minho (Portugal)	*Structural and functional changes in the growing eye: a holistic approach to diagnosis, prognosis and treatment.*
	11:50-12:10	**Prof. Brian Vohnsen** University College Dublin (Ireland)	*From the Stiles-Crawford effect towards optical sensing of photoreceptor dynamics*
	12:10-12:30	**Prof. Elvira Orduna** University of Zaragoza (Spain)	*Morphological changes in the retina: the influence of light and accommodation*
	12:30-13:00	**Discussion**	*Moderator: Jose Juan Castro Torres (UGr)*
	13:00-14:30	**Lunch**	
	14:30-16:30	**SESSION III. Microscopy, retina and beyond**	
	14:30-14:50	**Simone Mortal** ICFO-The Institute of Photonic Sciences (Spain)	*Spatial protein localization in photoreceptor discs revealed by expansion microscopy and nanoscopy*
	14:50-15:10	**Elena Gofas Salas** Institut de la Vision Paris (France)	*Biomarkers of inflammation in neurodegenerative disease using AOSLO*
	15:10-15:30	**Prof. Katarzyna Komar**	*Brightness of two-photon visual stimuli*

	International Center for Translational Eye Research (Poland)	
15:30-15:50	**Prof. Gloria Bueno** University of Castilla La Mancha (Spain)	*Computational approaches for biological imaging*
15:50-16:10	**Discussion**	*Moderator: María Viñas Peña (CSIC)*
16:10-16:30	**Break**	
16:30-17:30	**YOUNG RESEARCHERS SESSION**	
16:30-16:45	**Talk 1. Joan Goset** Technical University of Catalonia-UPC (Spain)	*Eye tracking parameters as biomarkers of cognitive performance in the Stroop Color-Word Test*
16:45-17:00	**Talk 2. Oliwia Kaczkoś** International Center for Translational Eye Research (Poland)	*Accommodation parameters in two-photon vision–application in Augmented Reality technology*
17:00-17:15	**Talk 3. Rosa M. Martínez-Ojeda** School of Optometry and Vision Science, University of Waterloo (Canada)	*Adaptive Optics Scanning Light Ophthalmoscopy of the Living Mouse Retina in Normal and Disease Conditions*
17:15-17:30	**Talk 4. Daniel Romero** Institute of Optics-CSIC (Spain)	*Investigating scleral tissues structural changes after riboflavin-mediated crosslinking with enhanced digital processing tools*
17:30-17:45	**Talk 5. Nathaniel Norberg** Institut de la Vision Paris (France)	*Dynamic Full-Field Optical Coherence Tomography to measure photosensitivity*
		Moderator: Juan Manuel Bueno (UMU)
20:00-22:00 pm	**SOCIAL EVENT. Carmen de la Victoria**	

		FRIDAY	
	9:00-11:00	**SESSION IV. New horizons in refractive, cataract and eye surgery**	
	9:00-9:20	**Aixa Alarcon** Johnson & Johnson (The Netherlands)	*New horizons in refractive and cataract surgery in the industry*
	9:20-9:40	**Prof. Walter Furlan** University of Valencia (Spain)	*Multifocal Intraocular lenses based on aperiodic structures: From design to optical bench evaluation*
	9:40-10:00	**Pablo Pérez Merino** Institute of Optics-CSIC (Spain)	*Ray Tracing Optimization for Personalized IOL Power Calculation*
	10:00-10:20	**Consuelo Robles García** Voptica SL (Spain)	*Advancing clinical vision through visual simulation*
	10:20-10:40	**Prof. E. Josua Fernández** University of Murcia (Spain)	*Correcting chromatic aberration*
	10:40-11:00	**Discussion**	*Moderator: María Sagrario Millán (UPC)*
6 JUNE	**11:00-11:30**	**Break**	
	11:30-13:30	**SESSION V. Visual Function, Smart Glasses and Diagnostics tools**	
	11:30-11:50	**Sonia Ortiz** University of Granada (Spain)	*Impact of Visual Function Changes on Everyday Activities*
	11:50-12:10	**Juan L. Aragón** University of Murcia (Spain)	*Optoelectronic glasses for automatic correction of presbyopia*
	12:10-12:30	**Harilaos Ginis** Diestia (Greece)	*Straylight and glare phenomena in cataract*
	12:30-13:00	**Discussion**	*Moderator: E. Josua Fernández (UMU)*
	13:00-14:30	**Lunch**	
	14:30-16:00	**POSTER SESSION + Coffee break**	
	16:00-17:00	**KEYNOTE TALK**	
		Prof. Pablo Artal University of Murcia (Spain)	*Future challenges in Visual Optics & Biophotonics*
	17:00-17:30	**CLOSING REMARKS. AWARDS CEREMONY**	
	18:00-22:00	**VISITS TO LA ALHAMBRA**	

.

slack Join BER2025 SLACK channel!!
https://shorturl.at/7Jvgo

WEDNESDAY, 4TH JUNE 2025

SESSION 0 BIOPHOTONICS: INDUSTRIAL APPLICATIONS

Advancing Ophthalmic Imaging and Surgery with Fiber Lasers: Innovations in Retinal Diagnostics and Corneal Procedures

Patrick Kolsch

Head of Global Market Development for Life Science and Biomedical. NKT Photonics

Fiber lasers are revolutionizing ophthalmology and other biomedical fields by enabling precise and high-resolution imaging, diagnostics, and surgical procedures. In ophthalmology, fiber lasers are instrumental in high-resolution retinal imaging, enhancing the early detection of retinal diseases. They also play a crucial role in femtosecond laser-assisted cataract surgery (FLACS), offering unparalleled precision to improve surgical outcomes and patient safety. Beyond ophthalmic applications, fiber lasers facilitate cell and tissue imaging, measurement of blood flow and oxygenation, activation of neural activity, and detection of cancer margins. This presentation will highlight key examples of how fiber lasers are advancing retinal diagnostics and corneal procedures, transforming the landscape of eye care and biomedical science.

PATRICK KOLSCH *is the Head of Global Market Development for Life Sciences and Biomedical Applications at NKT Photonics, specializing in fiber laser technologies for ophthalmic imaging and surgery. He focuses on advancing ultrafast and supercontinuum lasers for applications such as high-resolution retinal imaging and femtosecond laser-assisted cataract surgery (FLACS). Patrick collaborates closely with researchers and clinicians to develop photonic solutions that enhance diagnostic precision and surgical outcomes. Previously, he was a professor at the University of Washington, where he led research on nonlinear optical spectroscopy and innovative optical designs for biomedical applications.*

Simultaneous vision simulators: bridging research and industry applications in eye care

Lucie Sawides

Scientist & former Industry. Spanish National Research Council (CSIC) & 2EyesVision

A prime example of how research translates into industrial innovation is the SimVis Gekko (2EYESVISION), a binocular, see-through simultaneous vision simulator based on temporal multiplexing with an optotunable lens. This device has significantly evolved over the last decade[1-3] to accurately replicate different optical corrections, allowing real time simulation of a wide range of multifocal corrections such as intraocular lenses (IOLs)[4-5], contact lenses[6], and PresbyLASIK ablation profiles[7], providing valuable insights for both clinicians and patients.

The development of SimVis Gekko required overcoming key technological challenges, such as precise control of the optotunable lens in terms of dynamic[8-9] and temperature effect[10], the implementation of algorithms to ensure accurate simulation of multifocal patterns, and rigorous validation processes[5-6] and quality optimization efforts (optical, electronical, mechanical and aesthetical) to further enhanced its applicability in clinical settings. With the ability to accurately simulate multifocality, the next major endeavour in visual simulation is preoperative assessment of halos produced by multifocal IOLs, a factor that significantly influences patient experience and surgical outcomes. This challenge connects my previous work at 2EyesVision with my current research at IO-CSIC, focusing on the development of on-bench optical systems for the objective characterization of IOL optical quality and the optimization of an adaptive optics visual simulator for the subjective evaluation of halos in patients. These advancements aim to further improve the selection and personalization of ophthalmic corrections, ultimately enhancing visual outcomes for patients undergoing refractive and cataract procedures.

1. C. Dorronsoro, et al. Biomed. Opt. Express (2016)
2. C. Dorronsoro, et al. Optica (2016)
3. A. Radhakrishnan, et al. PLoS ONE (2019)
4. L. Sawides, et al. SPIEOptica Design&Engineering(2021)
5. P. Papadogiannis et al. Biomed. Opt. Express (2024)
6. E. Esteban-Ibañez, et al. Sci Rep (2024).
7. I. Siso-Fuertes, et al. ESCRS (2022)
8. V. Akondi, et al. Biomed. Opt. Express (2018)
9. C. Dorronsoro, et al. Opt Express (2019)
10. Y. Marrakchi, et al. Sci Rep (2023)

***LUCIE SAWIDES** has recently been appointed to Tenured Scientist in the Instituto de Óptica, CSIC (IO-CSIC), Spain after enjoying a Ramón y Cajal Research grant (RyC2021). She carried out her Doctoral Thesis in Vision Science (Univ. de Valladolid, 2013) in the IO-CSIC (FPI fellowship), and continued her career as a postdoctoral researcher first at Indiana Univ. USA (2013-2016) and then at the Univ. de Murcia, Spain (2016-2017). She then joined 2EyesVision, a technological spin-off of the CSIC for which she is also co-founder, through a H2020 European Innovation program where she has worked for 5 years as a R&D engineer and product performance area coordinator to validate the SimVis technology, before being granted the Ramón y Cajal Research grant to come back to the IO-CSIC. Her research has motivated research projects awarded at competitive public calls and with industrial collaborators. She is now actively working on the development of new technologies and tools for evaluating novel corrections for presbyopia and cataracts in close collaboration with 2EyesVision.*

SEBI RT1000 - TEYEDE: Wavefront Sensing - From Industrial Precision to Ophthalmic Innovation

Vanessa Morcillo

VP of Business Development Camera. Wooptix

The WaveFront Phase Imaging (WFPI) technology developed by Wooptix has its roots in the field of astronomy. Initially evaluated for high-precision metrology, it led to the development of measurement devices adapted for various applications. The SEBI RT1000 camera exemplifies this capability, offering nanoscale surface metrology for more demanding industrial applications. Wooptix identified WFPI's potential in ophthalmic diagnostics, resulting in the development of an ophthalmological prototype: t-eyede. This application required simplifying existing devices to allow their use in laboratory environments.

Wooptix applies WFPI technology in two key devices: the SEBI RT1000 camera and the t-eyede device. The SEBI RT1000 camera is designed to evaluate laboratory samples, allowing modifications without the need for intrusive interventions in patients. This is crucial for assessing deformations and determining applicability in real scenarios. On the other hand, the t-eyede device is a high-resolution ocular aberrometer specifically developed to directly examine human eyes, as it allows detailed analysis of the ocular wavefront in vivo, demonstrating great potential in the objective evaluation of corneal pathologies such as keratoconus and Fuchs' endothelial dystrophy. This work

demonstrates the versatility of WFPI technology, showing that it is possible to translate the technique from industrial environments to novel solutions in medical diagnostics. Advances in real-time high-resolution wavefront detection, including the use of electrically tunable lenses, open new possibilities for future applications in adaptive optics.

***VANESSA MORCILLO**, a physicist specialized in Medical Physics with a business vision and an MBI (Master in Business Innovation) from the University of Deusto, drives growth at Wooptix as Head of Business Development for the camera unit. An expert in MedTech, with extensive international experience (Iberia, LATAM, UK/IE, MEA), her passion for applied neuroscience has led her to become certified in Brain-Based Coaching by the Neuroleadership Institute in New York, and trained in Neuroscience for Business at MIT. Vanessa combines her scientific and business expertise to search for innovative applications in the field of camera technology, applying neuroscience principles to transform leadership and business strategy.*

KEYNOTE TALK

Visual Optics: An eye into the future

Prof. Susana Marcos

University of Rochester (US)

In the last years, innovations like Optical Coherence Tomography, Wavefront Aberrometry or Adaptive Optics have transformed optical diagnostic in ophthalmology and helped inspire new corrections. I will present key current projects exploring new paradigms for intraocular lens selection; the interplay between myopia development , crystalline lens remodeling and accommodation; retinal signaling pathways to scleral remodeling in myopia development and inhibition; or the corneal biomechanical response to corneal disease and mechanics. Optomechanical eye models capture the specific speficic geometrical, optical and biomechanical properties of the eye, while hey and optics while simulation technologies, such as SimVis Gekko, allow patient-specific testing of mee corrections. We will present our lab integration of 3D OCT imaging, biomechanics, machine learning, biomarkers, and advanced visual simulation aims to revolutionize optical diagnosis and treatment personalization. Altogether, this work envisions a future of fully customized, functional visual corrections supported by advances in materials science, AI, pharmacological agents and biomedical optics.

***SUSANA MARCOS** is currently the David R Williams Director of the Center for Visual Science, Nicholas George Professor of Optics at the Institute of Optics and Professor of Ophthalmology at the Flaum Eye Institute, at the University of Rochester, New York. She is the former Director of the Institute of Optics at the National Research Council in Spain. Susana Marcos obtained her PhD in Physics at the University of Salamanca, Spain, and was a Fulbright and Human Frontier Postdoctoral Fellow at the Schepens Eye Research Institute of Havard University. She is a leading researcher in visual optics, having pioneered multiple technologies of eye optical imaging diagnostics and treatments, including novel IOL designs. Shas published more than 240 highly cited publications, is a co-inventor of 28 patents and participated in two spin-out companies (Plenoptika and 2EyesVision). She is a Fellow of Optica, European Optical Society and the Association for Research in Vision and Ophthalmology. Her work has been recognized with numerous awards including the Adolph Lomb Medal, the Edwin Land Medal and the Edgar Tillyer Medal of Optica (formerly Optical Society of America), the ICO Prize by the International Commission for Optics, the Ramon y Cajal Medal by the Royal Academy of Sciences, the Alcon Award, the Physics, Innovation and Technology Award by the Royal Society of Physics, or the National Research Award in Engineering by the Spanish Government, the Jaime I Award in New Tecnologies.*

THURSDAY, 5TH JUNE 2025

KEYNOTE TALK

Live imaging of retinal cell dynamics with full field optical coherence tomography

Prof. Kate Grieve

Institut de la Vision Paris (France)

Full field optical coherence tomography (FFOCT) can reveal microscopic features in the living retina of patients in a compact simple device, and is being used in clinical trial for quantification of nerve fiber thinning. Dynamic FFOCT allows label free live imaging of cell cultures in the lab, including retinal organoids in disease modeling studies. I will explain the technology developments and present results on live imaging in patients in the clinic, along with live imaging in organoids in the lab.

KATE GRIEVE *(>4000 citations, h-index 32, i10 index 58), research director and team leader at the Vision Institute, Paris; scientific director of the "Paris Eye Imaging" ocular imaging unit, at the Quinze Vingts National Ophthalmology Hospital, Paris; president and founder of startup SharpEye, and co-founder of startup Lutèce Dynamics, is an expert in optical imaging. Her research aims to develop non-invasive optical measurements of retinal cell structure and function in the living human eye, as well as in cell cultures in the lab. This development contributes to significantly improving the diagnosis and monitoring of ophthalmological pathologies, as well as to evaluating the results of innovative therapies. She was awarded the 2024 Irène Joliot Curie prize for Women in Research and Business from the French Academy of Sciences.*

SESSION I OPTICS AND VISION

Vision: ocular optics, brain and beyond

María Vinas-Pena

Institute of Optics. Spanish National Research Council (CSIC) (Spain)

Vision relies on a complex system, which comprises an optical camera and a neural processor, adjusting to match visual coding and environment. Moreover, optical and structural properties of the eye change with age and with certain ocular conditions and treatments, altering the ocular optics, modifying the neural processes and consequently the visual function. Light-based technologies have allowed further understanding of the limits of visual function. In particular, phase modulation has allowed significant insights on visual science, in the understanding of the link between the ocular optics and the processes of neural adaptation behind them. Adaptive Optics (AO) based visual simulators are now able to couple the measurement of the ocular aberrations with their correction or manipulation by means of different active technologies (deformable mirrors, spatial light modulators, optotunable lenses), both in monochromatic and polychromatic conditions, which has revolutionized the management of Presbyopia and Myopia. The understanding of the interactions of these aberrations and their effect upon correction is essential to explore the limits of human spatial vision, and to design and optimize new alternatives of optical corrections.

MARIA VINAS-PENA *is a tenured scientist at the Institute of Optics of the Spanish National Research Council. She obtained her PhD in Physics (UCM, 2016) and since then enjoyed different postdoctoral positions at the IO-CSIC (Spain), as Marie Sklodowska Curie research fellow (2020-22) at Wellman Center for Photomedicine-MGH & Research fellow at Harvard Medical School (USA), and as visiting researcher (2022) at the University of Rochester (USA). In 2022, she was awarded a Ramon y Cajal fellowship to return to Spain. Her research focuses in the use of photonic technologies to the study of the physics of vision. First, through the use of polychromatic Adaptive Optics visual simulators, to image the eye, and to study visual function and neural adaptation in polychromatic conditions under a very wide range of artificially-simulated-conditions. Second, using a variety of microscopy tecniques to investigate emmetropization. Third, investigating the molecular and cellular mechanisms behind retinal stimuli processing which modulates the emmetropization process, using light/visual stimulation. She has received different awards and fellowships (OPTICA, ARVO), as well as being named OPTICA Ambassador &, senior member, and European Young Researcher Award EYRA2020.*

Eye Physiology, accommodation and crystalline lens

Alberto de Castro

Institute of Optics. Spanish National Research Council (CSIC) (Spain)

This session will review the physiological optics of the anterior segment of the eye focusing on the crystalline lens and its role in process of accommodation. The talk will describe the different methods employed to obtain quantitative information on the geometry of the surfaces of the crystalline lens and its optical properties.

ALBERTO DE CASTRO *works in the Instituto de Óptica - CSIC in Madrid. His research on optical technology and ophthalmology focus on the study of the ageing human eye using light-based imaging systems. He is interested in the development of methods to evaluate the optical quality of ocular structures, on the precise quantification of the structural properties of the anterior segment of the eye, and on the evaluation of the suitability of different optical corrections on a personalized basis using of the developed eye models.*

Retinal Structure Analysis through Two-Photon Imaging Microscopy

Juan M. Bueno

Laboratorio de Óptica, Instituto Universitario de Investigación en Óptica y Nanofísica, Universidad de Murcia (Spain)

Two-Photon Excitation Fluorescence (TPEF) microscopy has opened new research opportunities in Biomedicine.[1] This noninvasive and autoconfocal imaging method is used for exploring and mapping non-stained biological structures. Since 2004, it has become a powerful tool for the assessment of *ex vivo* retinal tissues,[2] in particular cell distribution in different animal models and humans has been a topic of interest.[3-6] However, whereas most studies were centered on healthy tissues, the characterization of pathological ones is scarce.[7] In this work we use this technology to quantify the changes in the spatial distribution and density of photoreceptors (PR) produced by diabetes. Moreover, neuroinflammatory effects are also analyzed. TPEF images of the PR layer were acquired in a diabetes-induced rat model using a research microscope.[4] The instrument uses an 800-nm pulse laser as illumination source, which is scanned across the specimen. The emitted signal travels in the backward direction reaching the photon-counter detection unit. Diabetes was induced by applying streptozotocin (STZ).[6] Blood tests showed high glucose levels in the animals 6 weeks after injection. The PR mosaic was imaged at different locations and density was quantified. Individual PR transversal size was assessed and used as cell neuroinflammation parameter. Non-stained retinas were imaged and compared in both control and STZ-injected animals. PR density was found to vary with eccentricity in both control and diseased retinas. The values are significantly higher in the former. A hexagonal packaging was dominant in control specimens and it was fairly maintained in diabetic retinas. Moreover, inflammatory abnormalities across the neural retina were also revealed. Although diabetic retinas presented larger PR transversal sections, the changes were not uniform and depended on the retinal location. These results demonstrate the usefulness of TPEF imaging to objectively assess retinal cell arrangement and to characterize inflammatory processes and retinal alterations. They also represent a step forward to understand the complex ocular inflammatory mechanisms.

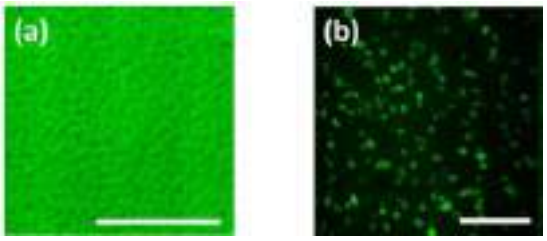

Figure 1: Example of TPEF images of the PR (a) and the ganglion cell layer (b). Bar length: 50 mm.

[1] *F. Helmchen and W. Denk; Nat. Methods (2005)*
[2] *Y. Imanishi, M. L. et al. Cell. Biol. (2004)*
[3] *R.-W. Lu, et al.; Biomed. Opt. Express (2011)*
[4] *J. M. Bueno, et al.; Biomed. Opt. Express (2011)*
[5] *S. He, et al.; Biomed. Opt. Express (2015.*
[6] *S. J. M. Bueno et al.; Biomed. Opt. Express (2020)*
[7] *M. Han, et al.; J. Biomed. Opt. (2006)*

JUAN M. BUENO *(PhD in Physics 1999, Doctorate Extraordinary Award) has been a faculty member since 1994 at the University of Murcia in Spain, where he currently holds a position as Full Professor of Optics. He has been President of the Vision Science Division of the Spanish Optical Society and is the actual Director of the Department of Physics. In 2017 he was elected Senior Member of the Optical Society of America (formerly OSA, now OPTICA). Dr. Bueno performs his research at the Center for Research in Optics and Nanophysics, leading the biomedical imaging section. Prof. Bueno's research focuses on biophotonics, with special emphasis on multiphoton microscopy of collagen-based structures and polarization properties of tissues. A number of his publications are considered as landmark works. He is also inventor/co-inventor in a number of patents in the field of Visual Optics and co-founder of Voptica SL a spin-off company.*

Computational approaches for eye research

Eva Acosta

University of Santiago de Compostela (Spain)

The study of retinal images requires high-precision optics to effectively detect various types of pathologies. The evolution of optics in fundus cameras has been constant, increasing in complexity as the detection of details becomes more crucial for medical diagnoses. However, in most commonly used retinoscopes today, two fundamental factors continue to affect the quality of retinal images: aberrations, both low and high order, and the presence of opacities in ocular tissues. These factors significantly degrade the quality of the obtained images, making the diagnosis of various pathologies more difficult. To mitigate these problems, a change in the system's optics and/or in the processing of the obtained images is required. Regarding aberration compensation, one of the main challenges is to develop solutions that do not excessively increase the cost of optical devices while maintaining the robustness of the equipment. In this study, we explore the application of the method known as wavefront coding to obtain images degraded by aberrations using simple optics, without requiring drastic changes in the design of the fundus camera. This method consists of the deliberate introduction of aberrations into the optical system. By carefully selecting the shape of the aberration, it is possible to generate a point spread function (PSF) that remains invariant under different types of aberrations, regardless of the subject or the moment of image acquisition. The resulting image, which contains the inserted aberration along with refractive errors and high-order aberrations, is referred to as the intermediate image. The key to the process is the deconvolution of the intermediate image with the system's PSF, which has only been degraded by the deliberately introduced aberration. Through this procedure, it is possible to recover a high-resolution final image, significantly improving diagnostic quality without requiring complex or expensive optics. On the other hand, in addition to aberration correction, another relevant issue is the restoration of images degraded by the presence of opacities in ocular tissues, such as in cases of cataracts or cloudy ocular media. To address this problem, we present an image processing method based on applying a filter designed to approximate the multiple scattering of light within the entire eyeball. This filter is based on the generalized Gaussian distribution and is used to characterize the point spread function in the presence of ocular opacities. Unlike simple light scattering, multiple scattering accounts for both the portion of light that is directly transmitted to the imaging system and the portion that is scattered and subsequently redirected toward the sensor by the regions causing the opacities. Once this filter is developed, the number of parameters that characterize it is reduced so that only one models the degree of opacity present in the ocular tissue (to facilitate use by medical professionals). Based on this simplified model, high-resolution images can be obtained through deconvolution with the optical transfer function (OTF) of the filter. In conclusion, the use of opto-computational techniques for aberration compensation and computational techniques for restoring images degraded by ocular opacities represents a significant advancement in retinal image acquisition. These strategies improve image quality without the need for excessively complex or costly optical systems, facilitating their implementation in clinical environments and contributing to more precise diagnoses of various ocular pathologies. Both methods are so fast that real-time implementation is possible.

EVA ACOSTA *received her M.S. in 1986 and her PH. D. degree in 1991 from University of Santiago de Compostela. From 1986 she joined the Department of Applied Physics of the University of Santiago de Compostela and became Assistant Professor in 1991, Associate Professor in 1993 and Professor in 2012. Supervisor of 10 Ph.D. Works and supervisor of more than 15 Master Works. She is permanent member of the Program Committee of the International Microoptics Conference since 1995, and collaborated as committee member of ICO, Optics in Atmospheric Propagation and Adaptive Systems among others. She was Vice-Dean of the Faculty of Physics from 2002 to 2006, leader of the group Optosensing (2002-2015), and currently senior member of Photonics4life. Her research background is in microoptics; her Ph.D. work is about propagation in Gradient index Optics for Optical Communications. She enjoyed a senior fellowship of EU in Nippon Sheet Glass Company in Tokyo Institute of Technology. She was involved in design and software for wavefront sensors and applications in atmosphere and visual optics and currently she is involved in the research and development of compact, robust and cheap optical systems for retinal imaging. She collaborates with LOUM (Murcia, Spain) and University of Arizona, USA.*

SESSION II STRUCTURAL & FUNCTIONAL DISRUPTIONS OF THE EYE

Structural and functional changes in the growing eye: a holistic approach to diagnosis, prognosis and treatment

José Manuel González-Méijome

Department and Center of Physics – Optometry and Vision Science, School of Science (Portugal)

This work applied a comprehensive short and medium-term physiological, structural and visual assessment in 20 subjects wearing spectacle lenses with different defocus lenslet distribution in random order. The protocol included an evaluation of high and low contrast visual acuity under photopic conditions, contrast sensitivity function (CSF) under photopic (95 cd/m^2) and mesopic (5cd/m^2) conditions, light disturbance analysis as well as multifocal global-flash (mf-gfERG), photopic 3.0 (Phot. 3.0), photopic on-off (Phot. On-off) and pattern (PERG) electroretinogram, as well as choroidal thickness and axial length in 3 visits: baseline, 30 minutes and after 15 days of wear. There was a clinically significant improvement of 0.05 to 0.10 LogMAR units in monocular HCVA from baseline to 30 minutes and after 15 days of wear. Photopic CSF was within normal limits for all spatial frequencies while medium frequencies (3 to 12 cycles per degree -cpd-) fall below normal under mesopic conditions with some lenses. Light disturbance analysis measured after 15 days of lens wear was significantly lower than baseline measurement under monocular and binocular conditions, with the binocular values being significantly lower than monocular ones ($p<0.05$). Pattern and multifocal electroretinogram analysis showed significant changes in amplitude (ganglion and bipolar cell activity upregulation) from baseline to 30 minutes and 15 days ($p<0.05$). Objective structural and functional metrics along with subjective and psychophysical analysis of visual function provide valuable information for future design of defocus incorporating optical devices.

JOSÉ MANUEL GONZÁLEZ-MÉIJOME g*raduated with honours in Optics and Optometry at the University of Santiago de Compostela in 1997. After a fellowship at CCLRU, University of New South Wales in Australia, joined the Universidade do Minho in Braga, Portugal where he is currently Full Professor and Dean of the School of Sciences, Vice-President elect of the European Academy of Optometry and Optics, Editor-in-Chief of the Journal of Optometry and member of the European Council of Optometry and Optics Qualifications Board. Along with teaching tasks in Optometry and Vision Sciences, different institutional management tasks, coordinates the Clinical and Experimental Optometry Research Lab with activities in clinical visual optics, specialty contact lenses, myopia management, presbyopia and epidemiology research. Published more than 220 articles in indexed journals (Web of Science h-index=42, > 5600 citations). Authored 3 books and 30 book chapters and has presented conferences in more than 30 countries. Received different prizes and awards including the UMinho Scientific Merit Award 2018 and International Optometrist of the Year by Catalonia Polyethnic University in 2016.*

From the Stiles-Crawford effect towards optical sensing of photoreceptor dynamics

Brian Vohnsen

School of Physics, University College Dublin (Ireland)

In this work the fundamentals of the Stiles-Crawford effect and photoreceptor directionality will first be discussed. This will be followed by an analysis of temporal changes, both on short and long timescales, of changes that occur in the retina and photoreceptors with adaptation, with diurnal changes, optically-induced changes and age. The pupil sets a physical limit on the angular range of waves at the retina, where the structure and size of the photoreceptors is well matched to the photopic pupil size. The optoretinograms reveal changes that are in part due to the photochemistry of the photon absorption, but potentially also heating due to thermal expansion. The photoreceptor outer segments renew their pigments on a two-week cycle, which is likely causing part of the adaptation to optical aberrations, and the visual pigments decrease potentially with disease and age, leading to

potential structural differences. The Stiles-Crawford effect can probe such changes psychophysically and may hold potential as a clinical tool.

***BRIAN VOHNSEN**, leads the Optics Group, School of Physics in University College Dublin, Ireland, where he programme director for the MSc in NanoBio Science and co-Chair for the EDI school committee. He is a Fellow of Optica and ARVO. He currently chairs Optica Vision & Colour on the Board of Meetings, and is current Chair-elect on the ARVO annual meeting programme committee as well as serving on their publications committee. His work spans from optical imaging and advanced microscopy to the optics of the eye, myopia, the retina and photoreceptors.*

Morphological changes in the retina: the influence of light and accommodation

Elvira Orduna-Hospital

University of Zaragoza (Spain)

The retina is a dynamic structure that undergoes morphological changes in response to different visual stimuli, particularly lighting conditions and accommodative demand. The aim is to present recent research exploring how illumination (photopic, scotopic, mesopic, blue, and red light) may influence retinal curvature, with variations that could be associated with myopia progression. The findings suggest a tendency for the retina to flatten under lower luminance conditions and become more curved in mesopic environments. Additionally, it will be discussed how accommodation appears to affect retinal thickness and curvature across different age groups. Preliminary results indicate a pattern of central retinal thinning and peripheral thickening with increasing accommodative effort, observed even in presbyopic individuals. Furthermore, retinal curvature may undergo changes, including a tendency to flatten under higher accommodative demands, suggesting a potential interaction between accommodation and retinal shape adaptation. These structural modifications highlight the need for further research to better understand the role of retinal dynamics in visual function, myopia control, and aging-related ocular changes.

***ELVIRA ORDUNA-HOSPITAL**, PhD, is an Associate Professor in the Department of Applied Physics (Optics) at the University of Zaragoza, Spain. She holds a degree in Optics and Optometry, a Master's in Vision Science Research, and a PhD in Biomedical and Biotechnological Sciences. Her research focuses on clinical optometry, ophthalmology, and binocular vision, with a growing emphasis on the impact of lighting on visual function and retinal changes. She has authored over 70 scientific articles, 10 book chapters, and presented more than 220 conference papers. She is actively involved in the Retina and Visual System Research Group at the Aragón Health Research Institute (IIS Aragón) and participates in multiple research projects on ocular dynamics, visual performance under different environmental conditions, and the study of retinal biomarkers in neurodegenerative diseases.*

SESSION III MICROSCOPY, RETINA AND BEYOND

Spatial protein localization in photoreceptor discs revealed by expansion microscopy and nanoscopy

Simone Mortal[1], Jesus Planaguma[2], Pablo Loza-Alvarez[1]

[1]The Barcelona Institute of Science and Technology, ICFO-Institut de Ciencies Fotoniques (Spain)
[2]Neuroimmunology Programme, Institut d'Investigacions Biomèdiques August Pi i Sunyer Hospital Clínic, University of Barcelona (Spain)

Vision originates within a stack of tightly packed disc-shaped membranes, or "discs", located in the outer segment of photoreceptor cells, where the most abundant protein is rhodopsin, the key player in phototransduction. Traditionally, discs have been observed using electron microscopy, which can reveal their structure but cannot provide a precise protein localization, leaving their exact distribution uncertain. To overcome this limitation, we combined expansion microscopy with STED nanoscopy, achieving a resolution below 15 nm, thereby surpassing previous limitations in observing discs. This enabled us to precisely identify proteins and outline their distribution in photoreceptors. Analyzing the disc composition, we observed that around 90% of the disc area is decorated by rhodopsin, and the inter-disc spacing is more irregular compared to what is observed in electron microscopy. Furthermore, we localized proteins such as peripherin-2, responsible for maintaining the disc shape and its structural components. Lastly, we investigated how the connecting cilium penetrates within the rod outer segment and its relationship with disc proteins, under physiological conditions and in an animal model of retinitis pigmentosa. Our results collectively suggest a larger spatial distribution of rhodopsin in the disc than previously described, leading to a lower protein concentration. Moreover, we found that the connecting cilium plays a significant role in determining the final shape and orientation of the disc. These findings provide new insights into the molecular architecture of photoreceptor discs, which could have significant implications for better understanding visual processes and the pathogenesis of retinal diseases like retinitis pigmentosa.

***SIMONE MORTAL** is a postdoctoral researcher in biophotonics at ICFO, Barcelona. His research focuses on the biophysical properties of retinal photoreceptors, specifically studying protein distribution at the ultrastructural level. Using advanced super-resolution techniques, he investigates structures previously observable only through electron microscopy. His work aims to uncover novel properties of photoreceptors and open new perspectives for studying retinal diseases.*

Biomarkers of inflammation in neurodegenerative disease using AOSLO

Elena Gofas Salas

Institut de la Vision Paris (France)

Inflammation plays a key role in neurodegenerative diseases such as multiple sclerosis (MS), yet studying the underlying cellular mechanisms remains challenging. The eye, as a transparent optical window, provides a unique opportunity for non-invasive exploration of neuroinflammatory processes. At the Quinze-Vingts hospital, we have developed high-resolution retinal imaging systems to observe immune responses at different stages of neurodegenerative diseases. This study characterizes cellular biomarkers of inflammation in MS patients with recent optic neuritis using phase-contrast Adaptive Optics Scanning Laser Ophthalmoscopy (AOSLO). Fifty MS patients and ten healthy controls underwent AOSLO imaging alongside clinical assessments at 3, 6, and 12 months. Round-

shaped cells (12.1 ± 4.2 µm) with compact cytoplasm and round intracellular structures were identified in the retinal ganglion cell layer (GCL) of affected eyes but were absent in controls. These cells were sometimes detected weeks before clinical ON onset, and their density declined post-ON, though at varying rates. Infiltrates were more frequently found in MS patients than in controls, even outside acute ON episodes. These findings demonstrate cellular infiltration in MS-associated optic neuritis and highlight phase-contrast AOSLO as a promising tool for assessing inflammatory mechanisms in MS and other neurodegenerative conditions.

ELENA GOFAS SALAS *– was recently appointed INSERM Researcher (CRCN) at the Vision Institute (1st November 2022). She works at the interface between optics and medicine. She defended her PhD in 2019 where she presented several novel imaging modalities that she developed. She then joined the ROSSI lab at University of Pittsburgh where she designed a new detection system revealing retinal ganglion and microglial cells. She joined in September 2020 Kate Grieve's team at the Vision Institute in collaboration with the Quinze Vingts hospital importing the technology she developed and detecting for the first time inflammatory in cells in multiple sclerosis patients. She has published 18 articles in international peer-reviewed journals with an h index of 12, and was awarded the French Young Talents Award from l'Oreal-Unesco Foundation (2022), WEAVR award (2022), EyeFind award (2022) and IUIS Sorbonne postdoctoral award (2021).*

Brightness of two-photon visual stimuli

Katarzyna Komar

International Center for Translational Eye Research (Poland)

Two-photon vision is a phenomenon of visual perception of pulsed infrared lasers caused by two-photon absorption of photons by visual pigments. The perceived color of projected stimuli is close to half of the laser wavelength. The intensity of two-photon stimulation depends quadratically on mean power of the laser, as the two-photon absorption is a nonlinear optical effect. The other factors that influences two-photon visual perception are: pulse length and repetition frequency of the laser, its wavelength and degree of focusing at retinal plane. All these factors affecting the perceived brightness of the two-photon stimuli will be discussed and supported by experimental results.

KATARZYNA KOMAR *graduated from Gdansk University of Technology (MSc in Technical Physics) and received a Ph.D. in Technical Sciences in 2007. Since 2011, she has worked in biomedical imaging of the human eye at Nicolaus Copernicus University in Torun. he is also working at the International Centre for Translational Eye Research in Warsaw, exploring two-photon vision, i.e., a phenomenon of perception of pulsed near-infrared lasers due to two-photon absorption in visual pigments. She focuses on developing optical systems and methods for psychophysical testing of this new way of perceiving light and integrating these methods into ophthalmic imaging systems.*

During both phases of her career, she has participated in and led nationally and internationally funded-research projects. Now, she is leading two projects devoted to a two-photon vision funded by the Foundation for Polish Science and by the National Science Centre, Poland.

Computational approaches for biological imaging

Gloria Bueno

University of Castilla La Mancha (Spain)

This module offers an overview of cutting-edge computational methodologies applied to the analysis of microscopic images in biological research, with a particular focus on the ocular domain. At the intersection of biophotonics and artificial intelligence (AI), we will explore how deep learning algorithms enable the extraction of structural and functional information from images acquired through optical and microscopy techniques. Approaches such as convolutional neural networks (CNNs), attention-based architectures and transformers for segmentation and classification, autoencoders for anomaly detection, and data augmentation strategies to model biological variability will be introduced. These methodologies will be illustrated through practical case studies, including: a) Classification of diseases such as glomerulonephritis at the glomerular level using CNNs with self-attention, an approach adaptable to the study of other tissue types[1,2]; b) Assessment of image quality in GAN-generated datasets and its impact on classification networks, particularly relevant in contexts with limited annotated data[3] and c) Semi-supervised segmentation of the corneal endothelium using geometric transformations, demonstrating how to model the natural variability of biological tissue[4].

Students will learn how these techniques not only enhance the accuracy and automation of microscopic image analysis but also improve reproducibility, efficiency, and applicability in real-world scenarios, from laboratory research to clinical diagnostics. The module aims to equip participants with innovative computational solutions to tackle current challenges in biological and biomedical research.

[1]G Bueno, et al. IEEE EMBS International Conference on Biomedical and Health Informatics (2024)
[2]I Mateos-Aparicio-Ruiz, et al. Computational and Structural Biotechnology Journal 27, 35-47 (2025)
[3]G Bueno, et al. Optics, Photonics, and Digital Technologies for Imaging Applications VIII, SPIE, (2024)
[4]S Sanchez, et al. PloS one 19 (11), e0311849, (2024)

GLORIA BUENO *(BSc in Physics, 1993; PhD in Computer Vision, 1998) is a Full Professor at the School of Industrial Engineering of the University of Castilla-La Mancha, where she has been working since 2003, leading the VISILAB research group in Computer Vision and Artificial Intelligence. She earned her PhD from Coventry University (UK) and later completed a Marie Curie postdoctoral fellowship at CNRS (France). She has conducted research at the Institut Physique Biologique (FR) and at CEIT (ES), applying AI techniques to both biomedical and industrial applications. She has served as Principal Investigator on 19 publicly funded research projects, including five at the European level. She maintains collaborations with leading institutions such as CERN, CEA, CNRS and INRIA. Her work has contributed to successful technology transfer to companies such as SIEMSA, INDRA and Leica Biosystems. In 2009, she was a visiting professor at Carnegie Mellon University (USA). She is a member of IEEE, SEIB, SPIE, a promoter of the ESDIP scientific society and a founding partner of the Ubotica spin-off.*

FRIDAY, 6TH JUNE 2025

SESSION IV NEW HORIZONS IN REFRACTIVE, CATARACT AND EYE SURGERY

New horizons in refractive and cataract surgery in the industry

Aixa Alarcon

Johnson & Johnson (The Netherlands)

More than 20 million cataract surgeries are performed per year, being the most common surgery in the world and one of the safest (90% of the patients see better after the surgery). Although around 90 % of the cataract patients receive a monofocal intraocular lens (IOL), this industry is strongly driven by innovation. Currently, there are many different technologies and a wide range of designs available to address the visual needs of the patients, from standard monofocal, toric lenses and to full visual range. This presentation reviews some of currently available technologies and the developments behind some of these innovations.

AIXA ALARCON *is a Senior Principal Scientist at Johnson and Johnson Vision in Groningen (the Netherlands). She graduated in Physics and Optics and Optometry in the University of Granada (Spain) and completed her PhD in Physics in 1022 at the same university. She worked as a Postdoctoral Research Associated at the University of Rochester (NY, US) and joined J&J in 2014 working on the R&D department since then. She has several published patents, publications in high impact journals and over 70 scientific communications at international meetings (e.g. ESCRS, ASCRS, ARVO). She has a h-index of 12 with 525 citations (Scopus Author Profile) and has been invited speaker for different international meetings, including Wavefront Congress and AECOS and instructional courses (e.g. ESCRS).*

Multifocal Intraocular lenses based on aperiodic structures: From design to optical bench evaluation

Walter Furlan

University of Valencia (Spain)

This talk presents how aperiodic mathematical structures, like the Cantor Set and the Silver Mean Sequence, can be used to design diffractive intraocular lenses with unique optical properties, that set them apart from conventional periodic designs. A comparative discussion of the main characteristics of these new designs is provided, evaluating merit functions such as the Point Spread Function (PSF) and the Modulation Transfer Function (MTF), both theoretically and experimentally on an optical bench. Additionally, comparative image formation results obtained using an adaptive optics visual simulator are presented.

WALTER D. FURLAN *earned his M.S. degree and Ph.D. in physics from the University of La Plata, Argentina. Until 1990, he worked at the Centro de Investigaciones Ópticas (CIOp) in Argentina. At the end of that year, he joined the Optics Department at the University of Valencia, Spain. His research has focused on two key areas within optics. The first is the theory and applications of phase-space representations, in which he has published over 30 papers in peer-reviewed scientific journals and contributed a chapter to Phase-Space Optics: Fundamentals and Applications (McGraw-Hill Professional, 2009). In recent years, his work has been dedicated to the study of non-conventional diffractive optical elements and their applications. He has co-authored more than 100 scientific papers and holds four patents related to these topics. Currently, he is a Full Professor at the University of Valencia and co-director of the Diffractive Optics Group (DiOG), where his research primarily focuses on the design of aperiodic structured*

diffractive lenses and their applications in optical trapping and ophthalmology. He is a member of SPIE and the European Optical Society.

Ray Tracing Optimization for Personalized IOL Power Calculation

Pablo Pérez Merino

Institute of Optics. Spanish National Research Council (CSIC) (Spain)

Cataract and presbyopia affect billions of people worldwide, these ocular conditions are usually related with the natural ageing and an established solution is to replace the crystalline lens by an intraocular lens (IOL). The implantation of an IOL is the most frequently performed surgical procedure in the world, with an estimation of 20 million-cataract operations/year globally, but the recent increase in optical lens designs has not been paralleled by a further sophistication of the IOL power calculation formulas.[1] Current methods of IOL power calculation generally fail in patients with irregular corneas, such as keratoconus or after corneal refractive surgery, because they rely on assumptions about the corneal shape or estimated lens position that may lead to postoperative refractive surprises.[2,3] One reason for this shortcoming is that IOL power calculations generally aim at minimizing the residual refractive error. In a previous study[4], we developed a novel method based on ray tracing optimization (RTO), which refines IOL power selection by using patient-specific eye modelling and through-focus simulated optical performance to determine the optimal refractive target (Figure 1).

The present study examines the application of this method for IOL power calculation in patients with high level of HOAs, investigating its potential to improve IOL selection based on natural corneal aberrations in a cohort of post-LASIK and keratoconus patients who underwent cataract surgery. To achieve this, 3D corneal elevation data, along with axial distances, were incorporated into custom computer eye models to estimate WF aberrations and to derive retinal image quality. The following parameters were evaluated: (i) corneal astigmatism, (ii) corneal HOAs (e.g., spherical aberration, coma, trefoil, and secondary astigmatism) and (iii) through-focus Visual Strehl as optical quality metric. By analyzing these parameters, we identified the sphero-cylindrical correction that maximizes visual performance in combination with the corneal HOAs. The defocus and astigmatism producing the maximum VSOTF was determined as the optimal target refraction, and compared with postoperative subjective refraction. For the spherical equivalent, 76.3% (post-LASIK) and 68.2% (keratoconus) were within ±0.5D, while 98.2% (post-LASIK) and 86.3% (keratoconus) were within ±1.0D. The RTO method demonstrated a high degree of precision in refraction estimation.

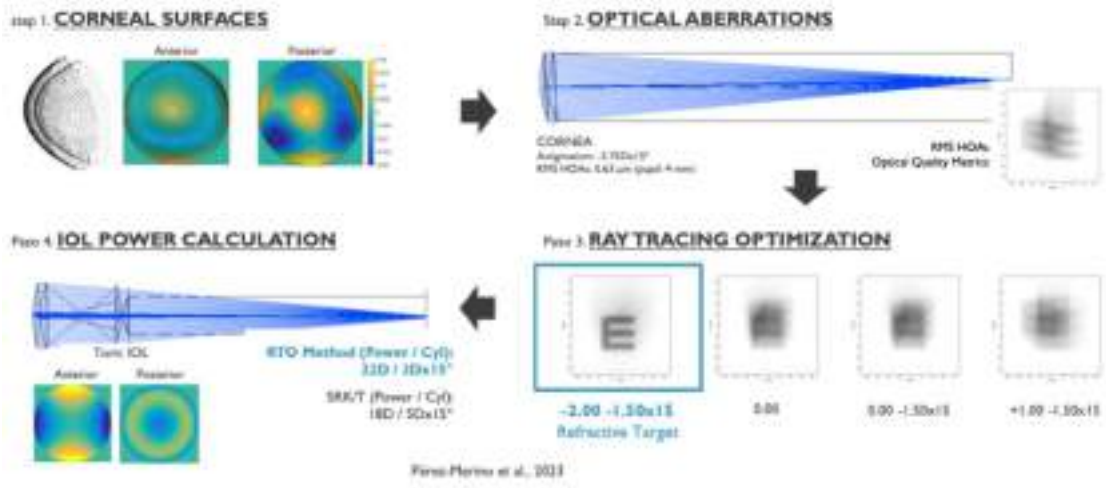

Figure 1. Illustration of the ray tracing optimization (RTO) method for IOL power calculation

[1] S. Marcos et al.; *Annu Rev Biomed Eng* (2021).
[2] R. B. Melles et al.; *Ophthalmology* (2018).
[3] J. X. Kane et al.; *Ophthalmology* (2020).
[4] P. Pérez-Merino et al.; *Sci Rep* (2023)

PABLO PEREZ-MERINO *is a tenured Scientist at the Institute of Optics, Consejo Superior de Investigaciones Científicas (CSIC, Spain), where he develops smart optical systems and advanced imaging technologies for ophthalmic applications. He obtained his Ph.D. in the Visual Optics and Biophotonics group at the Institute of Optics (CSIC, Spain). He completed postdoctoral fellowships as a Juan de la Cierva post-doctoral fellow at the Institute of Biomedical Research Fundación Jiménez Díaz and Autonomous University of Madrid (Madrid, Spain), and as a Marie Skłodowska-Curie Fellow at the Centre for Microsystems Technology (CMST) at Ghent University and imec (Ghent, Belgium). He later joined CSIC as a Ramón y Cajal Fellow. His research has contributed to the development of optical coherence tomography (OCT) systems, wavefront sensing technologies, optical simulations, digital image correlation (3D-DIC) imaging technique, and smart optical systems. He has a proven track record of achievements and independent research, with 45 high-impact publications (15 as leading and corresponding author; h-index: 27, >1800 citations), one patent, 7 book chapters, a popular science book, more than 50 congress contributions and over 10 invited talks.*

Advancing clinical vision through visual simulation

Consuelo Robles García

Voptica SL (Spain)

Visual simulation has transformed vision research, but it also has significant implications for clinical practice. This technique allows a more efficient workflow while integrating new visual tests into routine examinations. One of its most impactful applications is the preoperative simulation of optical profiles, such as intraocular lenses, enabling the selection of the most suitable option for each patient. In this talk we will see the benefits of visual simulation in cataracts patients.

CONSUELO ROBLES *works as a Clinical Specialist at Voptica since 2018, where she has contributed to multiple clinical studies on ocular aberrations, visual simulation, and intraocular lenses, among other topics. She finished her PhD in Vision Sciences in 2023 and is currently a substitute lecturer at the University of Murcia.*

Correcting chromatic aberration

E. Josua Fernández

Laboratorio de Óptica, Centro de Investigación en Óptica y Nanofísica (CiOyN), Universidad de Murcia (Spain)

This course will explore various aspects of chromatic aberration, with a strong focus on its correction and the methods used to achieve it. It will begin with an examination of the origins of chromatic aberration and its characterization through geometrical optics. Next, the course will introduce the most widely used chromatic eye models in the field[1], providing a foundation for understanding how chromatic aberration manifests in vision. A portion of the course will be dedicated to experimental methods for determining chromatic aberration in the eye[2], emphasizing practical challenges and the effectiveness of current techniques. Both subjective and objective measurement methods will be analyzed and compared to assess their limitations and reliability. The course will then address the impact of chromatic aberration on vision[3], particularly its role in accommodation. A key discussion will focus on the paradox of chromatic aberration correction: despite its potential for visual enhancement, its actual benefits in normal vision remain modest at best[4].

A major emphasis will be placed on the correction of chromatic aberration in retinal imaging. Optical coherence tomography (OCT), the only ophthalmic imaging technique that inherently utilizes polychromatic light, will be introduced in this context. Experimental methods for correcting chromatic aberration in OCT will be explored, along with their implications for improving imaging performance[5,6,7]. The course will assess the practical limits of chromatic aberration correction in OCT and its overall impact on imaging quality.

[1]D. A. Atchison and G. Smith; J. Opt. Soc. Am. A (2005)
[2]M. Vinas, et al. Biomed. Opt. Express (2015)
[3]N. Suchkov, et al. Opt. Express (2019)
[4]E. J. Fernandez, et al. Opt. Express (2020)
[5]E. J. Fernandez and W. Drexler; Opt. Express (2005)
[6]E. J. Fernandez, et al. Opt. Express (2006)
[7]E. J. Fernandez, et al. Opt. Express (2008)

ENRIQUE JOSUA FERNANDEZ *received the M.S. degree in Physics, specialty in Astrophysics, and the International Student Diploma in 1999 from the University of La Laguna, Spain, and Imperial College, London, UK, respectively. In 2004 he received his Ph.D. degree in Physics from University of Murcia, Spain, applying Adaptive Optics (AO) techniques to the human eye. From 2004 to 2006, he was Associate Researcher at University of Vienna, Austria, where he worked in ophthalmic Optical Coherence Tomography (OCT). Since 2007, he is Associate Professor (tenured) at Physics Department, University of Murcia. He is the author of more than 50 articles, and more than 10 inventions, most of them licensed to the industry. He has been the cofounder of the spin-off company Voptica, being the first author of several patents of ophthalmic instruments for diagnosis and visual simulation based on AO technology, and several types of intraocular lenses. He has chaired the sections of Vision and Applications in the Spanish Optical Society (SEDOPTICA) and in OPTICA, formerly OSA. Among other distinctions, Dr. Fernandez was the recipient of the International Pascal Rol Award in 2006, SPIE; and the recipient of Young Researcher Award, Royal Spanish Physic Society and Spanish Optical Society in 2003. Currently he serves as vice-dean of Physics at the University of Murcia. His current research interests include new and efficient forms to generate high photon-bunching light sources for Biomedical Optics applications and Physiological Optics.*

SESSION V VISUAL FUNCTION, SMART GLASSES AND DIAGNOSTICS TOOLS

Impact of Visual Function Changes on Everyday Activities

Sonia Ortiz-Peregrina

Department of Optics, Laboratory of Vision Sciences and Applications, University of Granada (Spain)

Visual function can be subject to change or alteration in several circumstances. These include the adaptation to a myopia control method, the development of ocular pathologies, or ocular surgeries. These factors can determine variations in the way in which an individual perceives visual stimuli. The precise characterization of these changes is typically undertaken within clinical or laboratory settings, employing research methodologies and standardized approaches. However, the extent to which these changes manifest as challenges in daily activities remains largely unknown.[1] This issue is particularly relevant, as it is the impact of impairments in visual function on our ability to carry out everyday activities that ultimately determine whether it constitutes a true disability, thereby diminishing the quality of life of the affected individual. It is evident that object manipulation, mobility and driving are three activities that require the greatest visual resources. These activities are directly related to our autonomy and work capacity. For personal mobility, visual function is a determining factor. A recent study found that peripheral blur induced by standard intraocular lenses or myopia control methods (such as astigmatic and myopic defocus) affects simulated driving, primarily by worsening the ability to maintain lane position.[2] However, the implantation of inverted meniscus intraocular lenses, which have been shown to improve this aspect, may provide drivers with greater self-security.[3] Another key aspect of personal mobility is how obstacles are managed while walking. It has been found that myopic and astigmatic peripheral blur impacts step negotiation, resulting in more cautious behavior and increased foot displacement in such situations.[4] In fine motor skills, which are essential for object manipulation, contrast sensitivity has been identified as a critical visual function.[5] The findings demonstrate that a comprehensive evaluation of visual function at various stages and under different circumstances can facilitate the anticipation of difficulties in daily activities. Consequently, it is possible to contribute to the minimization of risks associated with tasks such as driving vehicles or falls in older adults, thereby helping to maintain quality of life.

[1] *J. Wood, et al. Ophthalmic and Physiological Optics (2011)*
[2] *S. Ortiz-Peregrina, et al. Biomed. Optics Express (2022)*
[3] *Casares-López, M., et al. Scient Reports (2025)*
[4] *C. García-Pedreño, et al. Invest Ophthalmology & Visual Science (2024)*
[5] *P. Granados-Delgado, et al. Life, **14**, 1354 (2024)*

***SONIA ORTIZ PEREGRINA** is an Associate Professor at the University of Granada. She holds a Degree in Optics and Optometry (2014), a Master's in Advanced Optics and Optometry (2015), and a PhD in Physics and Space Sciences (2020). She has authored 33 JCR-indexed scientific articles, 2 book chapters, and has made over 40 contributions to national and international conferences. She has participated in 6 competitive research projects (3 National Plan, 2 Regional Plan, 1 UGR), acting as Principal Investigator in two ongoing projects. Her research focuses on visual optics, particularly the impact of visual quality on daily tasks such as driving, the effects of cannabis on vision, dry eye disease biomarkers, myopia control, and contact lens fitting optimization.*

Optoelectronic glasses for automatic correction of presbyopia

Juan L. Aragón

University of Murcia (Spain)

Presbyopia is an unavoidable condition that affects the entire world population over the age of 45 due to aging. It impairs the eye's ability to accommodate, leading to a loss of focus on near objects. This results in blurry vision and discomfort when performing common tasks such as using a smartphone, working on a computer, or reading a book. This talk focuses on the development of a wearable device to dynamically and automatically correct presbyopia,

which we are designing at LOUM (University of Murcia). The device consists of a pair of optoelectronic lenses driven by efficient pupil tracking. The system is fully portable and provides a wide range of defocus correction, up to 10 D. Several prototypes will be described, up to the latest wearable device, in which all computing tasks are performed directly on the glasses. To develop a truly autonomous and wearable device, fast, robust and energy-efficient pupil tracking must be performed. Our latest prototype incorporates AI-based pupil tracking using a deep learning model, which outperforms classical pupil tracking approaches (PuRe, ElSe, and ExCuSe) as well as other deep neural network models (such as DeepVOG). This enables real-time presbyopia correction using portable, low-power computing devices.

JUAN L. ARAGÓN *is a Full Professor in Computer Architecture at the University of Murcia (Spain). He received his M.Sc. degree in Computer Science in 1996 and his Ph.D. degree in Computer Engineering in 2003, both from the University of Murcia (Spain). In 1999 he joined the Computer Engineering Department at the University of Murcia as an Assistant Professor. In 2003-2004, he did a 1-year post-doctoral stay as a Visiting Assistant Professor in the Computer Science Department at the University of California, Irvine. He has also been a Visiting Researcher at EPFL (Lausanne, Switzerland) in 2013; and a Visiting Researcher at Princeton University (NJ, USA) in 2015, 2017, 2018, 2019 and 2022.*

His research interests are focused on computer architecture, energy-efficient processors, microarchitecture design, application-specific accelerators, GPUs in addition to applied research in the field of human visual optics. Dr. Aragón has advised 7 Ph.D. theses and has co-authored +80 research papers in major conferences and journals in computer architecture. He has been a PC member for HPCA'2022, HPCA'2023, MICRO'2023, MICRO'2025, EuroMicro-PDP for 14 years (2009-2022), ISLPED'2010 and has been the Workshop Chair of ISCA'2017. Prof. Aragon is a regular reviewer in top-class conferences and international journals, and he is a member of the HPCA Test of Time Award Committee.

Straylight and glare phenomena in cataract

Harilaos Ginis

Diestia (Greece)

Cataract impairs visual quality by inducing significant light scattering and a rapid increase in wavefront aberrations. Various methods are available to measure this scattering and assess its impact on visual performance. Following surgery, despite the replacement of the opacified crystalline lens with an artificial intraocular lens (IOL), patients may experience new entoptic phenomena. These include glare, straylight, and dysphotopsias, often associated with IOL design. Both the pre- and postoperative visual disturbances are examined to provide a comprehensive understanding of the optical challenges in cataract patients.

HARILAOS GINIS *is a physicist with a background in biomedical optics and over 30 years of experience in vision science and ophthalmic technology. His work focuses on the development of diagnostic instruments, surgical systems, and intraocular implants aimed at improving visual outcomes in clinical practice. He has contributed to both academic research and product development through roles in industry and university settings. Harilaos is currently involved in projects related to optical quality assessment, diagnostic / imaging devices and intraocular lenses.*

KEYNOTE TALK

Future Challenges in Visual Optics

Pablo Artal

University of Murcia (Spain)

Visual optics has advanced significantly, yet challenges remain in optimizing vision correction and developing advanced diagnostic tools. In this presentation, I will explore key future directions, including wearable adaptive optics, novel intraocular lens designs, innovative strategies for myopia control and presbyopia correction, and the role of infrared two-photon vision in expanding our understanding of human visual perception. This talk will provide insights into the future of visual optics research, bridging fundamental discoveries with clinical applications to advance vision care.

PABLO ARTAL *studied physics at the University of Zaragoza (Spain) and completed his PhD at the Instituto de Óptica (CSIC) in Madrid. He pursued postdoctoral research at Cambridge University (UK) and the Institut d'Optique in Orsay, France, before securing a permanent research position at the Instituto de Óptica. In 1994, he became the first full Professor of Optics at the University of Murcia, where he founded the Laboratorio de Óptica. His research focuses on the optics of the eye and retina, as well as the development of optical and electronic imaging techniques for vision, ophthalmology, and biomedicine. He has published over 400 peer-reviewed papers (h-index:87), holds more than 30 international patents, and has co-founded two spin-off companies. He has received numerous prestigious awards, including the Edwin H. Land Medal (2013), the King Jaime I Award in New Technologies (2015), the Spanish National Research Award "Juan de la Cierva" (2018), the Edgar D. Tillyer Award (2019), and the 2021 medal of the Spanish Royal Physics Society. A Fellow of Optica (OSA), ARVO, EOS, and SPIE, he continues to contribute significantly to both fundamental and applied optics.*

YOUNG RESEARCHERS SESSION: ORAL

TALK 1. Eye tracking parameters as biomarkers of cognitive performance in the Stroop Color-Word Test

Joan Goset[1], Valldeflors Viñuela[1], Clara Mestre[1], Luis Pérez-Mañá[1], Mikel Aldaba[1], Meritxell Vilaseca[1]

[1] Center for Sensors, Instruments and Systems Development, Universitat Politècnica de Catalunya, Rambla Sant Nebridi 10, 08222, Terrassa (Barcelona), Spain

Contact: joan.goset@upc.edu

***Introduction*:** Diagnosing neurological disorders relies on detecting cognitive decline. This is usually conducted in clinical practice by means of neuropsychological tests, as the Stroop Color and Word Test (SCWT)[1], a key tool for assessing inhibition and processing speed. The standard neuropsychological tests, including the SCWT, are time-consuming, require trained professionals, face cultural barriers, and often miss early diagnosis[2]. Therefore, new approaches are needed for earlier and easier detection of neurological diseases. Since eye movements are influenced by cognitive decline, eye tracking offers a promising alternative[3] to overcome the limitations of standard neuropsychological tests.

Within this context, the objective of this study is to examine the relationship between the cognitive score of a widely used neuropsychological test, the SCWT, and eye movement parameters.

***Methods*:** Participants first completed the SCWT that requires to name the ink color of mismatched words rather than reading them. This test score consists of the number of correct answers in one minute. Eye movements were recorded on a separate day. To do so they were positioned 60 cm from a 17" LCD monitor and stabilized with a chinrest. Eye movements were tracked using an EyeLink 1000 Plus (SR Research) with visual tasks to induce different eye movements: saccades, antisaccades, fixation and smooth pursuit. In the saccade task, participants fixated on a central point and shifted gaze to a peripheral target as quickly as possible. During antisaccades, participants were instructed to shift their gaze in the opposite direction of the peripheral stimulus while mirroring its amplitude. From saccades and antisaccades we retrieved the accuracy in terms of deviation from the horizontal line [º], amplitude[º], velocity [º/s] and latency [s]. In the fixation task, they maintained gaze on a central cross while peripheral distracting dots appeared and disappeared. In this case the fixation stability was measured with the root mean square error (RMS) [º] of the gaze points. The smooth pursuit task involved tracking a stimulus moving following linear (horizontal/vertical) and sinusoidal trajectories at a constant speed. For this task, we measured accuracy using the root mean square error (RMS) in degrees [º] between the gaze points and the stimulus position, as well as the number and amplitude of intrusive saccades.

Partial Spearman correlations were conducted to examine the relationships between test scores and eye tracking metrics, adjusting for participants' years of education and age as covariates. A p-value < 0.05 was considered statistically significant.

Beyond the correlation analysis, a machine learning-based k-means clustering approach was applied to identify hidden patterns and subgroups within the eye tracking data. To facilitate this, Principal Component Analysis (PCA) was first used to reduce all eye tracking variables into three principal components. For each identified cluster, differences in the test performance across clusters were assessed using the Kruskal-Wallis test.

Results: Eye movement data from a total of 103 participants were included in the final analysis. Participants had a mean ± SD age of 50.75 ± 7.43 years. Higher test performance was associated with improved eye movement metrics. The following significant correlations between the SCWT score and the eye tracking parameters were found: fixation RMS during distractors -0.290 (p=0.003), saccades horizontal deviation -0.325 (p=0.020), anti-saccades amplitude 0.365 (p=0.009) and vertical smooth pursuit RMS -0.289 (0.003). PCA analysis and k-means

clustering grouped participants into three clusters (0, 1, and 2), resulting in a Silhouette coefficient[4] of 0.32. Cluster 0 had the lowest median performance, followed by Cluster 1, while Cluster 2 performed the highest. SCWT scores varied significantly between clusters, and the post-hoc Bonferroni corrections identified specific differences, with significant p-values, medians, and IQRs presented in Figure 1.

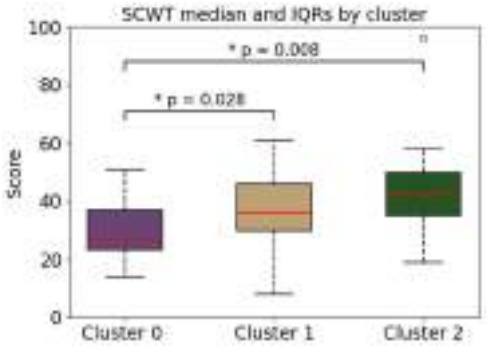

Figure 1: Median and interquartile range (IQR) scores of SCWT for each cluster. Significant differences between clusters are indicated by brackets. Cluster 0 differs significantly from Cluster 1 (p = 0.028) and Cluster 2 (p = 0.008).

***Discussion*:** This study investigated the relationship between eye movement parameters and cognitive performance measured by the SCWT. Our results show statistically significant moderate correlations between eye movement features and SCWT scores. Our findings align with previous research demonstrating meaningful relationships between eye movement metrics and neuropsychological testing[5,6]. Moreover, the use of cluster analysis revealed that oculomotor performance can distinguish participant groups with different cognitive profiles, as defined by SCWT score. This indicates that eye movement data may be used to classify individuals in a way comparable to traditional cognitive assessments. Given the known limitations of traditional neuropsychological evaluations (time demands, cultural and language barriers, and the reliance on trained professionals) eye tracking emerges as a viable, non-invasive alternative. A limitation of this study is the separate-day administration of SCWT and eye tracking which may have introduced variability in the participants performance. To further validate its clinical value, future studies should explore longitudinal changes in eye movement behaviour with cognitive performance.

Acknowledgements: This publication is part of the project TED2021-130409B-C54 and TED2021-130409B-C51, funded by MCIN/AEI/10.13039/501100011033 and the European Union "NextGenerationEU"/PRTR.

1 Charles J. Golden, *Test de Colores y Palabras (Stroop)*, TEA Ediciones, Madrid, 2005.
2 D. Howieson, *The Clinical Neuropsychologist*, 2019, **33**, 200–208.
3 L. Tao, Q. Wang, D. Liu, J. Wang, Z. Zhu and L. Feng, *Neurol Sci*, 2020, **41**, 1697–1704.
4 C. Yuan and H. Yang, *J*, 2019, **2**, 226–235.
5 A. C. Gran Ekstrand, M. Nilsson Benfatto and G. Öqvist Seimyr, *Front. Educ.*, 2021, **6**, 643232.
6 J. L. Gills, N. T. Bott, E. N. Madero, J. M. Glenn and M. Gray, *GeroScience*, 2021, **43**, 297–308.

TALK 2. Accommodation parameters in two-photon vision – application in Augmented Reality technology

Oliwia Kaczkoś[1,2,3], Maria Viñas Peña[4], Jacek Pniewski[3], Maciej Wojtkowski[1,2], Katarzyna Komar[1,2,5]

[1] International Centre for Translational Eye Research, Institute of Physical Chemistry, Polish Academy of Sciences, Skierniewicka 10A, 01-230, Warsaw, Poland.
[2] Department of Physical Chemistry, Institute of Physical Chemistry, Polish Academy of Sciences, Kasprzaka 44/52, 01-224, Warsaw, Poland.
[3] Faculty of Physics, University of Warsaw, Pasteura 5, 02-093, Warsaw, Poland.
4 Instituto de Optica, Consejo Superior de Investigaciones Cientificas, C. de Serrano 121, 28006, Madrid, Spain.
5 Institute of Physics, Faculty of Physics, Astronomy and Informatics, Nicolaus Copernicus University in Torun, Grudziądzka 5, 87-100, Torun, Poland.

Contact: kkomar@fizyka.umk.pl

Accommodation parameters play a crucial role in retinal image quality, which is particularly important in the context of retinal displays and augmented reality (AR) technology. The aim of this study was to evaluate the accommodation amplitude of the eye for two-photon vision and investigate the impact of defocus on image quality. Two-photon vision phenomenon is based on visual perception of pulsed infrared lasers (800-1300 nm) due to isomerization of visual pigments caused by two-photon absorption [1]. Two-photon visual stimuli are subjectively perceived as highly clear and sharp, which is particularly important in the context of using two-photon vision in retinal displays and AR technology. The quality of the image formed on the retina is strongly conditioned by the accommodation parameters of the eye. The aim of the study was to assess the accommodation amplitude of the eye for two-photon vision and evaluate the impact of defocus on the perceived image.

Ten healthy volunteers with no diagnosed visual system pathologies participated in the study. To measure accommodation amplitude, a letter stimulus "E" of 0.2° size was displayed through fast scanning of the retina with a pulsed laser beam at a wavelength of 1040 nm for two-photon vision and 520 nm for one-photon vision, with both stimuli perceived as green. Both beams were generated by a femtosecond laser (τ_p=250 fs, F_{rep}=63 MHz). Using a brightness matching method, both stimuli were adjusted to have the same subjective brightness [2]. The measurement involved increasing the stimulus for accommodation by adjusting defocus in 0.5 D steps until the participant observed subjective blurring of the stimulus. Additionally, the study assessed the defocus level at which the participant could no longer correctly identify the orientation of the presented optotype using a four-alternative forced-choice procedure. The obtained accommodation amplitudes were higher for two-photon vision: 4.0 ± 0.6 D compared to one-photon vision: 2.7 ± 0.6 D. The threshold for optotype recognition did not differ significantly between one- and two-photon vision (6.8 D ± 0.8 D and 6.6 D ± 0.7 D, respectively). The results suggest that two-photon vision is characterized by a higher accommodation amplitude, allowing for the maintenance of a high-quality image over a wider range of defocus than one-photon vision. The findings confirm the potential for applying the phenomenon of two-photon vision in retinal displays and AR technology.

Figure 1: Schematic representation of the effect of defocus on perceived stimuli in one-photon (VIS) and two-photon (IR) vision.

ACKNOWLEDGEMENTS: The International Centre for Translational Eye Research (FENG.02.01-IP.05-T005/23) project is carried out within the International Research Agendas programme of the Foundation for Polish Science co-financed by the European Union under the European Funds for Smart Economy 2021-2027 (FENG).

[1] G. Palczewska et al.; *Proc Natl Acad Sci*, **111**, 5445 (2014).
[2] O. Kaczkoś et al.; *Biomed Opt Express,* **15,** 5818 (2024).

TALK 3. Adaptive Optics Scanning Light Ophthalmoscopy of the Living Mouse Retina in Normal and Disease Conditions

Rosa M. Martínez-Ojeda[1], Wuao Jia[1,2] and Jennifer J. Hunter[1]

[1] School of Optometry and Vision Science, University of Waterloo, 200 University Av. W, N2L 3G1, Waterloo, CAN
[2] The Institute of Optics, University of Rochester, 480 Intercampus Dr., 14627, Rochester, USA

Contact: rosa.martinezojeda@uwaterloo.ca

Adaptive Optics Scanning Light Ophthalmoscopy (AOSLO) is a technique that achieves high resolution images of the retina by correcting the aberrations of the eye. Functional and structural changes in the different layers of the retina can appear due to different retinal pathologies, such as retinitis pigmentosa[1,2] (RP). The use of animal models is helpful to study the feasibility of different diagnostic techniques[3] and AOSLO has been shown to be capable of non-invasive imaging of the eye of live mice[4,5].

Here, we study in vivo structural differences between the retinas of Thy1-EGFP mice (with GFP- labelled ganglion cells) and rhodopsin knockout (Rho-/-) mice (model for retinitis pigmentosa) with an AOSLO. The experimental setup is a custom-built AOSLO6. The illumination source for the AO module is a 940 nm super luminescent diode (SLD, QPhotonics), a deformable mirror (ALPAO) corrects the wavefront aberrations measured by a Hartman-Shack wavefront sensor. Reflectance images of the retina were acquired with a 670 nm SLD (Superlum) and a Ti:Sapphire femtosecond laser (tunable λ = 730 - 920 nm, 80 MHz, ~70 fs, SpectraPhysics) that also allowed us to acquire two-photon excited fluorescence (TPEF) images. The individual images are the result of the registration and average of 1000 frames. The reflectance images from the retina of the GFP mice, used as a control here, show a well-maintained retinal structure, and due to the confocal modality, we can image different layers. The left panel in Figure 1, shows the nerve fiber layer (inner retina), with the nerve fiber bundles behind a wide blood vessel and some capillaries. On the other hand, Rho-/- mice don't show the fiber bundles in the NFL as clearly as the EGFP mice (Figure 1, center). However, due to the lack of the photoreceptors outer segment (OS) in Rho-/- mice1, the RPE mosaic is clearly visible (Figure 1, right).

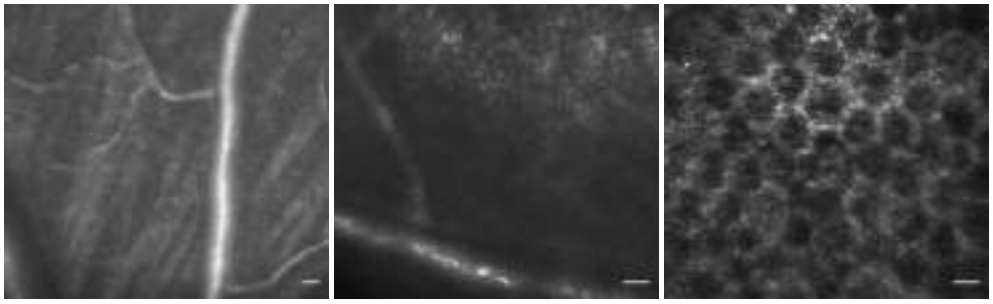

Figure 1: In vivo confocal images of the nerve fiber layer (NFL) of the Thy1-EGFP (left) and Rho-/- (center), and retinal pigmented epithelium (RPE) in Rho-/- (right). Scale bar: 20 µm.

In conclusion, high resolution confocal reflectance images of the living mouse retina have been acquired with a custom-build AOSLO. Structural differences have been found in the retinas of control and RP model mice, such differences can be studied and described.

ACKNOWLEDGEMENTS: Funding from National Institutes of Health (NIH) R01 EY022371 and NSERC Canada Discovery grant RGPIN-2024-05140.

[1] *J. Lem et al.; Proc. Natl. Acad. Sci. U.S.A., 96, 736 (1999).*
[2] *C. Punzo, K. Kornacker and C. Cepko; Nat. Neurosci, 12, 44 (2009)*
[3] *H. O. Orlans, A. R. Barnard and R. E. MacLaren; Exp. Eye Res, 190, 107895 (2020)*
[4] *K. Kunala et al.; Invest. Ophthalmol. Vis. Sci., 62,50 (2021)*
[5] *Y. Geng et al.; Biomed. Opt. Express, 3, 715 (2012)*
[6] *S. Steven; Thesis (Ph. D.) University of Rochester. The Institute of Optics (2020)*

TALK 4. Investigating scleral tissues structural changes after riboflavin-mediated crosslinking with enhanced digital processing tools

Daniel Romero[1*], Gloria Bueno[2,4], Yoonha Hwang[3], Gabriel Cristóbal[1,4], María Vinas-Pena[1,4]

[1]P4EyeLab. Institute of Optics. Spanish National Research Council. Serrano, 121, 28006 Madrid, Spain
[2]VISILAB, Universidad de Castilla-La Mancha, E.T.S. Ingeniería Industrial, Avda Camilo Jose Cela, Ciudad Real, Spain
[3]IVIM Technology. #B-415, Daedeok BizCenter, 17 Techno 4-ro, Yuseong-gu, Daejeon, 34013, Republic of Korea
[4]OPTICAI, CSIC Associated Research Unit (IO-VISILAB), Madrid-Ciudad Real, Spain

Contact: danrom06@ucm.es

Introduction. The sclera, which covers the entire eyeball except for the cornea, and is composed of collagen fibrils arranged in irregular and interlacing bundles, responsible for the stiffness of the eyeball, undergoes significant remodeling in refractive eye development. Light-based technologies have allowed a partial understanding of structural[1]/mechanical[2]/molecular[3,4] changes in ocular tissues. However, structural dissection of scleral tissues has been hampered by the spatially heterogeneous, anisotropic, and varying regionally scleral properties, as well as its highly scattered properties. We combine second harmonic generation (SHG) microscopy and enhanced digital processing tools to analyze scleral structural properties, and changes following collagen crosslinking (SCXL) treatments.

Methods. (1) Images acquisition. Measurements were performed in a porcine eye model (10 porcine eyes, Animal Biotech Industries) in control and treated regions, with riboflavin-UVA light cross-linking (UVX-SCXL) (Dresden protocol, 370nm, 3mW/cm2, 30min), using a commercial device (Avedro, Glaukos). After SCXL, scleral strips were cut from both treated and non-treated regions and measurements performed in the treated/non-treated riboflavin immersed strips. Porcine eyes were imaged using time-correlated single photon counting (TCSPC) and SHG. SHG measurements were performed using a two-photon microscope (IVM-MS2, IVIM Technology) using fluorescent microbeads as precise 3D landmarks (Figure 1, upper row); (2) Images stacks analysis (Figure 1, lower row). The initial analysis consisted of adapting previously validated computational methodologies for the cornea to our sclera images. Processing techniques were implemented, such as Hessian filtering for fiber enhancement and noise suppression[5], 3D Fourier transforms on the full image stack[6], and calculation of frame-by-frame gradients as a basis for deriving dominant orientation (DoI) maps or the structure tensor [7].

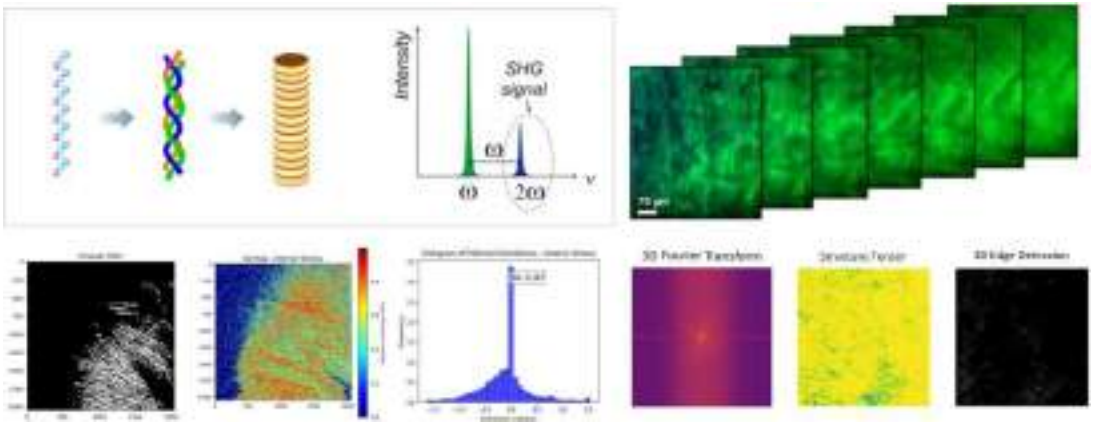

Figure 1: Second harmonic generation and initial images stacks analysis

After validating the applicability of existing corneal analysis methods on the sclera, complementary advanced processing methods were implemented. Including energy filters and Fourier transform fitted lines to isolate main fibers (Figure 2, upper row), along with quantitative analysis of their orientation and distribution in depth using orientation.py (Figure 2, lower row).

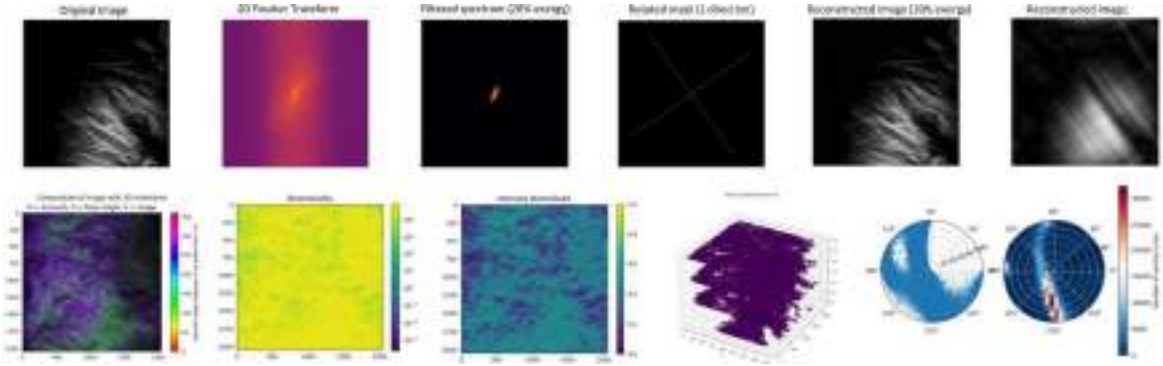

Figure 2: Implemented advanced methods of images stacks analysis

Results. Figure 1 shows that Hessian filtering effectively removes noise, highlighting only the main collagen fibers, while DoI and structure tensor reveal their behavior, useful for applications such as edge detection. On the other hand, Figure 2 evidences how computational refinement yields significantly more information-rich results through: (a) advanced filtering protocols, including 20% energy thresholds for full reconstruction and adaptive line algorithms for spatial targeting; (b) multidimensional visualization techniques that allow three-dimensional layered representation of the fibrillar architecture; and (c) spatial modeling of orientations by stereoplots, thus establishing a superior analytical paradigm for microstructural characterization.

Discussion & Future steps. The initial results with the newly implemented methods were promising but revealed the need for a more selective analysis. To improve this, the approach of working with smaller pixel windows within the frames is proposed, or alternatively, a more recent strategy involves selecting only the main fibers using a line filter adapted to the Fourier transform. This filter is adjusted based on the spectrum: if it is directional (horizontal/vertical), a linear filter is applied; if it is isotropic (circular/square), a combination of two linear filters in the principal directions is used, thereby recovering information that might otherwise have been lost.

ACKNOWLEDGEMENTS: This research has received funding from the Spanish Government under the PID2022 (PID2022-139840OA-I00-MYOFLUOGOLD) and the CNS2022 (CNS2022-135326-GOLDENEYE) and the RyC2021 (RYC2021-034218-I) programs to MV.

[1] *Ávila, F. J. et al. Applied Optics 54, (2015).*
[2] *Vinas-Pena, M. et al. Biomedical Optics Express 13, (2022).*
[3] *Dysli, C. et al. Prog Retin Eye Res 60, (2017).*
[4] *Vinas-Pena, M. et al. Investigative Ophthalmology & Visual Science 64, (2023).*
[5] *A. A. Zeitoune, P. A. Bersanetti, P. Schor, L. A. Erbes, C. L. Cesar, and J. Adur; International Journal of Biological Macromolecules, 165, 346 (2020).*
[6] *T. Y. Lau, R. Ambekar, and K. C. Toussaint; Optics Express, 20, 21822 (2012).*
[7] *J. M. Bueno, F. J. Ávila, and M. C. Martínez-García; BioMed Research International,* ***2019****, 3860498 (2019)*

TALK 5. Dynamic Full-Field Optical Coherence Tomography to measure photosensitivity

Nathaniel Norberg[1], Olivier Thouvenin[3], Salvatore Azzollini[1], Julia Granier [1,2], Tual Monfort[1,2], Kate Grieve[1,2]

[1] Sorbonne Université, INSERM, CNRS, Institut de la Vision, 17 rue Moreau, F-75012Paris, France
[2] CHNO des Quinze-Vingts, INSERM-DGOS CIC 1423, 28 rue de Charenton, F-75012 Paris, France
[3] Institut Langevin, ESPCI Paris, Université PSL, CNRS, 1 rue Jussieu, 75005 Paris, France

Contact: nathanielonorberg@gmail.com

PURPOSE Functional assessment of photoreceptors in in-vitro/ex-vivo environments typically relies on methods like electrophysiology and fluorescence. These techniques, though powerful, are invasive and unsuitable for longitudinal studies. Optophysiology—an all-optical probing of retinal function viavisible light—emerges as a non-invasive alternative for quantitatively assessing photoreceptor function[1,2]. In vivo, optoretinography using adaptive optics scanning laser ophthalmoscopy (AOSLO)[3] and optical coherence tomography (OCT)[4] has enabled non-invasive functional assessment of neurons. In vitro, developing equivalent tools is essential for non-invasive functional assessment of retinal samples, important for disease modeling and therapy testing. Here, we adapt in- vivo post-processing tools for the lab environment, focusing on photoreceptors in an ex-vivo macaqueretinal explant.

NOVELTY: This work presents the first use of a signal processing technique for assessing photoreceptor responsiveness in an ex-vivo setting using dynamic full-field optical coherence tomography (D-FF-OCT). D-FF-OCT is a label-free, non-invasive method ideal for functional assessments in a lab environment, maintaining cell culture conditions and providing high-resolution imaging. While D-FF-OCT has shown structural measurements of retinal samples[5], we extend its application to probing cell behavior in response to light, paving the way for non-invasive evaluation ofretinal samples and therapy testing. Our results show the promise of intensity-based optophysiology as a quantitative measure of cone function in the macaque retina.

METHODS: The setup, previously described[5,6], includes a Linnik interferometer with sample and reference arms and a stage-top incubator for cell culture maintenance. The interferometric signal was recorded using a CMOS camera at 400 Hz. The system's resolution (0.4 µm lateral, 0.7 µm axial) allows visualization of subcellular structures. D-FF- OCT images were acquired from datasets with dimensions (1440x1440 pixels, 512 frames), with statistical metrics of the intensity profile assigned to Hue, Saturation, and Brightness channels, revealing metabolic activity. For optophysiology, a reference D-FF-OCT image was recorded, followed by raw recordings (1440x1440 pixels, 2500 frames) capturing the entire light stimulation-induced event. D-FF-OCT recordings were obtained from a dark-adapted (5 min) macaque photoreceptor explant using an infrared LED (810 nm) source, focusing on the photoreceptor outer nuclear layer.

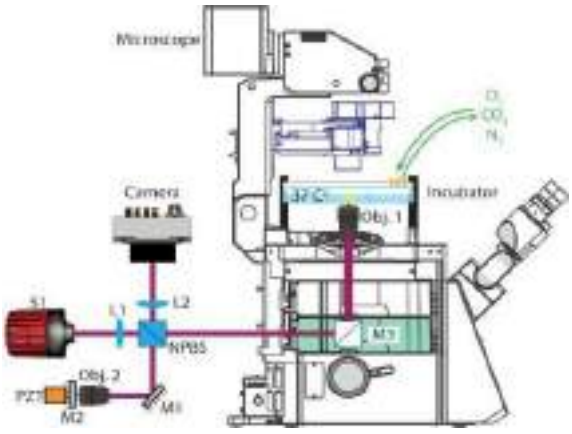

Figure 1. D-FF-OCT optical set-up

At frame 650, a single green light flash (530 nm, 100 ms) was delivered. Control recordings without a flash were also acquired. Intensity signature comparisons before and after the flash were analyzed. Regions of interest (ROIs) corresponding to individual photoreceptor nuclei were identified using the Cellpose GUI [7], with manual adjustments for accuracy. Standardization of signal intensity, removal of stimulus-independent fluctuations, and classification of ROIs into responders and non-responders were performed. ROIs exceeding ±2 standard deviations (STDs) were classified as responders. The variability of responding cells was then calculated to generate photostimulation responsiveness curves(Fig. 3b).

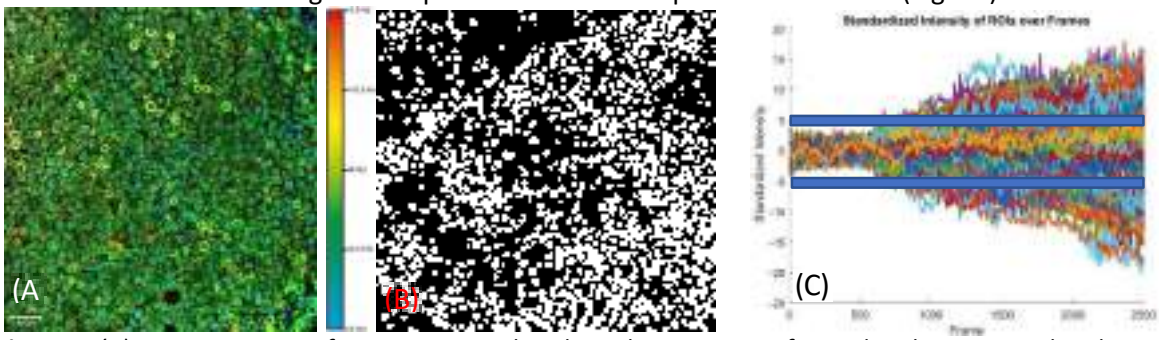

Figure 2. *(A) D-FFOCT image of macaque retinal explant photoreceptors focused in the outer nuclear layer. Scale bar 200 µm. The color scale is representative of the metabolic state of the cells. (B) Cellpose segmented image showing the ROIs selected (n=1075). (C) Standardized intensity of ROIs over time. Each plot represents the standardized intensity of a single ROI. Blue bars indicate the threshold for non-responders (n=405) within the blue bars, and responders (n=670) outside the blue bars.*

RESULTS: Figure 3a shows 62% of photoreceptors responding to light stimulation. Identifying these responsive cells may reveal biomarkers of photosensitivity. Figure 3b shows photostimulation responsiveness curves, with control and stimulated data diverging significantly post-stimulus, indicating substantial cellular behavioral changes in response to light.

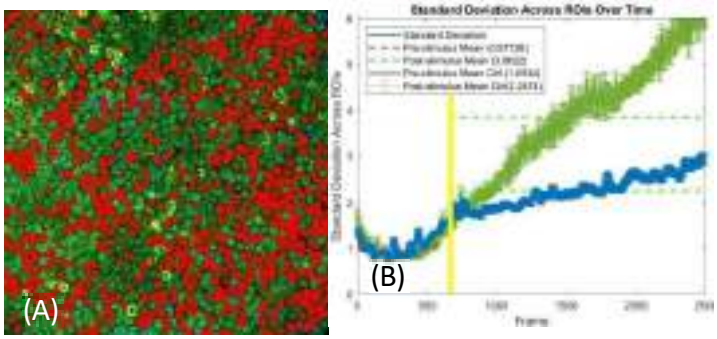

Figure 3. ***(A)*** *Overlay mask of responding ROIs in red (n=670), 62% of the photoreceptors responded*
(B) *Photostimulation responsiveness curve for stimulation (green) and control (blue). Light stimulus delivery represented in yellow. Error bars represent the standard error of the mean (SEM).*

CONCLUSION: We have extended a signal processing pipeline to assess photoreceptor function using D-FFOCT, demonstrating the feasibility of optophysiology in an ex-vivo environment.

REFERENCES

[1]*Bizheva, K. Pflug, et al. (2006). Depth-resolved optical probing of retinal physiology with functional ultrahigh resolution optical coherence tomography. PNAS 5066- 5071*
[2]*Yao X, Wang B. Intrinsic optical signal imaging of retinal physiology: a review. J Biomed Opt. 2015 Sep;20(9):090901.*
[3]*Cooper RF, et al. Optoretinography of individual human cone photoreceptors. Opt Express. 2020 Dec 21; 28(26): 39326-39*
[4]*Vienola, Kari V., et al. 2022. "Velocity-Based Opto-retinography for Clinical Applications." Optica 9(10): 1100.*
[5]*Monfort, T., J. et al. Dynamic full-field OCT module adapted to commercial microscopes allows longitudinal in vitro cell culture study. CommunBiol **6**, 992 (2023).*
[6]*Scholler, J., et al. Dynamic full-field OCT tomography: 3D live-imaging of retinal organoids. Light Sci Appl 9, 140 (2020).*
[7]*Stringer, C., et al. Cellpose: a generalist algorithm for cellular segmentation. Nat Methods **18**, 100–106 (2021).*

POSTERS SESSION

ID	TITTLE	AUTHOR
1	Analysis of the relationship between accommodation and age: structural and functional changes in the eye	**María Arcas Carbonell** Universidad de Zaragoza
2	Analysis of Visual Performance and Pupil Dependency in Intraocular Lenses with Extended Depth of Focus Design	**Inas Baoud Ould Haddi** University Complutense of Madrid
3	Next-Generation Ophthalmic Glasses for Circumventing Presbyopia	**Sunil Kumar Chaubey** University College Dublin, Ireland
4	Measurement of detection intensity thresholds of stimuli presented behind the halos produced by multifocal corrections	**Diego Chorrero Labrador** Instituto de Óptica (IO - CSIC)
5	Do diffractive intraocular lenses break the beneficial interaction between chromatic and monochromatic aberrations in the eye?	**Laura Clavé** Universidad Politécnica de Cataluña
6	Optical performance and predicted visual resolution of two presbyopia-correcting intraocular lens designs	**Fátima Cuéllar Santiago** Universidad Politécnica de Cataluña
7	Analysis of optical properties and halo effects in five intraocular lens designs	**Paulina Dotor Goytia** Instituto de Óptica (IO - CSIC)
8	Optical imaging performance of an extended depth of focus intraocular lenses compared to its monofocal platform	**Júlia Hernàndez Ris** UPC
9	Objective assessment of halos in diffractive multifocal intraocular lenses through optical simulation	**Anabel Martínez Espert** Universitat de València
10	Image correction through cataracts by wavefront shaping	**Alba M. Paniagua-Diaz** University of Castilla La-Mancha
11	Halo size evaluation produced by multifocal intraocular lenses using a binocular visual simulator	**Petros Papadogiannis** 2EyesVision
12	Lensless holographic reconstruction of a highly diffractive profile of a multifocal intraocular lens	**Rosa Vila** Universitat de València
13	A new algorithm for anterior cornea segmentation and shape quantification in optical coherence tomography (OCT) images	**André Amorim** Universidade do Minho
14	Preliminary study on the reflectance of eye fundus structures using a portable multispectral fundus camera	**Marina Bou i Marin** Universitat Politècnica de Catalunya
15	Stokes Vector Analysis of the Lamina Cribrosa using Linear and Second-Harmonic Generation Microscopy	**Aishwarya Chanady Babu** University College Dublin
16	Improving a Multispectral Camera for Simultaneous Retinal Oximetry and Multispectral Image Acquisition	**Armin Eskandarinasab** Universitat Politècnica de Catalunya (UPC)
17	A Hybrid Algorithm for Artifact Removal in Shack-Hartmann Sensor Images: Combining Correlation and Hough Transform	**Sarvenaz Kalantarinejad** Universitat Politècnica de Catalunya (UPC)
18	Reconstruction of the full Shape of the Crystalline Lens from Off-Axis OCT Images	**Javier Rodríguez Sánchez** Instituto de Óptica (IO - CSIC)
19	The Heidelberg FLIO and aCustom AOFLIOShowConsistent FluorescentLifetime Phasor Signatures	**Michelle Peimann** University of Waterloo
20	Multimeridional analysis of brightness artifacts in corneal densitometry and the role of eye color	**Ana Ramos Arizcuren** Universidad de Zaragoza
21	Unorthodox parameters in machine learning-based keratoconus detection	**Juan Casado Moreno** Universidad de Zaragoza

22	Changes in the Corneoscleral Profile Induced by Soft Contact Lens	**Laura Remón** Universidad de Zaragoza
23	Analysis of changes in intraocular pressure and ocular perfusion pressure in young athletes: a preliminary study.	**Aida Ramón Campillo** Universitat de València
24	Assessing Intraocular Pressure During Fenestrated Scleral Lens Wear: A Novel Methodology	**Rita Maria Serra Seco** Universidade do Minho
25	Driving performance under the influence of visual distraction from smartwatch and navigation system use	**Miriam Casares López** Universidad de Granada
26	Colour Vision in Early Parkinson's Disease: MUC Test Assessment	**Alba Herrero-Gracia** University of Valencia
27	Does cannabidiol use affect visual function and optical quality?	**Francesco Martino** University of Granada
28	Age-related changes of the foveal neural contrast sensitivity function	**Sara Silva-Leite** Zeiss Vision Science Lab - Carl Zeiss International
29	Clinical implications of high-order aberrations for accommodation measurement in subjective refraction	**Aina Turull-Mallofré** Universitat Politècnica de Catalunya
30	Visual field assessment using an automatic eye tracking perimetry	**Eduardo Esteban-Ibañez** DIVE-Medical SL /Aragón Health Research Institute (IIS Aragón),
31	Validation of aLaptop-Webcam-BasedEye TrackingSystem for SaccadeMeasuremen	**Lorenzo Fratini** UPC
32	Impact of Bangerter foils on non-strabismic binocular anomalies and fine motor skills analysed using eye-tracker and motion-capture camera	**Pilar Granados Delgado** Universidad de Granada
33	Eye movements and visual performance from eye-tracking in table tennis players	**Alejandro Guiseris Santaflorentina** Universidad de Zaragoza
34	Video-ophthalmoscope to measure retinal reflectance changes to flickering light	**Radim Kolar** Brno University of Technology
35	Comparison of eye movements in a Head-mounted and a Table-top implementations of the visual simulator SimVis Gekko2	**Pilar Urizar** 2EyesVision
36	A novel approach to assess oculomotor behaviour in amblyopia	**Maite Valentino** CD6-UPC
37	Application of optofluidic tunable lens for dioptric power measurement in ophthalmic lenses	**Sara Ferrer Altabás** University of Valencia
38	Validation of a Novel Computerized Contrast Sensitivity Test: Comparison with the F.A.C.T.	**Paula García Balaguer** University of Valencia
39	Macroscopic modelling of absorption in the retina and its relation to the Stiles-Crawford effects	**Amy Fitzpatrick** University College Dubliin
40	Development and evaluation of a holographic stereo-acuity test	**Jorge Lasarte Sanz** Technological University Dublin
41	Direct comparison between an LED monitor and DMD projection in creating shades of grey for visual stimuli	**Chiara Maria Mariani** University College Dublin
42	Retinal Image Quality Assessment of Myopia Control Lenses in a Synthetic Accommodative Wavefront Model	**María Mechó García** University of Minho
43	Chromatic Temporal Defocus Sensitivity	**Victor Rodriguez-Lopez** Institute of Optics (IO-CSIC)

44	Exploring the clinical potential of a manual tunable lens in amplitude of accommodation assessment	**Raquel Salvador Roger** Universitat de València
45	Statistical Shape Modelling of Eyes with Eigeneyes	**Estela Vadillo Polo** Instituto de Óptica (CSIC)
46	Comparative Analysis of three different implementations of SimVis Gekko in Clinical Workflow	**Alejandra Varea** 2EyesVision, SL & IO-CSIC

Analysis of the relationship between accommodation and age: structural and functional changes in the eye

María Arcas Carbonell[1,2], Elvira Orduna Hospital[1,2], Sara Oliete Lorente[1], María Mechó García[3] and Ana Sánchez Cano[1,2]

[1] Departamento de Física Aplicada, Facultad de Ciencias, Universidad de Zaragoza (Pedro Cerbuna, 12, 50009, Zaragoza, España)
[2] Instituto de Investigación Sanitaria de Aragón (IIS Aragón) (San Juan Bosco, 13, 50009, Zaragoza, España)
[3] Clinical & Experimental Optometry Research Lab, Physics Center of Minho Porto Universities (CF-UM-UP), School of Sciences, University of Minho, 4710-057, Braga, Portugal

Contact: marcas@unizar.es

Purpose: To investigate the influence of accommodative demand on ocular structures, analyzing variations in anterior chamber depth (ACD), retinal shape, and visual function across different age groups.

Methods: The study adhered to the Declaration of Helsinki and was approved by the Clinical Research Ethics Committee of Aragón (CEICA) (approval number 23/479). Ninety-six right eyes from healthy individuals aged 18 to 66 years were assessed to encompass a range of accommodative capacities, from normal levels in younger individuals to reduced capacities in older adults with presbyopia. Preliminary measurements were taken to assess accommodative amplitude and monocular accommodative facility, among other parameters, categorized by study age groups (Table 1). Accommodation was measured using an IRX3 Shack-Hartmann aberrometer (Imagine Eyes, Orsay, France) under demands of up to 5D. Anterior segment and retinal images were captured with the Galilei G2 Dual Scheimpflug Analyzer (Ziemer Ophthalmic Systems AG, Port, Switzerland) and the 3D OCT-1000 (Topcon Corporation, Tokyo, Japan) respectively. They were taken under three accommodation demands (0D, 1D, 3D and 5D) and analyzed with custom software ImgOCT 1.12 (University of Zaragoza, Zaragoza, Spain) that fitted surfaces to conic curves to quantify changes in retinal shape and ACD.

Results: The mean age of participants was 35.42 ± 13.55 years. While accommodation adequately responded to low demands (up to 1D), under-accommodation was observed at higher demands (Figure 1A). Related-relative values of retinal curvature exhibited significant flattening with increased accommodative demand (Figure 1B), and age-group analysis revealed statistically significant differences among groups G1, G2, and G3, also indicating progressive retinal flattening. ACD significantly decreased with accommodation due to forward lens displacement, with a more pronounced reduction in older age groups ($p<0.001$ in all cases) (Figure 1C).

Discussion: Our results indicate that accommodation effectively meets low demands (up to 1D) but declines at higher levels, likely due to presbyopia. These findings are consistent with previous evidence indicating a reduction in accommodative response with age, associated with an increase in ocular rigidity[1]. A significant flattening of retinal curvature was observed with increasing accommodative demand, which may correlate with findings from previous research showing central retinal thinning and peripheral thickening during accommodation, highlighting the complex structural adaptations of the retina[2]. These findings highlight the influence of age-related structural modifications on accommodative function. The reduction in ACD with accommodation suggests a progressive decline in lens mobility, while retinal curvature changes may indicate a compensatory mechanism. Further research is needed to validate the observed retinal flattening trend and its

implications for accommodative performance.

	n	Age (years)	Gender (M/F)	AL (mm)	ACD (mm)	SE (D)	AA (D)	MAF (cpm)
TG	96	35.42±13.55	38/58	23.98±0.91	3.47±0.37	-2.08±1.72	5.88±5.61	6.06±6.85
G1	48	24.58±2.15	14/34	23.87±0.90	3.61±0.30	-1.96±1.40	10.39±3.27	11.71±4.61
G2	18	34.00±3.32	10/8	24.35±0.39	3.63±0.21	-3.50±1.23	9.31±5.86	7.10±7.78
G3	10	46.00±3.24	6/4	24.79±1.06	3.43±0.34	-2.80±1.89	1.63±2.59	1.56±4.22
G4	12	54.67±3.01	8/4	23.82±1.06	3.20±0.23	-1.04±2.35	0.73±0.99	0±0
G5	8	61.50±1.00	6/2	23.04±0.55	2.77±0.09	-0.31±0.38	0.47±1.00	0±0

Table 1. Sample characteristics regarding the number of subjects (n), gender distribution with the number of males and females (M/F), mean axial length (AL), anterior chamber depth (ACD), spherical equivalent (SE), accommodative amplitude (AA), and monocular accommodative facility (MAF) of the right eye, considering the total sample (TG) and age groups.

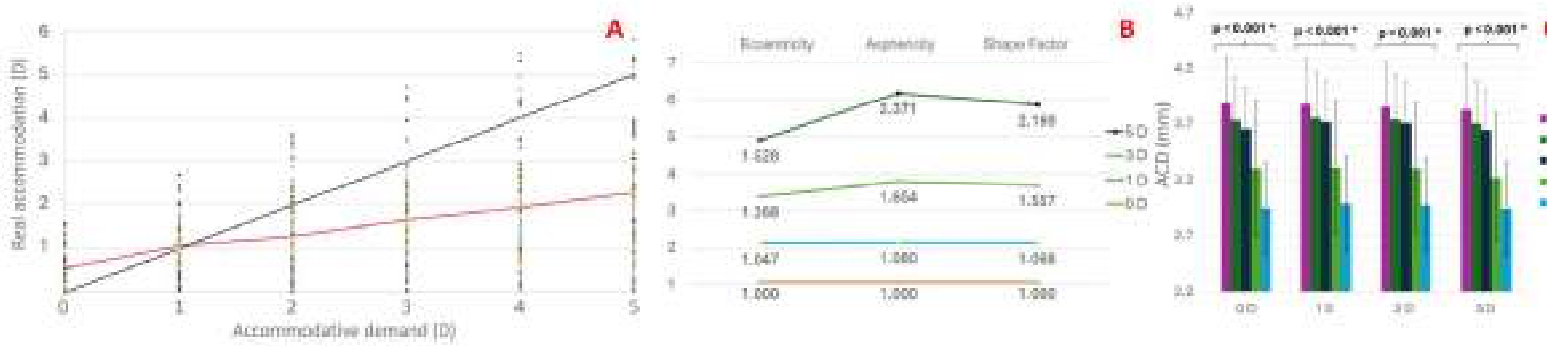

Figure 1: (A) Average results of the visual function of the study subjects, showing the actual accommodation in diopters (D) performed at the five measured accommodative demand levels in D, as obtained with the aberrometer. (B) Mean relative results of the studied parameters of the posterior pole: eccentricity, asphericity, and shape factor of the retina in the total group. Results of the baseline measurement, taken as a reference with a value of 1, are shown, along with the stimulation under three accommodation demands using -1D, -3D, and -5D lenses. (C) ACD mean results for baseline measurements and under accommodation stimulation with -1D, -3D, and -5D lenses in different age groups. Statistically significant differences ($p<0.005$), as calculated using the Friedman test with Bonferroni correction, are marked with an asterisk (*). Standard deviations are represented with error bars for each case.

---

[1] D.S. Laughton, A.L. Sheppard, E. A. H. Mallen, S. A. Read & L. N. Davies. Does transient increase in axial length during accommodation attenuate with age? Clinical and Experimental Optometry, **100(6)**, 676–682 (2017).

[2] M. Arcas-Carbonell, E. Orduna-Hospital, G. Fernández-Espinosa, M. Mechó-García, J.J. Castro-Torres & A. Sánchez-Cano. Anterior Chamber and Retinal Morphological Changes During Accommodation in Different Age Ranges. Current Eye Research, **1-11** (2008).

Analysis of Visual Performance and Pupil Dependency in Intraocular Lenses with Extended Depth of Focus Design

Inas Baoud Ould Haddi[1], Dayan Flores Cervantes[1,2], Emilio Dorronzoro Ramirez[2], Cristina Bonnin Arias[1] and Vanesa Blázquez Sánchez [1]

[1] Departament of Optometry and Vision, Faculty of Optics and Optometry, Universidad Complutense de Madrid, C. de Arcos de Jalón, 118 (28037, Madrid, Madrid).
[2] Hospital Universitario Sanitas La Moraleja, Ana de Austria, C. Arroyo de Valdebebas, 5 (28050, Madrid, Madrid).

Contact: ibaoud@ucm.es

Introduction.

Monofocal plus and extended depth of focus (EDOF) intraocular lenses (IOLs) have been developed to enhance functional vision at various distances—particularly intermediate—while minimizing the typical adverse effects associated with multifocal lenses.[1,2]

However, the visual performance of these IOLs may be influenced by physiological factors such as pupil size.[3] Despite this, their behavior in response to changes in pupil diameter remains not fully understood.

Objective.

To assess functional visual performance using defocus curves and evaluate the correlation between visual acuity (VA) and pupil diameter in three advanced IOL models: Tecnis® Eyhance™, PhysiOL® IsoPure 123™, and AcrySof® IQ Vivity™.

Material and method.

This study was conducted at Sanitas La Moraleja University Hospital (Madrid, Spain), in accordance with the Declaration of Helsinki. All surgeries were performed by the same experienced surgeon (E.D.R.). A total of 61 patients with bilateral cataracts were enrolled. Inclusion criteria required absence of ocular pathology, prior ocular surgery, and uncontrolled systemic disease. Exclusion criteria included astigmatism >0.75 D, need for toric IOLs, and the presence of AMD, glaucoma, uveitis, or other visual impairments. All patients provided written informed consent.

Each subject underwent bilateral IOL implantation, but for monocular measurements, the right eye (OD) was selected and used for analysis. Participants were randomly assigned to one of three groups: Tecnis® Eyhance™ (n = 20), PhysiOL® IsoPure 123™ (n = 20), or AcrySof® IQ Vivity™ (n = 21). Postoperative assessments were conducted one month after surgery. Pupil diameter was measured with the Power Refractor II (Plusoptix, Germany). Defocus curves were obtained under photopic conditions by placing trial lenses ranging from −3.00 D to +1.00 D in 0.50 D increments over the final subjective refraction. Monocular VA (OD) was measured in LogMAR. Spearman's correlation coefficients (r_s) were calculated between pupil diameter and VA at distance (0.00 D), intermediate (−1.50 D), and near (−2.50 D). Defocus curves were compared using repeated-measures ANOVA and post hoc analysis.

Results.

The mean pupil diameter was 3.87 ± 0.89 mm for the Tecnis® Eyhance™ group, 3.92 ± 1.28 mm for the PhysiOL® IsoPure 123™ group, and 3.96 ± 0.52 mm for the AcrySof® IQ Vivity™ group, with no statistically significant differences between them (p = 0.750).

PhysiOL® IsoPure 123™ showed a very weak correlation between pupil size and VA at all distances: distance (r_s = 0.15), intermediate (r_s = 0.08), and near (r_s = 0.10). Tecnis® Eyhance™ demonstrated

a moderate correlation at distance vision (r_s = 0.30) and weak correlations at intermediate (r_s = 0.12) and near vision (r_s = 0.18). AcrySof® IQ Vivity™ showed a moderate correlation at intermediate vision (rs = 0.28), and weaker correlations at distance (r_s = 0.20) and near vision (r_s = 0.12).
All IOLs achieved VA values close to 0.00 LogMAR at the emmetropic focus (0.00 D). At intermediate vision (−1.50 D), AcrySof® IQ Vivity™ provided significantly better VA (0.10 ± 0.06 LogMAR) compared to Tecnis® Eyhance™ (0.22 ± 0.09 LogMAR) and PhysiOL® IsoPure 123™ (0.24 ± 0.08 LogMAR) ($p < 0.0001$ for both comparisons). At near vision (−2.50 D), AcrySof® IQ Vivity™ also showed significantly superior performance (0.25 ± 0.11 LogMAR) versus Tecnis® Eyhance™ (0.36 ± 0.12 LogMAR) and PhysiOL® IsoPure 123™ (0.38 ± 0.13 LogMAR) ($p < 0.0001$).
Under positive defocus conditions, at +0.50 D, the AcrySof® IQ Vivity™ lens achieved significantly better VA (0.14 ± 0.08 LogMAR) compared to Tecnis® Eyhance™ (0.22 ± 0.07 LogMAR) and PhysiOL® IsoPure 123™ (0.24 ± 0.09 LogMAR) ($p = 0.026$). Similarly, at +1.00 D, AcrySof® IQ Vivity™ showed significantly better results (0.18 ± 0.10 LogMAR) than Tecnis® Eyhance™ (0.28 ± 0.09 LogMAR) and PhysiOL® IsoPure 123™ (0.30 ± 0.11 LogMAR) ($p = 0.021$).

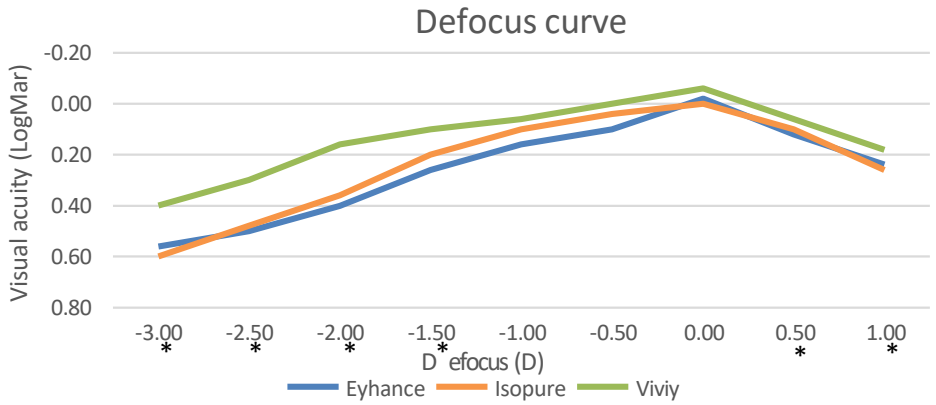

Figure 1: Monocular defocus curve one month after cataract surgery.

Conclusions.
Pupil diameter has a limited impact on VA one month after cataract surgery with the evaluated IOLs. AcrySof® IQ Vivity™, despite exhibiting slight pupil dependency at intermediate distances, offers a broader functional range and better tolerance to defocus, making it a strong candidate for patients with high visual demands. Tecnis® Eyhance™ and PhysiOL® IsoPure 123™ displayed stable, low pupil dependency, representing predictable choices for patients with more standard visual needs. These results highlight the importance of accounting for both IOL optical design and individual pupil characteristics when selecting the most appropriate lens for each patient.

---

[1]D.R.H. Breyer and H. Kaymak et al.; Asia Pac J Ophthalmol (Phila), 6, 339 (2017).
[2]J.H. Lee and S.Y. Moon; J Cataract Refract Surg, 48, 61 (2022).
[3]I.D. Baur, W. Yan, and G.U. Auffarth; J Refract Surg, 39, 668 (2023).

Next-Generation Ophthalmic Glasses for Circumventing Presbyopia

Sunil Kumar Chaubey and Brian Vohnsen

Optics Group, School of Physics, University College Dublin, Ireland

Contact: sunil.chaubey@ucd.ie

As humans age, eyes undergo natural changes, leading to a gradual decline in near and intermediate vision. This progressive worsening results in squinting at intermediate and close-up objects[1] and marks the onset of presbyopia - a natural middle-age milestone. Presbyopia is characterized by a reduction in ocular accommodation, causing blurriness in near vision and significantly impacting the quality of life[2]. In 2015, an estimated 1.8 billion people worldwide were affected by presbyopia, a number projected to rise to 2.1 billion by 2030[3].

Several well-established solutions exist to address presbyopia, including ophthalmic lenses, contact lenses, refractive surgeries, prescription eye drops, intraocular lens implants, and corneal inlays. Among these, ophthalmic lenses remain the most widely used, accounting for approximately 63% in Guangzhou[4], 39% in Los Angeles, and 82% in Saudi Arabia[5].

In our pursuit towards next-generation presbyopia corrective glasses an innovative application with advanced optical technology for passive vision correction was explored. Field tracing using finite difference time domain (FDTD) analysis and physical optics propagation of the wavefront within a modified Gullstrand eye model using optical design software. Through this simulation, key visual performance metrics were evaluated, including modulation transfer function (Figure 1), point spread function, light efficiency, and visual acuity (Figure 2) for the object located at near (0.5 meter), mid (1 meter), and far (6 meter) distances. This initial proof of concept highlights a promising alternative to bifocal and multifocal progressive glasses, offering advantages in cost, visual outcomes, appearance, and comfort.

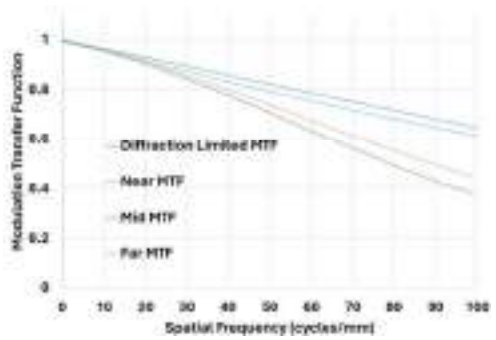

Figure 1: Modulation Transfer Function (MTF)

Figure 2: Visual Acuity (VA)

DISCLOSURE:
The intellectual property (IP) filing for this research is currently in progress. As a result, the details of the technology cannot be disclosed at this moment. A comprehensive disclosure will be provided during the conference.

ACKNOWLEDGEMENTS:
The authors would like to express their gratitude to European Union Horizon MSCA 2022; ACTIVA; for financial support under Grant No. 101119695.

---

[1]**T**.**R**. Fricke, **N**. Tahhan, **S**. Resnikoff, **E**. Papas, **A**. Burnett, **S**.**M**. Ho, **T**. Naduvilath, and **K**.**S**. Naidoo; *Ophthalmology*, no. 10 **125**, 1492-1499 (2018).
[2]**A**. Sivardeen, **C**. McAlinden, and **J**.**S**. Wolffsohn; *Ophthalmology*, no. 1 **13**, 29-34 (2020).
[3]**M**. Markoulli, **T**.**R**. Fricke, **A**. Arvind, **K**.**D**. Frick, **K**.**M**. Hart, **M**.**R**. Joshi, **H**. Kandel, **A**. Filipe Macedo, **D**. Makrynioti, **N**. Retallic, **N**. Garcia-Porta, **G**. Shrestha, and J.S. Wolffsohn; *British Contact Lens Association*, no. 4 **47**, 102157 (2024).
[4]**J**.**S**. Wolffsohn, **L**.**N**. Davies, and **A**.**L**. Sheppard; *BMJ Open Ophthalmology*, 8, e001122 (2023).
[5]**A**.**M**. Alsaqr, **A**.**M**. Alasmi, **R**. Fagehi and **A**. Ali; *BMC Public Health* 24, 1950 (2024).

Measurement of detection intensity thresholds of stimuli presented behind the halos produced by multifocal corrections

Chorrero, Diego[1]; Casilla, María Ángela[1,2]; Rodríguez-López, Víctor[1]; de Castro, Alberto[1]

[1] Visual Optics and Biophotonics Lab. Instituto de Óptica, IO-CSIC, Madrid, Spain.
[2] Facultad de Óptica y Optometría, Universidad Complutense de Madrid, Madrid, Spain

Contact: diego.chorrero@io.cfmac.csic.es

Aim: Presbyopia is the age-related loss of accommodation that is typically corrected with multifocal corrections. These corrections combine different optical powers within the same optical region and are a known source of halos around bright light sources, in some cases affecting night vision[1]. This is partly due to the overlapping of focused and defocused images on the retina. In this study, psychophysical methods were used to characterize both the size of the halo and the minimum intensity required to detect objects behind the halo in order to objectively evaluate the visual performance with different multifocal intra-ocular lenses (MIOLs).

Methods: Four young subjects (aged 23–28 years) participated in experiments in which the halo was produced by a circular light source (196.45 cd/m²) with radius 6, 15 and 30 arcmin (') generated with a 43 inches monitor (LG, 43UR78006LK UHD 4K, Seoul, South Korea) in a room with dim illumination (225 lux). The size of the halo was subjectively determined by adjusting the radial position of four peripheral stimuli. The just noticeable intensity within the halo was assessed by gradually increasing the luminance of a 6 arcmin radius stimulus positioned tangent to the light source until it became visible. The stimulus was randomly presented in four different positions and the experiments repeated three times. The value obtained was used as a measurement of the minimum intensity needed to detect objects of that size behind the halo. A commercial visual simulator (SimVis Gekko, 2EyesVision, Madrid, Spain)[2] was used to assess halo perception with six simulated optical corrections: three bifocal designs with +1.5 D, +3.0 D, +4.5 D addition power and three trifocal lenses (FineVision, PanOptix, and Synergy). The total duration of the experiment was approximately 30 minutes. The retinal image of the light source with each correction was simulated using standard Fourier optics to determine the relative intensity of light at the position of the stimulus.

Results: For bifocal lenses, the subjective size of the halo increased with the addition and the light source size. As the circular light source radius increased from 3 to 15', a progressive increase in the size of the halo was observed for all corrections. For the bifocal corrections, the size of the halo increased from 10.1±0.5 to 16.14±1.08', 16.6±1.20 to 20.1±0.8', and 21.8±0.8 to 26.3±0.7', for 1.5, 3.0, and 4.5 D addition respectively. Bifocal corrections with 4.5 D addition showed always the largest halo radius in all conditions tested. Trifocal lenses also showed an increase in the size of the perceived halo that ranged from 14.1±1.2 to 18.3±0.8' for FineVision, 13.1±0.8 to 18.5±0.6' for Panoptix, and 13.2 ± 1.0 to 18.6 ± 0.8' for Synergy, when the light source radii increased from 3 to 15', respectively. The halo size produced was similar across the three trifocal designs, with no significant differences between the studied designs.

The minimum intensity needed to detect objects behind the halo decreased in bifocal lenses when the addition of the correction increased and increased with the size of the light source for all corrections. For the 3 arcmin light source, the mean threshold intensity for the bifocals with 1.5, 3.0 and 4.5 D addition was 97 ± 17, 94 ± 36, and 84 ± 21 cd/m^2, respectively. This threshold intensity value increased when the light source size increased for all bifocals. For the three trifocals studied (FineVision, Panoptix and Synergy), the just noticeable intensity increased on average from 85±17

to 116 ± 18, 77 ± 21 to 114 ± 20 and 80 ± 16 to 122 ± 17 cd/m2, respectively when the light source size increased from 3 to 15'. Overall, the trifocal lenses showed a more homogeneous increase in threshold intensity with light source size. Figure 1 shows the relationship between the size of the halo and the just noticeable intensity with the correction for all light source sizes.

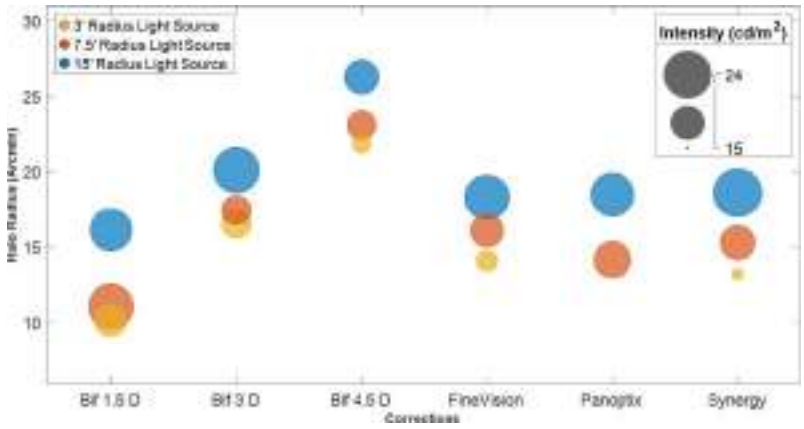

Figure 1: Halo size and detection threshold intensity for the optical corrections and light source sizes studied.

Computational simulations of the retinal image produced with each light source and correction are shown in Figure 2. The relative intensity of light at the location where the stimulus was presented experimentally to calculate the just noticeable intensity was calculated and compared with the subjective value obtained. The comparison between simulated local intensity and threshold detection intensity values experimentally showed a positive correlation, r^2= 0.73.

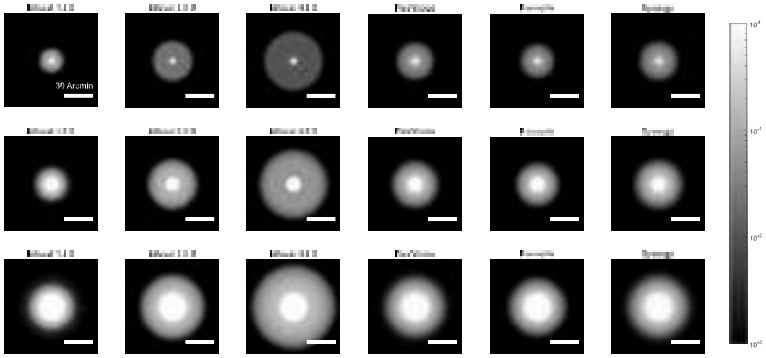

Figure 2: Computational simulations representing the halo as a function of different optical corrections and varying central stimulus sizes: 3, 7.5, and 15 arcmin radii.

Conclusion: Halo size increases with both addition power and light source size. Just noticeable intensity thresholds decrease with increasing addition and increase with halo source size for all corrections. A correlation was found between the subjective just noticeable intensity and the relative local intensity calculated by simulating the projected image, implying that as the halo intensity increases, the intensity of objects presented adjacent the halo source must increase to be detected. This result has interesting clinical implications for subjects with multifocal corrections.

ACKNOWLEDGEMENTS: PID2023-152641OA-I00, CPP2021-008388, LCF/TR/CI24/56010018

References:

[1]S. Pieh and B. Lackner; *Br J Ophthalmol*, **85**, 816 (2001).
[2]Vinas, Benedí-García, Aissati, Pascual, Akondi, Dorronsoro, Marcos; *Sci Rep*, **9**, 1539 (2019).

Do diffractive intraocular lenses break the beneficial interaction between chromatic and monochromatic aberrations in the eye?

Laura Clavé[1], Maria S. Millan[1]

1 Departament d'Òptica i Optometria, Universitat Politècnica de Catalunya – BarcelonaTech, Violinista Vellsolà 37, 08222 Terrassa, Spain

Contact: Laura.clave@upc.edu

Human vision operates in white light. Although optical aberrations typically degrade the retinal image quality, the existence of positive interactions between chromatic and monochromatic aberrations have proved to benefit visual acuity (VA)[1–3]. This study investigates whether diffractive presbyopia-correcting multifocal intraocular lenses (IOLs) disrupt the beneficial interaction between chromatic and monochromatic aberrations in the eye. It evaluates the performance of these lenses for both far and near vision, where the lens utilizes different diffraction orders depending on its design, and examines their effect under different light conditions. To achieve this, monocular VA of pseudophakic subjects will be assessed under white and green light conditions using standard methods, procedures, and materials employed in routine clinical examinations.

Method

Monocular visual acuity (VA) was assessed in pseudophakic subjects implanted with diffractive trifocal IOLs (Finevision Micro F12, PhysIOL, n= 20; AT LISA tri 839MP, Zeiss, n= 20) and compared to those with monofocal IOLs (Y601075, AJL Ophthalmic, n=30). The study also included presbyopic phakic subjects wearing a diffractive bifocal contact lens (CL) (Pilkington Diffrax, n=9). We consider diffractive designs based on the zero-diffraction order for far vision and the first diffraction order for near vision (i.e., 0F/+1N design). VA was measured under broadband white light (W) (White LED, CCT=6500K) and narrow-band green light (G) (Green LED, nominal wavelength of 530 nm with a full width at half maximum of 33 nm) conditions. The intensities of both light sources were adjusted to maintain a constant luminance of 25.3 ± 0.10 cd/m² for all charts throughout the evaluation.

Results

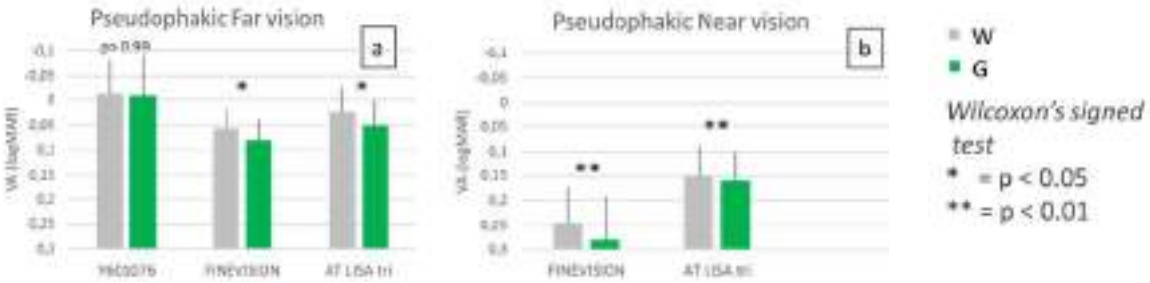

Figure 1. VA W and G light:(a) Pseudophakic patients at far distance (mean ± sd). (b) Pseudophakic patients at near distance (mean ± sd) with the diffractive trifocal IOLs. p values under 0.05 show statistical difference between G and W VA values. (Wilcoxon test).

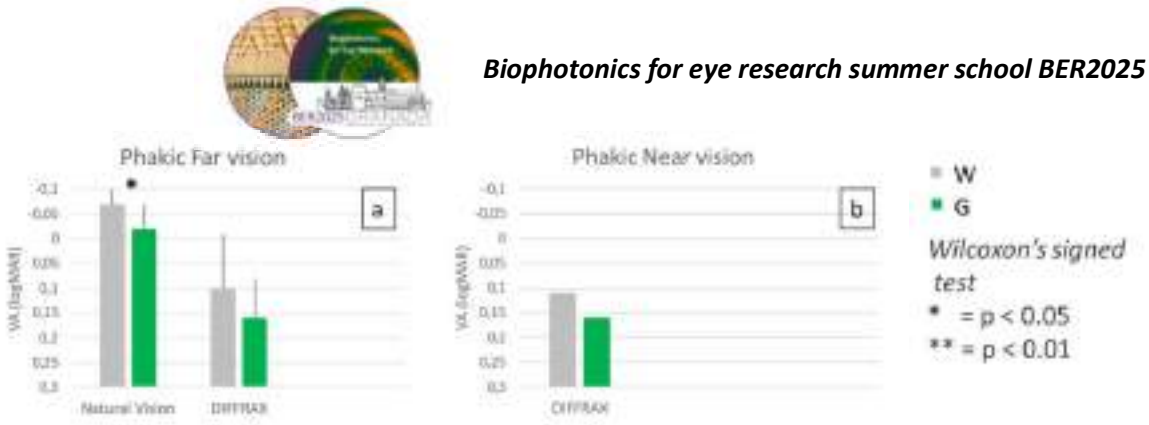

Figure 2 a) Phakic observers at far distance (mean ± sd) with natural vision (spectacle lens if needed) and wearing the Diffrax CL. (b) Phakic observers at near distance (mean ± sd) with the Diffrax CL. p values under 0.05 show statistical difference between G and W VA values. (Wilcoxon test).

Discussion

These results indicate that diffractive IOLs with a 0F/+1N design maintain the beneficial interaction between chromatic and monochromatic aberrations[4]. VA was consistently slightly higher under white light compared to green light, likely due to defocus effects arising from residual refractive errors.

For trifocal IOLs, VA differences between far and near vision were more pronounced due to energy efficiency distribution favouring far vision[5]. Conversely, bifocal CLs maintained a more balanced VA at both distances[6]. The study suggests that diffractive presbyopia-correcting lenses do not disrupt the beneficial interaction between chromatic and monochromatic aberrations but emphasizes that findings are specific to the 0F/+1N design.

ACKNOWLEDGEMENTS:

Agencia Estatal de Investigación (PID2020-114582RB00-I00/AEI/10.13039/501100011033). The authors thank Prof. Norberto López Gil (Universidad de Murcia) for providing the Diffrax lenses.

References

1. J. S. McLellan, S. Marcos, P. M. Prieto, *et al.*, "Imperfect optics may be the eye's defence against chromatic blur," Nature 417(6885), 174–176 (2002).
2. S. Aissati, C. Benedi-Garcia, M. Vinas, *et al.*, "Matching convolved images to optically blurred images on the retina," J. Vis. 22(2), 12 (2022).
3. C. Benedi-Garcia, M. Vinas, C. Dorronsoro, *et al.*, "Vision is protected against blue defocus," Sci. Rep. 11(1), 352 (2021).
4. L. Clavé, MS. Millán. "Do diffractive intraocular lenses break the beneficial interaction between chromatic and monochromatic aberrations in the eye?," *Biomed Opt Express*. 15(12):6977(2024).
5. MS. Millán, L. Clavé, A. Torrents, *et al., "*Spatio-chromatic vision with multifocal diffractive intraocular lens," *Eye and Vision*. 10(1):32(2023).
6. L. Clavé, M. Faria-Ribeiro, MS. Millán. "Chromatic changes in vision with diffractive ophthalmic optics," *Opt Express*. 32(6):10348 (2024).

Optical performance and predicted visual resolution of two presbyopia-correcting intraocular lens designs

F. Cuéllar[1]*, F. Vega[1], D. Madrid-Costa[2] and M. S. Millán[1]

[1] Applied Optics and Image Processing Research Group (GOAPI), Department of Optics and Optometry, Universitat Politècnica de Catalunya BarcelonaTech, Terrassa, Spain.
[2]Clinical and Experimental Eye Research (CEER). Optometry and Vision Department, Faculty of Optics and Optometry, Universidad Complutense de Madrid, Spain.
Contact: fatima.cuellar@upc.edu

This study compared the in vitro optical performance of two intraocular lenses (IOLs): a trifocal (Optiflex Trio 22.0 D) and an extended depth of focus (EDOF) lens (Asqelio 19.0 D). For this purpose, through-focus modulation transfer function (TF-MTF) was measured in a model eye with pupil diameters of 3.0 and 4.5 mm in the IOL plane and the visual acuity (VA) was estimated from the area under the TF-MTF curve. Unwanted photopic effects, such as halos, were also evaluated.

The optical image quality of the IOLs was measured in vitro using an optical bench according to ISO 11979-2:2024 and ANSI Z80.35 2018 standards[1,2]. The setup (Figure 1) is formed by an illumination system (550nm), a model eye and an image acquisition system. The model eye complies ANSI type 2 specification (i.e., artificial cornea with spherical aberration SA= +0.27 µm for 5.15 mm aperture at the IOL plane). A four-slit test was used to measure MTF. For halo measurement, we used a 200 µm pinhole, equivalent to a visual angle of 3.44 arc minute in diameter. A translation holder allowed the camera to scan in the image space.

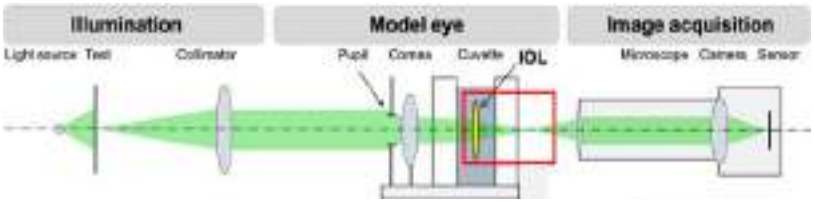

Figure 1: Scheme of the optical setup.

The area under the MTF (MTFa) was calculated through integration from 0 to 50 cyc/mm (15 cyc/deg in the model eye). We calculated the expected VA (logMAR) from the TF-MTFa values for both IOLs using the equation recommended by ANSI ($VA = 0.085\ (MTFa)^{-1} - 0.21$).[3] Figure 2 shows the results, expected VA versus defocus (spectacle plane), obtained for 3.0 mm pupil.

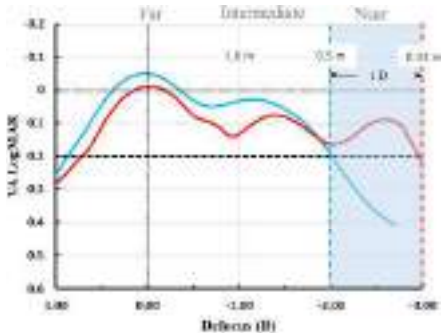

Figure 2: Expected VA (LogMAR) defocus curves for Asquelio (blue) and Optiflex Trio (red) IOLs.

Figure 3 shows the intensity distribution of the pinhole image in the far, intermediate and near focus planes with 4.5 mm pupil. They are displayed on logarithmic scale for better visualization. Below each pinhole image, the intensity is plotted versus the visual angle in minutes of arc. The graphics include a central part with the highest energy (core) corresponding to the focused pinhole image. Around the core, all graphs show a lower energy pedestal corresponding to the surrounding halo.

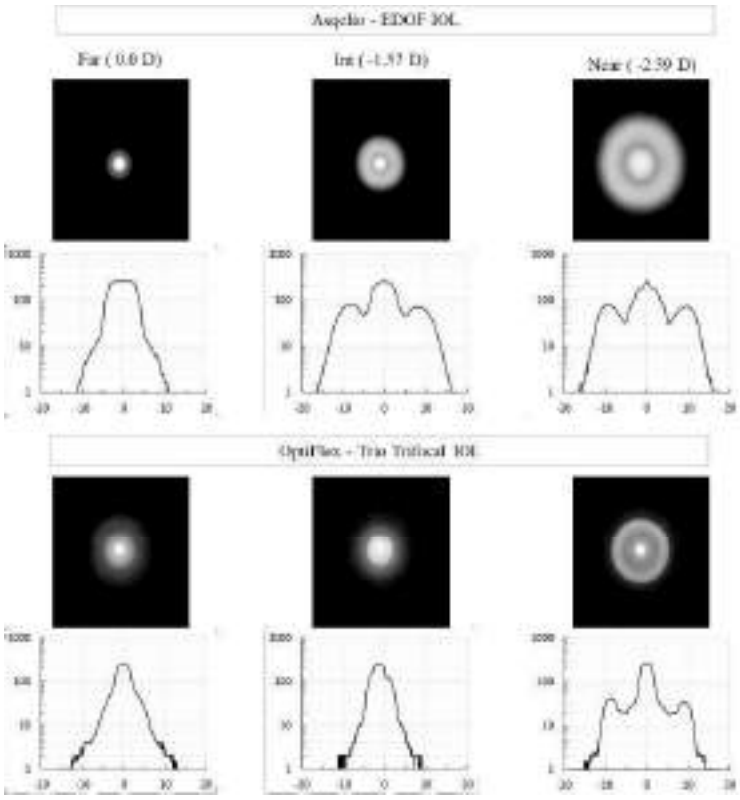

Figure 3: Halo. Each pair represents the image of a pinhole (top) and its intensity profile (bottom).

In conclusion, with a 3.0 mm pupil, the EDOF IOL provides better expectation for far and intermediate vision quality. The trifocal lens offers a 1 D (negative) extended range of vision compared to the EDOF IOL, providing superior near-distance vision. The intensity of halos is significantly influenced by the lens design. For distance vision with a relatively large pupil (4.5 mm), the EDOF lens produces smaller halos than the trifocal lens. However, at intermediate and near distances, the trifocal lens generates smaller halos than the EDOF lens, with the halo intensity being further impacted by defocus.

ACKNOWLEDGEMENTS:
Ministerio de Ciencia e Innovación, Agencia Estatal de Investigación (PID2020-114582RB-I00/AEI/ 10.13039/501100011033). Fátima Cuéllar acknowledges a pre-doctoral contract (PRE2021-100674).

[1] Ophthalmic implants. Intraocular lenses. Part 2: Optical properties and test methods. ISO 11979-2:2024.
[2] American National Standards Institute, ANSI Z80.35-2018. (2019). Extended depth of focus intraocular lenses. Alexandria, VA U.S.A.: The Vision Council.
[3] Alarcon, A., Canovas, C., Rosen, R., Weeber, H., Tsai, L., Hileman, K., Piers, P. (2016). Preclinical metrics to predict through-focus visual acuity for pseudophakic patients. Biomedical Optics Express, 7(5), 1877.

Analysis of optical properties and halo effects in five intraocular lens designs

Paulina Dotor-Goytia[1], Alejandra Varea[1,2], Alvaro de la Peña[1], Alberto de Castro[1], Lucie Sawides[1]

[1] Visual Optics and Biophotonics Lab. Instituto de Óptica, Consejo Superior de Investigaciones Científicas (Serrano, 121, 28006, Madrid, Spain)

[2] 2EyesVision (Pl. del a Encina, 10, 28760, Tres Cantos, Madrid, Spain)

paulina.dotor@csic.es

Background and purpose: Presbyopia-correcting intraocular lenses (IOLs) were developed to meet the growing demand for restored vision at all distances after cataract surgery without the need for additional corrective lenses. Early multifocal IOLs (MIOLs) were bifocal, improving distance and near vision but offering limited intermediate vision. Newer designs include trifocal and extended depth of focus (EDOF) IOLs. Trifocal IOLs add a third focal point to enhance intermediate vision, but the simultaneous projection of multiple focal points can reduce contrast and induce visual disturbances such as halos and glare. EDOF IOLs extend the range of focus to improve intermediate vision, although they may not provide the same level of near vision as trifocal IOLs and might not significantly reduce dysphotopsia. The purpose of this study is to evaluate the through-focus optical quality of five IOLs at 3- and 4.5-mm pupil diameters for three different wavelengths and to assess the IOL-induced halos under these experimental conditions.

Methods: A new optical test bench for IOL characterization was developed to evaluate the optical and retinal image quality of IOLs. The system includes an aberration-free corneal model and a slide mechanism for immersing an IOL in distilled water within a polished quartz cuvette mounted on a 3D translational stage. Illumination was provided by a white LED projecting a USAF test image, a pinhole (20, 50, 100, and 200 µm diameter), or a crosshair target (10 µm). A bandpass filter allowed measurements at 490 nm (blue), 550 nm (green) and 650 nm (red). A variable aperture controlled the optical diameter at the IOL plane (3 and 4.5 mm). A Mitutoyo 10X microscope objective and an x1 tube lens were used to magnify the image and transfer it to a 5MP 12-bit CMOS camera. These three elements were mounted in a 3D translational stage motorized along the optical axis for automated through-focus measurements. Experimental calibration of the motorized camera was performed using seven monofocal intraocular lenses with different base powers ranging from 16D to 26D. Linear regression analysis was applied to the measurements to obtain the mm/diopters ratio, and the resulting calibration was compared to theoretical predictions obtained from a Zemax optical design model where the monofocal IOL surface shapes were extracted from OCT images. The optical and retinal image quality of the five IOLs were evaluated: a monofocal IOL (24D base power), two EDOF IOLs (Vivity, Alcon base power 22D and Symfony, J&J base power 20D), one diffractive trifocal IOL (FineVision BVI, base power 19D) and a refractive trifocal IOL (PanOptix, Alcon, base power 20D). The TF optical quality of the USAF images and the retinal image quality for different pinhole sizes were evaluated across the three wavelengths and both pupil diameters. Halo intensity was quantified using custom software to calculate the through focus energy efficiency[1] from the amount of light inside and outside the pinhole image considering the magnification of the system.

Results: Experimental calibration provided a slope of 0.27 mm/diopter for the camera displacement. Through focus RGB images at far distances showed the green (G) focus located

between the red (R) and blue (B) foci, with B shifted 0.4 D toward higher power and R shifted 0.4 D toward lower power (Monofocal and EDOF Vivity). A similar trend was observed for the trifocal FineVision IOL at far, although the shift reversed at near distances for R-focus. In comparison, the trifocal PanOptix IOL showed G-focused images consistently centered between R and B at all distances (although the separation decreased with proximity with 0.55D (far), 0.4D (intermediate) and 0.2D (near). For the EDOF Symfony, R was focused slightly before G at far (0.2D), and the B focus was not clearly defined whereas at intermediate distances, B and G foci were nearly coincident. At far, the Energy Efficiency (EE) increased with decreasing pupil and with increasing pinhole sizes, with the G-EE consistently between the R-EE and B-EE. At 3-mm pupil diameter, EE was 42% lower for the trifocal and 24% lower for the EDOF IOLs compared to the Monofocal.

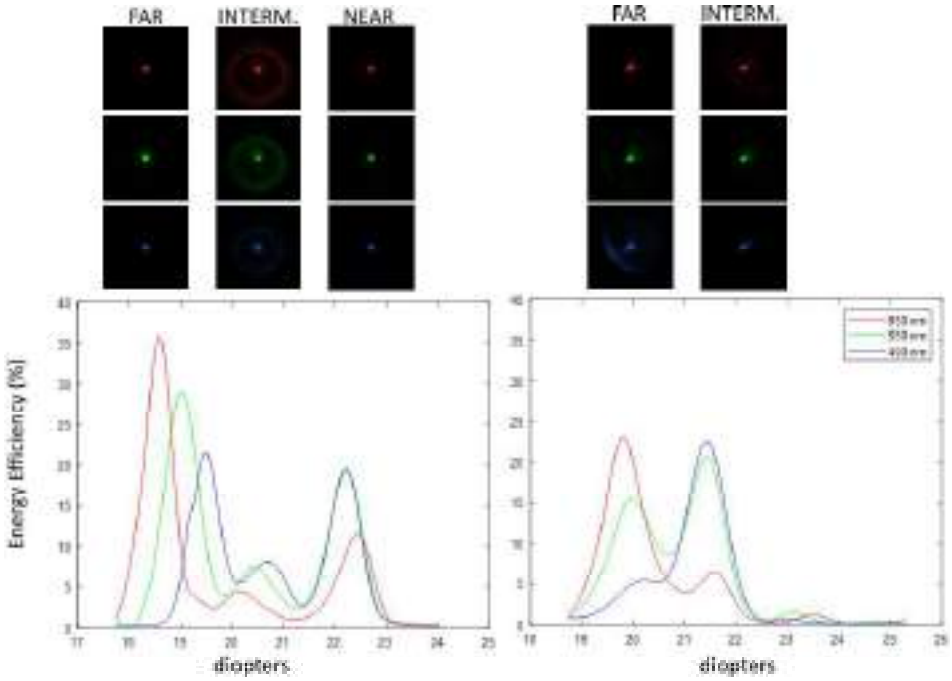

Figure1. Through Focus Energy Efficiency (TF-EE) calculated for the 20-micron pinhole and 3 mm pupil diameter for the FineVision (left) and Symfony (right) IOLs for the RGB wavelengths. Images at the peaks of the TF-EE (far, intermediate and near distance) are displayed above the plots. Red, green and blue color maps were used for illustration purposes.

Conclusions: The newly developed experimental system effectively characterized TF optical and retinal image properties of different IOL designs. Pinhole imaging provided valuable insights into halo size and intensity across a wide range of conditions, revealing significant differences among the tested IOLs.

ACKNOWLEDGEMENTS: PID2023-152641OA-I00 (LS), IND2023/BMD-27723 (PD, AV), CPP2021-008388 (AdC)

[1]M.S. Millán, F. Vega. Trans Vis Sci Technol. 9;9(12):13 (2020).

Optical imaging performance of an extended depth of focus intraocular lenses compared to its monofocal platform

J. Hernàndez-Ris[1], F. Cuéllar[1], D. Madrid-Costa[2], F. Vega[1] and M. S. Millán[1]

[1] Applied Optics and Image Processing Research Group (GOAPI), Department of Optics and Optometry, Universitat Politècnica de Catalunya BarcelonaTech, Terrassa, Spain.
[2] Clinical and Experimental Eye Research (CEER). Optometry and Vision Department, Faculty of Optics and Optometry, Universidad Complutense de Madrid, Spain.

Contact: julia.hernandez@estudiantat.upc.edu

The objective of this study is to compare in vitro the optical imaging quality and halo formation of the Extended Depth of Focus (EDOF) TECNIS™ PureSee™ (model DEN00V) intraocular lens (IOL) to the standard monofocal TECNIS™ one-piece (model ZCB00). Both IOLs are produced by the same manufacturer (Johnson & Johnson Vision, Inc) and share the same platform.

The optical performance of both IOLs was evaluated using a 550 nm light source and an ANSI Z80.35-2018 compliant model eye 2 on optical bench[1,2] The artificial cornea had spherical aberration SA= +0.27 µm for 5.15 mm aperture at the IOL plane. A four-slit test was used to measure imaging quality through the Modulation Transfer Function (MTF at 50 cycles/mm) and the Area under the MTF (MTFa, calculated through MTF integration from 0 to 50 cyc/mm -15 cyc/deg in the model eye-). A 200 µm pinhole, which simulated an object of small visual angular dimension, was used to assess halos. For through-focus (TF) analysis, the camera captured images along the optical axis in the image space.

Measurements determine the IOL's ability to maintain image quality across different image vergences and thus, allowing the estimation of the focus extension. The best focus for distance vision was identified based on the highest MTF value at 50 cycles/mm with a 3-mm aperture. TF-MTF and MTFa analysis was carried out across a defocus range from +2.50 to -5.00 D for apertures of 2-, 3-, and 4.5-mm (IOL plane) (Fig.1). Simulated visual acuity for a 3-mm pupil was calculated in the +1.00 to -3.00 D range using an ANSI Z80.35-2018 – recommended formula.

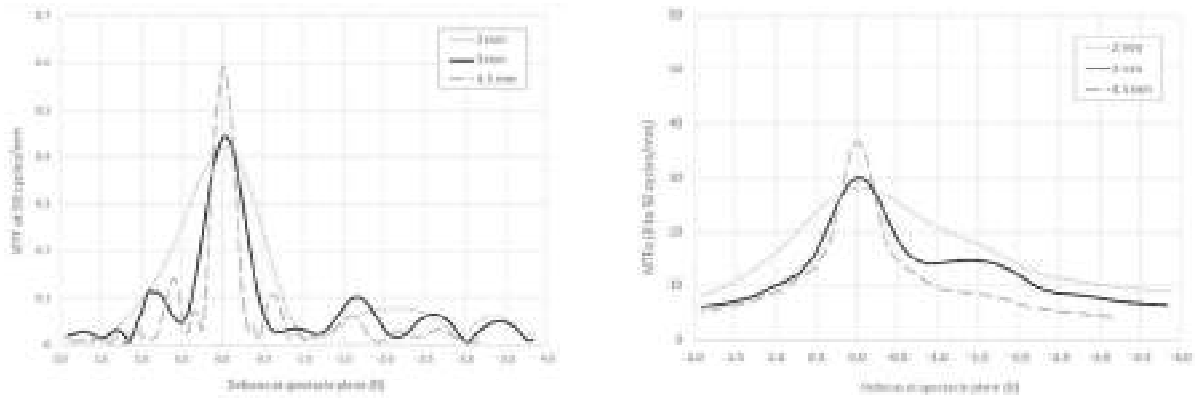

Figure 1: (A) Through-focus modulation transfer function (TF-MTF) and (B) TF-MTF area (TF-MTFa) curves obtained with the TECNIS PureSee IOL for a 2-, 3-, and 4.5-mm aperture. D = diopters

Halo measurements followed ANSI guidelines[1] They were taken in different conditions: first, at the best focus plane with varying pupil size of 2-, 3-, and 4.5-mm (Fig. 2a) and second, with 4.5 mm pupil and varying defocus (±0.50 D) (Fig. 2b) to assess the joint effect of mild refractive errors and mesopic light condition (such as driving at night).

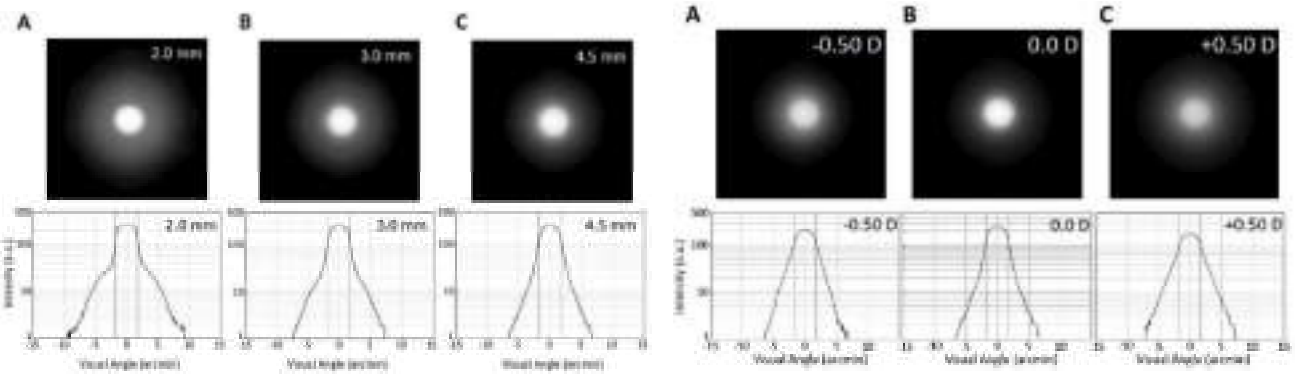

(a) (b)

Figure 2: Halo measures of TECNIS™ PureSee™ EDOF IOL. Images of the pinhole displayed with gamma correction of 0.5 (top) and their intensity profiles on logarithmic scale (bottom). (a) At the best focus plane with varying pupil size: 2-, 3-, and 4.5-mm; (b) with 4.5 mm pupil and varying defocus (±0.50 D).

The preliminary results with TECNIS™ PureSee™ [3] EDOF IOL indicated high-quality distance vision and increased depth of focus for smaller pupils. No power shifts in either the far distance (0.0 D defocus) MTF and MTFa peaks were appreciated with varying aperture. Simulated visual acuity for 3 mm pupil remained good (equal or better than 0.2 logMAR) across a broad defocus range at the spectacle plane (2 D approximately). Halos were smaller and less intense with larger pupils, and mild refractive errors had low impact.

The results with the standard monofocal TECNIS one-piece ZCB00 IOL will provide a more complete context for comparison of such reported properties of the TECNIS PureSee.

ACKNOWLEDGEMENTS:
Ministerio de Ciencia e Innovación, Agencia Estatal de Investigación (PID2020-114582RB-I00/AEI/10.13039/501100011033).

[1] American National Standards Institute. ANSI Z80.35:2018. (2019). Extended depth of focus intraocular lenses. Alexandria, VA, USA. The Vision Council.
[2] Ophthalmic implants. Intraocular lenses. Part 2: Optical properties and test methods. ISO 11979-2:2024.

Objective assessment of halos in diffractive multifocal intraocular lenses through optical simulation

Anabel Martínez-Espert[1] and Walter D. Furlan[1]

[1] Departamento de Óptica y Optometría y Ciencias de la Visión, Universitat de València, Dr. Moliner 50, 46100, Burjassot, Spain.

Contact: anabel.martinez@uv.es

Introduction: It is well known that, the images formed by multifocal intraocular lenses (MIOLs) at each focal plane are accompanied by a background or halo, which introduces blur and reduces image contrast. These halos are primarily produced by the out-of-focus image corresponding to the other foci of the lens and generally depend on the add power and on how the MIOL distributes the energy among its foci[1]. For a given pupil size, the fraction of the energy that is out of focus also depends on the residual high order aberrations, higher diffraction orders, and the light scattering produced by the diffractive steps (straylight). However, there is no consensus in the scientific literature regarding the specific influence of the diffractive profile on halo formation. The objective of this study is to clarify this issue by isolating the effect of the diffractive profile from all other factors contributing to the halo produced by MIOLs.

Methodology: A numerical method to evaluate halos using the point spread function (PSF) obtained in Zemax OpticStudio (v. 18.7, LLC, Kirkland, WA, USA) is proposed. The profiles of two well-known commercial MIOLs were analysed, each featuring a different diffractive pattern: the Acriva Trinova (VSY Biotecnology, The Netherlands), which produces an intermediate and near addition of + 1.50 D and + 3.00 D, respectively[2], and the FineVision POD F (PhysIOL, Liege, Belgium) which produces an intermediate and near addition of + 1.75 D and + 3.50 D, respectively[3].The analysis was performed on a simplified model eye in which the anterior surface of the IOL is a Grid sag surface. All other model eye parameters were kept constant across the evaluation of both profiles. The halo effect at each focus was estimated using as previously method described by Lago et al.[4], using a custom-made code written in Matlab R2018b (The MathWorks, Inc). Retinal images of a 2 arcmin pinhole stimulus were simulated taking into account the PSF of the eye, with a pupil diameter of 4.5 mm. The diameter (*d*) encircling 50% of the intensity was calculated for polychromatic light using the V(λ) function provided by Zemax software. In addition, the percentage of intensity within a 2 arcmin diameter was also calculated.

Results: The halo diameters and the percentage of intensity for each lens at the three main focal planes are shown in Figure 1. A logarithmic scale was used in this figure to enhance the differences between both MIOLs.

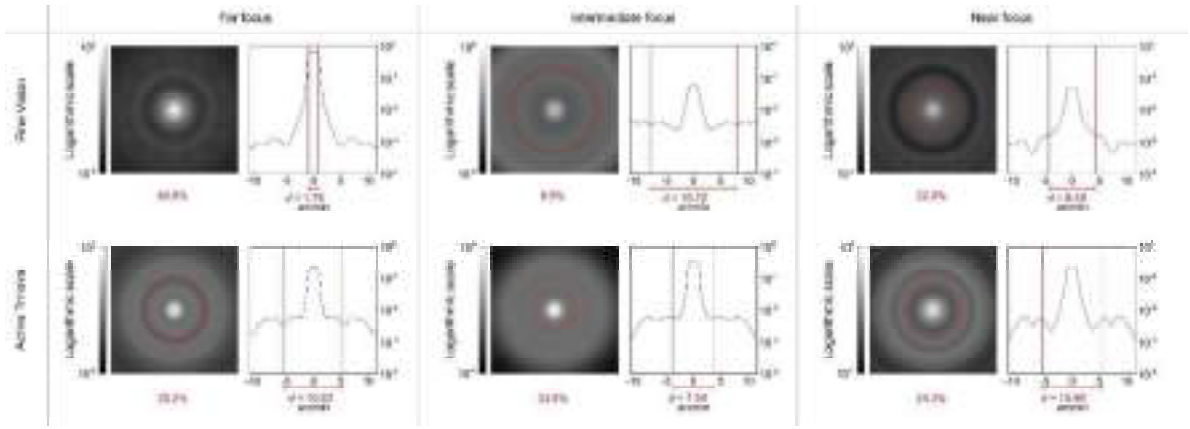

Figure 1: Simulated halos obtained with polychromatic light and a 4.5 mm pupil diameter: The images were obtained by convolving the PSF with a 2 arcmin pinhole. The numerical values correspond to the diameter that encircles 50% of the intensity at the retina (*d*) and to the percentage of intensity.

As can be seen in this figure, the FineVision lens exhibits the lowest halo effect at the far focus and the highest at the near focus. In contrast, the Acriva Trinova lens shows the lowest at the intermediate focus and the highest halo effect at the near focus. Comparatively, the FineVision lens shows a lower impact of dysphotopic phenomena than the Acriva Trinova, at the far focus, while the opposite occurs in the intermediate and near foci. In fact, in the near focus, although the calculated diameter for the FineVision is smaller, the percentage of intensity at 2 arcmin is higher for the Acriva Trinova, as shown in Figure 1.

The differences observed between the two lenses are likely due to the distribution of energy among the diffractive orders of the lenses. The FineVision lens features an apodized diffractive pattern, composed of two superimposed profiles, that produce the intermediate and near foci with the 1st diffraction order, leaving the 0th order for the far focus. In contrast, the Acriva Trinova lens has a sinusoidal diffractive profile, where the intermediate focus corresponds to the 0th diffraction order, while the far and near foci are formed by the negative and positive 1st orders, respectively.

Conclusions: We demonstrated that by isolating the effect of the diffractive profile of a MIOL**,** an objective and quantitative evaluation of the induced halos—including halo diameter, and intensity percentage—can be obtained. It was shown that the MIOL's design has a clear influence on the image at each focus.

ACKNOWLEDGEMENTS: Generalitat Valenciana (CIPROM/2022/30); Ministerio de Ciencia e Innovación (PID2022-142407NB-I00); A. M.-E. acknowledges financial support from Universitat de València (UV-INV-PREDOC21-1915492).

[1] F. Alba-Bueno, F. Vega, and M. S. Millan; *Archivos de la Sociedad Española de Oftalmología*, **89**, 397(2014).
[2] F. Vega, M. Valentino, F. Rigato, and M. S. Millán; *Biomedical Optics Express*, **12**, 3338 (2021).
[3] D. Gatinel, C. Pagnoulle, Y. Houbrechts, and L. Gobin; *Journal of Cataract & Refractive Surgery.* **37**, 2060 (2011).
[4] C. M. Lago, A. de Castro, and S. Marcos; *Journal of Cataract & Refractive Surgery,* **49**, 1153 (2023).

Halo size evaluation produced by multifocal intraocular lenses using a binocular visual simulator

Petros Papadogiannis[1], Victor Rodriguez-Lopez[2], Alejandra Varea[1,2], Diego Chorrero[2], Lucie Sawides[2], Alberto de Castro[2] and Carlos Dorronsoro[1]

[1] 2EyesVision SL, Pl. de la Encina 10, 28760, Madrid, Spain
[2] Institute of Optics, Spanish National Research Council (IO-CSIC), C. de Serrano 121, 28006, Madrid, Spain

Contact: ppadogiannis@2eyesvision.com

Purpose: The purpose of the study was to assess the halo size of multifocal Intraocular Lenses (IOLs) produced by a binocular visual simulator (SimVis Gekko, 2EyesVision). The aim was to estimate the halo size using computer simulations, to measure it using psychophysical procedures, and to evaluate the visual symptoms using a subset of the AIOLIS questionnaire.

Methods: A commercial visual simulator (SimVisGekko) was used to simulate 10 IOLs in randomized order: 3 trifocals (Synergy-Johnson & Johnson, PanOptix-Alcon, FineVision PodF-BVI), 3 Extended Depth of Focus (EDOF - Vivity-Alcon, Symfony-Johnson & Johnson, ISOPURE-BVI), 3 generic bifocals (1.5, 3.0 and 4.5 D near addition) and a monofocal. The experiment with subjects consisted of 3 phases. Phase 1: Ten subjects aged between 27-51 years old participated. A modified version of the Halo Software v1.0[1] with a central LED (instead of the original central main stimulus) was utilized to measure halo size as perceived from the subjects for each IOL. Phase 2: A custom psychophysical method (scrolling method) was developed to measure halo size, based on detecting peripheral dim stimuli around a central glare source (LED point source). Ten subjects aged between 23-41 years old indicated when the stimuli reached the perceived halo from the outside (variation 1, Out-In) or the inside (variation 2, In-Out) utilizing the scrolling wheel of a computer mouse to move the stimuli further from or closer to the LED. Phase 3: Three questions from the AIOLIS questionnaire were asked to assess the visual symptoms. Finally, computer simulations were performed convolving the Point Spread Function (PSF) of each multifocal correction with a flat aperture of 1.2 mm that acted as the LED. An energy threshold of 99% was considered to determine the halo size.

Results: Out-In and In-Out variations provided very similar results ($r=0.95$, $p<0.05$), with high repeatability (0.77 arcmin across repetitions), thus the average across both methods will be shown as results of the scrolling method. Figure 1 shows the average halo radius and the standard deviation across subjects with the Halo V1.0 software, the scrolling method and the computational estimation; no statistically significant difference between the three ($p<0.05$) was found.

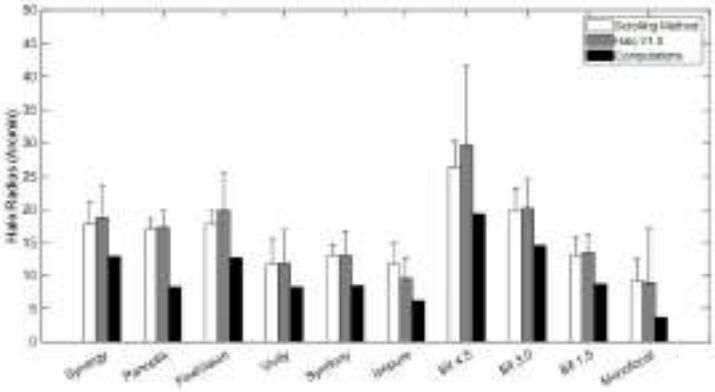

Figure 1. Average halo radius of the Halo V.1 software, the scrolling method and the computational estimation.

In terms of time per experiment, the scrolling method requires much less time than the Halo V1.0; 29.6±16.2 and 283.8±1.7 seconds, respectively. Figure 2 presents the average scores of the AIOLIS questionnaire. The bifocal IOL with 4.5 D of addition yielded the highest disturbance scores, whereas the monofocal the smallest. Results of halo size obtained with the Halo V1.0 software and the scrolling method were highly correlated (r=0.97, p<0.05) with the results of the AIOLIS questionnaire, showing that larger halos disturbed the subjects more.

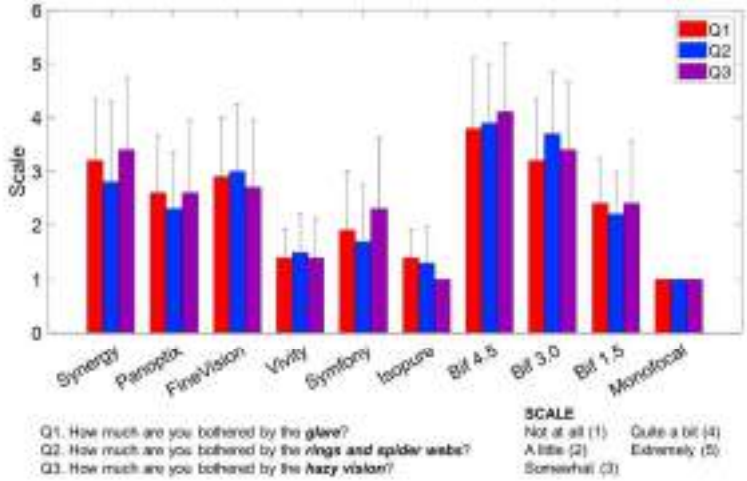

Figure 2. Average scores of the AIOLIS questionnaire.

Figure 3 shows the correlation between the addition of the simulated lenses and the halo size measured with the Halo V.1 software and the scrolling method. The correlation is very high in both cases (r=0.98, p<0.05).

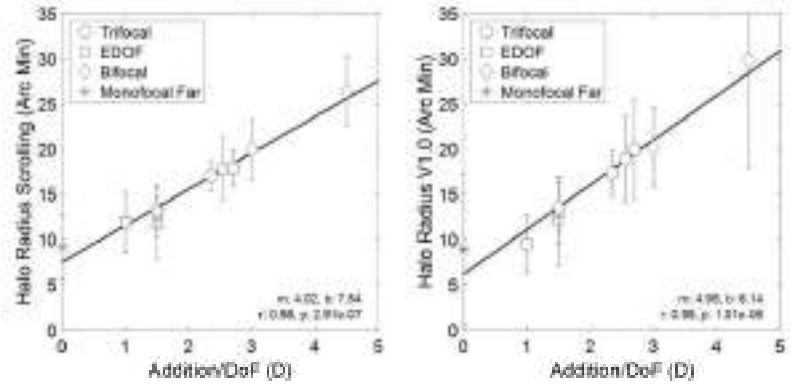

Figure 3. Correlation between the addition of the simulated lenses and the size of the halo.

Conclusion: Results from the Halo V1.0 software and the scrolling method showed that trifocals produced larger halos than EDOFs, the 4.5 D bifocal yielded the biggest halo and the monofocal the smallest. The scrolling method required much shorter time to measure halo size compared to the Halo V1.0 software. The AIOLIS questionnaire responses score aligned linearly with halo size, indicating that larger halo is associated with greater disturbance. Finally, as also predicted by computer simulations, halo strongly depends on the addition. Combining SimVis Gekko for commercial IOLs simulations, with the fast method developed to subjectively measure halo, allows to experience and to quantify halos fast and reliably prior to surgery.

[1] Jiménez Cuesta et al. 2008, Laboratory of Vision Sciences and Applications, University of Granada

Lensless holographic reconstruction of a highly diffractive profile of a multifocal intraocular lens

Rosa Vila-Andrés[1], Anabel Martínez-Espert[1], José J. Esteve-Taboada[1] and Vicente Micó[1]

[1] Department of Optics and Optometry, Faculty of Physics, Universitat de València (C/ Doctor Moliner, 46100, Burjassot, Spain)

Contact: rosa.vila@uv.es

Introduction:

Having access to the independent phase profile of manufactured Multifocal Intraocular Lenses (MIOLs) could provide even more reliable information about their optical performance. Various techniques have been developed for measuring MIOL surface characteristics. In this context, digital in-line holography under Gabor's regime (DIH-G) has emerged as a promising compact, single-shot, and contactless method for reconstructing the diffractive topography of MIOLs. Originally introduced by Dennis Gabor, DIH-G records interference patterns between a non-diffracted reference beam and a diffracted object beam, allowing phase retrieval and topographic reconstruction through numerical propagation techniques. Despite its inherent twin-image artifacts, iterative phase-retrieval algorithms enable reliable phase reconstructions. Therefore, this technique has been successfully validated for the inspection of different diffractive profiles of MIOLs[1]. The aim of this work is to improve the reconstruction of a sawtooth diffractive surface by achieving a wider field of view (FOV) and reducing background noise. This is accomplished by removing from the inspection cuvette the lens holder with a circular diaphragm used in a previous work[1].

Methods:

Sample: The measured MIOL was the FineVision POD F (PhysIOL, Liege, Belgium) with a power of +13 D (n=1.42, 550 nm wavelength). This trifocal lens features a diffractive profile with 26 rings[2].

Experimental assembly and image processing: The experimental setup for DIH-G consisted of a pigtailed diode laser emitting at 532 nm directly illuminating the sample. The MIOL was placed inside a horizontally positioned cuvette filled with saline solution (n_s=1.34). The lens was laying on the bottom of the cuvette to permit the reference beam to pass through and outside the diffractive area of the lens. The recorded hologram was captured using a CMOS located 5 mm after the cuvette. The optical configuration was pre-defined in Zemax OpticStudio (Ansys, Canonsburg, PA USA) and the source was placed at the focal plane of the inspected sample, thus ensuring an outgoing collimated beam in order to provide a lateral magnification of M=1 on the sensor while capturing both intermediate and short-distance beams related to power additions as converging beams. A single hologram was recorded and processed using MATLAB 2023a (The Mathworks, Inc., Natick, MA, USA). The hologram was numerically back propagated using the Angular Spectrum Method in order to retrieve an in-focus image of the lens, and a modified Gerchberg-Saxton algorithm was applied to obtain an accurate phase estimation reducing twin-image artifacts[33]. The retrieved phase data was translated into optical path differences (OPD) to be converted to the height of the diffractive structure. The obtained surface map was background-subtracted to obtain the information related to the diffractive profile.

Results and discussion:

Figure 1 shows the reconstruction of the diffractive surface topography after background subtraction and the comparison of the 360° averaged experimental profile with the theoretical one[2]. The reconstruction obtained with the improved system (Fig. 1B) shows good agreement with the theoretical profile up to a radius of 2.3 mm, thus offering improvements over previously reported measurements[1] (Fig. 1C). These prior measurements only retrieved rings up to a radius of 1.9 mm. These results also suggest an enhancement of background noise provided by a larger recording area irradiated by the reference beam. While the configuration with the holder permitted the light to pass only through the optical area of the lens and could also have introduced residual diffraction contributions coming from the edge of the diaphragm, the cuvette without the holder favoured classical requirements of Gabor. Moreover, the introduction of a partially coherent light source should be explored to reduce background noise caused by laser coherence.

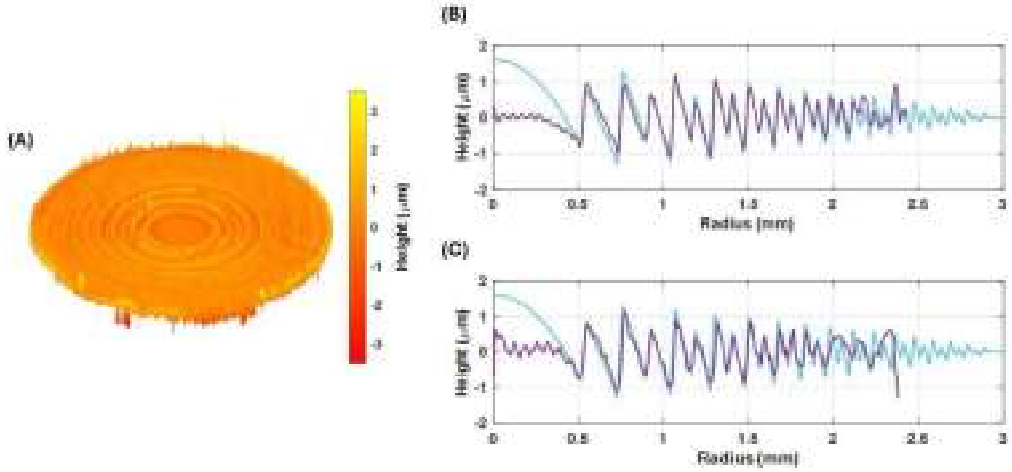

Figure 1: (A) Surface map of the diffractive profile of the FineVision POD F. (B) Averaged experimental profile (purple line) compared to the theoretical profile[2] (blue line). (C) Previous measurement (purple line) compared to the theoretical profile[2] (blue line) using a cuvette with a diaphragm.

Conclusions:

This work demonstrates significant improvements in the reconstruction of sawtooth diffractive surfaces, achieving a wider FOV and reduced background noise. The single-shot reconstruction shows good agreement with the theoretical profile and the enhanced system successfully reconstructs up to a 2.3 mm radius, enhancing previous measurements. These findings and the previously reported ones confirm DIH-G as a lensless, powerful, contactless, and extremely compact technique for inspecting diffractive MIOL profiles.

ACKNOWLEDGEMENTS: R.V-A, V.M. and J.E-T.: Grant PID2023-153363NB-C21 from MCIN/AEI/10.13039/501100011033 (Spanish Ministerio de Ciencia, Innovación y Universidades). R.V-A.: Spanish Ministerio de Universidades (FPU21/05151). A.M-E: Spanish Ministerio de Ciencia e Innovación (PID2022-142407NB-I00) and Generalitat Valenciana (CIPROM/2022/30), and Universitat de València (UV-INV-PREDOC21-1915492).

[1]R. Vila-Andrés et al.; *Scientific Reports*, **15**, 566(2025).
[2]D. Gatinel et al.; *Journal of Cataract & Refractive Surgery*, **37**, 2060(2011).
[3]U. Schnars et al.; W. *Digital holography and wavefront sensing,* **2nd Ed**, (2015)**.**

A new algorithm for anterior cornea segmentation and shape quantification in optical coherence tomography (OCT) images

André Rino Amorim, Miguel Faria Ribeiro

Department or Physics, School of Science, University of Minho, Largo do Paço 4704-553 Braga, Portugal

amorim.andre.89@gmail.com

Introduction

We propose a new algorithm to segment and characterize the shape of the cornea in optical coherence tomography (OCT) images. Corneal segmentation allows to extract shape parameters of the cornea such as the radius and asphericity, crucial for applications such as contact lens fitting and surgery planning. Several cornea segmentation algorithms have been described in literature, but most of them have flaws, ranging from being too simple[1], using hard-coded parameters[2], being defined only in the central part of the cornea[3], using shape assumptions that are not always true[4], or requiring large training datasets[5]. Our goal is to provide a simple and fast algorithm, that does not use artificial intelligence and can accurately segment the cornea in both low- or high-quality OCT images. We also intend to rely as little as possible on shape assumptions, as pathologies such as keratoconus significantly affect the shape of the cornea.

Methods

Blinking artifacts are common in OCT images and result in unwanted structures. To remove them, images were smoothed using a gaussian filter, followed by a custom binarization using Otsu's method. A vertical gradient filter allowed to extract the eye surface curve Figure 1-Left. A visual inspection allows us to conclude that each transition from the cornea to the eyelid corresponds to a valley in the curve. These transitions were identified by analysing the first and second derivatives of the curve and removing unwanted valleys. Results are shown in Figure 1-Center.

A pilot segmentation of the anterior surface of the cornea was initially performed. First, the cornea apex y-coordinates of the cornea extremities at the first and last column of the image were determined from projected reflectivity. The apex and extremities were used to fit a parabola, whose normal vectors were used to weight the x and y gradients used in a customized columnwise edge detector. The signal-to-noise ratio (SNR) of each edge was computed. A morphological grayscale opening operation followed by a Savitzky-Golay filter smoothed all major bumps from the initial segmentation. Regions with too many columns with SNR smaller than 1 were interpolated from the remaining regions. Horizontal edges near the borders of the image were truncated and a final large window Savitzky-Golay filter smoothed the eye surface.

To refine the segmentation, two concentric curves around the pilot edge defined a ROI, which was flattened. A graph cut algorithm was then applied to the flattened ROI. The resulting segmentation was unflattened and uncropped, providing the final segmentation (Figure 1-Right). A fit using the Taubin method[6] was applied to the cornea region ranging between the apex and 4.5 millimetres to each side, and the corneal radius and asphericity were estimated.

Results and discussion

The algorithm was implemented in MATLAB and applied to 223 images taken from 13 subjects through the CASIA 2 OCT scanner (Tomey GmbH). The dataset included images with low and high SNR, various degrees of blinking, different numbers of frame averages, different eye alignments, and two keratoconus cases. The complete segmentation worked very well in all images, with a mean duration 1.2 seconds per image, which is well satisfactory in a programming language not

optimised for performance. Some errors in the graph cut occurred due to the algorithm confusing the corneal epithelium with the Bowman layer and due to A-scans that escaped the blinking artifact removal. But this only happened in a few pixels close to the sclera transition and did not affect the conic fit.

The mean, standard deviation, minimum and maximum of the radius and asphericity are shown in Table 1. Two outliers were removed, which corresponded to the keratoconus images, with R equal to 4.91mm and 4.22mm and Q equal to -1.81 and -1.71 respectively.

The results show that the estimated metrics are well in the normal range of the human cornea. This suggests the algorithm presented here has potential for the quantification of the shape of corneal structures. Further improvements are currently being made, namely the segmentation and characterization of the posterior surface of the cornea.

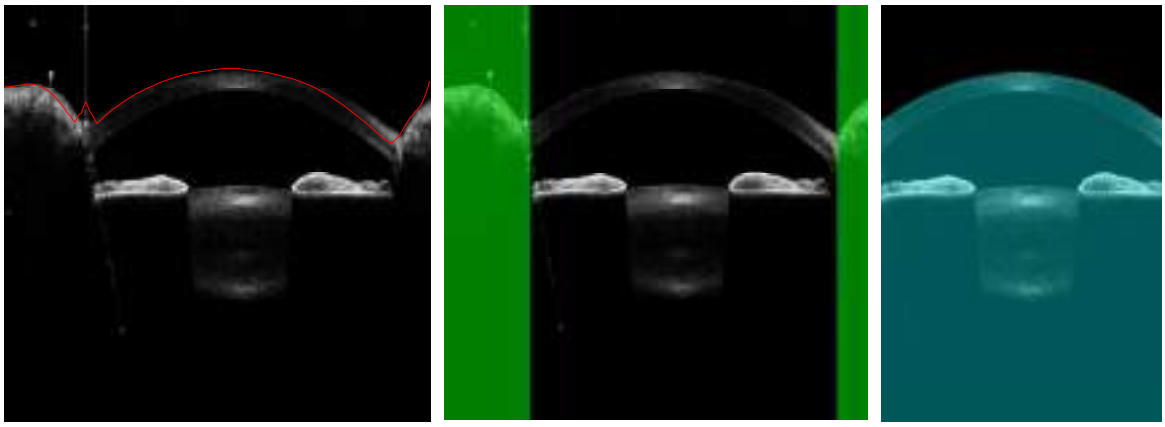

Figure 1: Anterior cornea segmentation. Left: Original image with the curve extracted to detect blinking artifacts overlapped. Center: Detected regions corresponding to blinking artifacts. Right: Final segmentation, after truncating the blinking artifacts.

	Radius, R (mm)	Asphericity, Q
Mean	7.41	-0.31
STD	0.20	0.11
Min	6.94	-0.61
Max	7.80	0.07

Table 1: Summary statistics of the corneal radius and asphericity estimated from the presented algorithm.

ACKNOWLEDGEMENTS: Work financed by FCT - Foundation for Science and Technology (UI/BD/154546/2022)

1 F. Graglia, J.-L Mari, G. Baikoff; *IEEE*; 5612–5615 (2007).
2 Y. Garcia-Marin et al., *Biocybernetics and Biomedical Engineering*; *41* (3), 903–915 (2021).
3 F. LaRocca et al.; *Biomed. Opt. Express*; (6), 1524 (2011).
4 T. Zhang et al.; *IEEE Access*; *5*, 10352–10363 (2017).
5 M. Jahromi et al.; *J Med Signals Sens*; *4* (3), 171 (2014).
6 V. Lockett-Ruiz, R. Navarro, N. López-Gil; *Ophthalmic Physiologic Optic*; *44* (2), 334–346 (2024).

Preliminary study on the reflectance of eye fundus structures using a portable multispectral fundus camera

Marina Bou-Marin, Meritxell Vilaseca and Francisco J. Burgos-Fernández

Centre for Sensors, Instruments and Systems Development, Universitat Politècnica de Catalunya, Rambla Sant Nebridi 10, Terrassa 08222 (Barcelona), Spain

Contact: marina.bou@upc.edu

In ophthalmology, one of the most widespread techniques to evaluate eye fundus pathologies is fundus imaging. For this, an RGB camera is used to obtain a colour image of the eye fundus[1]. These cameras give excellent spatial resolution, but their spectral resolution is limited, causing some alterations to be undetected or labelled as healthy. Multispectral (MS) cameras are a potential solution to this limitation, giving both high spatial and spectral information of the eye fundus, thus resulting in the detection of diseases at early stages[2]. These systems offer more than three spectral channels, and not only in the visible (VIS), but in the near-infrared (NIR) range, allowing the visualization of deeper layers such as the choroid and its vessels[3,4]. However, tabletop approaches have a high-cost, are bulky and difficult to use. To overcome this, a portable MS fundus camera has been developed to work in the 470–850 nm spectral range, offering high spatial and spectral resolution. A preliminary study has provided fundus spectral images of human eyes and the reflectance of different fundus structures have been retrieved. The prototype is based on a PanOptic™ ophthalmoscope (Hill-Rom Holdings, Inc.) as the optical module to illuminate the eye fundus and collect the reflected light. A 12-bit CMOS monochromatic camera UI-1480SE-M-GL (Imaging Development Systems GmbH) with an 8-mm objective lens is attached to it (Fig. 1 A). A six fiber-coupled LEDs sequentially illuminates the eye fundus from 470 to 855 nm (Thorlabs, Inc.) (Fig. 1 B). For positioning purposes, two NIR LEDs (830 nm) as fixation targets and lineal sliders were included.

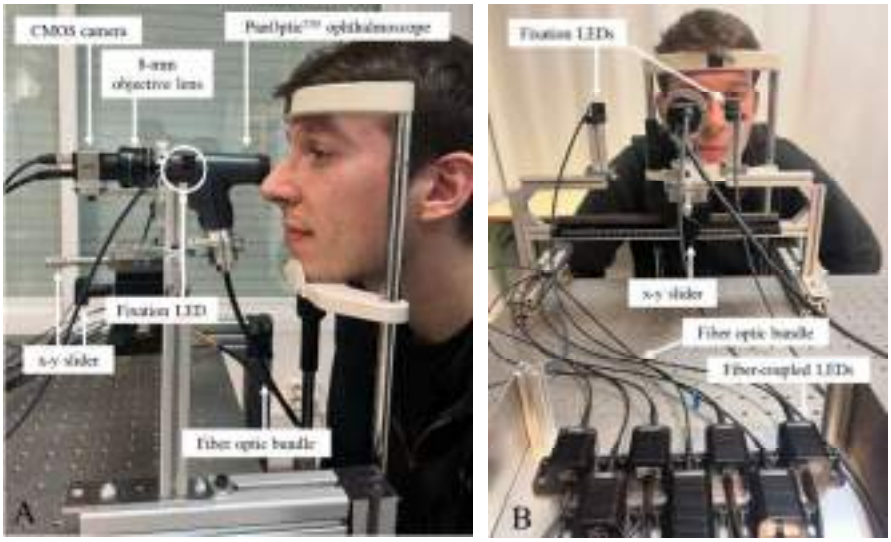

Figure 1: Portable MS fundus camera. A) Lateral view; B) Frontal view.

A customized software was implemented in Matlab R2022b to control and synchronize the LEDs and the camera to obtain the six MS images; a complete sequence is obtained in 1 s. Background and dark images of an absorptive black sheet with the LEDs turned on and off, respectively, were also captured for each patient, to compensate for internal reflections from the system. In order to calibrate and retrieve reflectance data, a calibrated white standard (BN-R98-SQC, Gigahertz-Optik

GmbH) was used. Equation 1 describes how compensation of reflections and calibration was performed, where $I_C(\lambda)$, $I(\lambda)$, $I_B(\lambda)$, $I_D(\lambda)$, and $I_w(\lambda)$ correspond to the digital levels of the corrected, non-corrected, background, dark, and white reference images, respectively, and R_W is the calibration factor given by the white standard's manufacturer.

$$II_{GG}(\lambda\lambda) = RR_{WW}(\lambda\lambda)\frac{\left\|II(\lambda\lambda) - II_{DD}(\lambda\lambda)\right\| - \left\|II_{BB}(\lambda\lambda) - II_{DD}(\lambda\lambda)\right\|}{\left\|II_{WW}(\lambda\lambda) - II_{DD}(\lambda\lambda)\right\|}$$

Equation 1

In this first study the optic disc, veins and arteries were spectrally analysed by retrieving their reflectance. To compare them, the global contrast, $GGGG(\lambda\lambda)^2$ (equation 2), was calculated for each channel, where $RR(\lambda\lambda)$ is the reflectance of the structure under study, and $RR_{FFFFFF}(\lambda\lambda)$ is the mean reflectance of the whole fundus image.

$$GC(\lambda) = \frac{R(\lambda)}{R_{FOV}(\lambda)}$$

Equation 2

A complete sequence of MS fundus images obtained with the prototype is shown in figure 2 (A) after image processing. It can be observed that the optic disc has a high reflectance in the VIS range compared with the fundus. This behaviour is also seen when analyzing the GC (figure 2B), where its values remain above one in all the VIS range while it decreases in the NIR range. Regarding the blood vessels, the higher difference between them can be observed around 600 nm, where arteries show a higher reflectance than veins, and can be observed brighter than them[5].

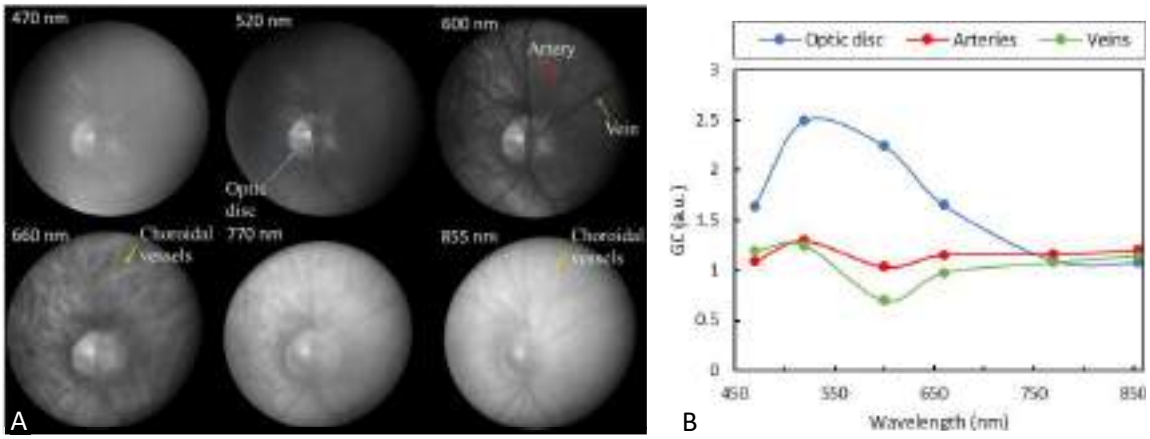

Figure 2: A) complete sequence of spectral images of a healthy eye acquired with the multispectral fundus camera. B) Global contrast (GC) of the optic disc, veins and arteries in the spectral range evaluated.

ACKNOWLEDGEMENTS: This publication is part of the project PID2023-147541OB-I00, funded by MCIU /AEI /10.13039/501100011033 and by FEDER, UE. The first author gratefully acknowledges the Universitat Politècnica de Catalunya and Banco Santander for the financial support of her predoctoral grant FPI-UPC.

[1] N. Panwar et al., "Fundus Photography in the 21st Century—A Review of Recent Technological Advances and Their Implications for Worldwide Healthcare," Telemed. E-Health **22**(3), 198–208 (2016).
[2] F.J. Burgos-Fernández et al., "Reflectance evaluation of eye fundus structures with a visible and near-infrared multispectral camera," Biomed. Opt. Express **13**(6), 3504–3519 (2022).
[3] C. Zimmer et al., "Multiple-wavelength imaging of the retina and choroid.," Retina Today **9**(7), 94–99 (2014).
[4] T. Alterini et al., "Fast visible and extended near-infrared multispectral fundus camera," J. Biomed. Opt. **24**(09), 096007-1-096007–7 (2019).
[5] F.C. Delori, and K.P. Pflibsen, "Spectral reflectance of the human ocular fundus," Appl. Opt. **28**(6), 1061–1077 (1989).

Stokes Vector Analysis of the Lamina Cribrosa using Linear and Second-Harmonic Generation Microscopy

Aishwarya Chanady Babu[1], Ian A Sigal[2] and Brian Vohnsen[1]

[1]Optics Group, School of Physics, University College Dublin (Belfield, D04P7W1, Dublin, Ireland)
[2]Department of Ophthalmology, School of Medicine, University of Pittsburgh (Locust Street, PA15219, Pittsburgh, USA)

Contact: aishwarya.chanadybabu@ucdconnect.ie

Introduction

The Lamina Cribrosa (LC) is a complex, mesh-like structure located at the opening of the nerve head, composed primarily of collagen fibrils that provide structural and nourishing support to the retinal ganglion cells as they leave the eye on their path to the brain. Abnormalities in the collagen fibril organization in the LC alter its mechanical and physiological environment potentially leading to neural tissue damage and irreversible vision loss[1]. Therefore, visualizing the distribution of collagen fibrils within the LC is of particular interest. To achieve this, polarimetric imaging has been incorporated into both second-harmonic generation (SHG) microscopy and widefield linear transmission microscopy. By calculating the Stokes vector, these techniques enable quantitative mapping of collagen fibril distribution, facilitating more precise data analysis and interpretation[2].

Method

A cryosection of the lamina cribrosa of normal sheep eyes, prepared at 25µm thicknesses under 0 mmHg intraocular pressure (IOP), was imaged using two setups. The first was an SHG microscopy system with an ultrafast Ti:Sapphire femtosecond laser (Micra-5, Coherent Inc.) as the source, galvo-mounted mirrors for scanning along with a motorized XY-stage. The second was a widefield transmission microscopy setup, where a white light source was filtered at 633 nm using a bandpass filter (3 nm bandwidth) and passed through a linear polarizer. Polarimetric analysis was performed by placing a polarization state analyzer in the detection path, consisting of a rotating quarter-wave plate followed by a linear polarizer, using the same method for both setups. Four sets of images were acquired with the quarter-wave plate positioned at -45°, 0°, 30°, and 60°. These images were then used to calculate the Stokes vector using the method described by Bueno et al[3].

Results

Stokes vector (S0, S1, S2 and S3) was derived for both linear and SHG Microscopy using the images captured at different angles of the polarization state analyzer (Figure 1). A direct comparison of polarimetry in linear and SHG Microscopy is made by calculating the degree of polarization, entropy and standard deviation across the images. The stokes vector can quantify the state of polarization in the SH signal allowing a more accurate determination of collagen fibril orientation across the LC.

Conclusion

Polarimetric analysis with linear and nonlinear microscopy give complementary information on the collagen organization and enriches the understanding of the contrast observed. In linear microscopy S3 gives added insight into the crimp seen as regular ondulations in the image, whereas in SHG microscopy the crimp is most apparent in the original SHG intensity images.

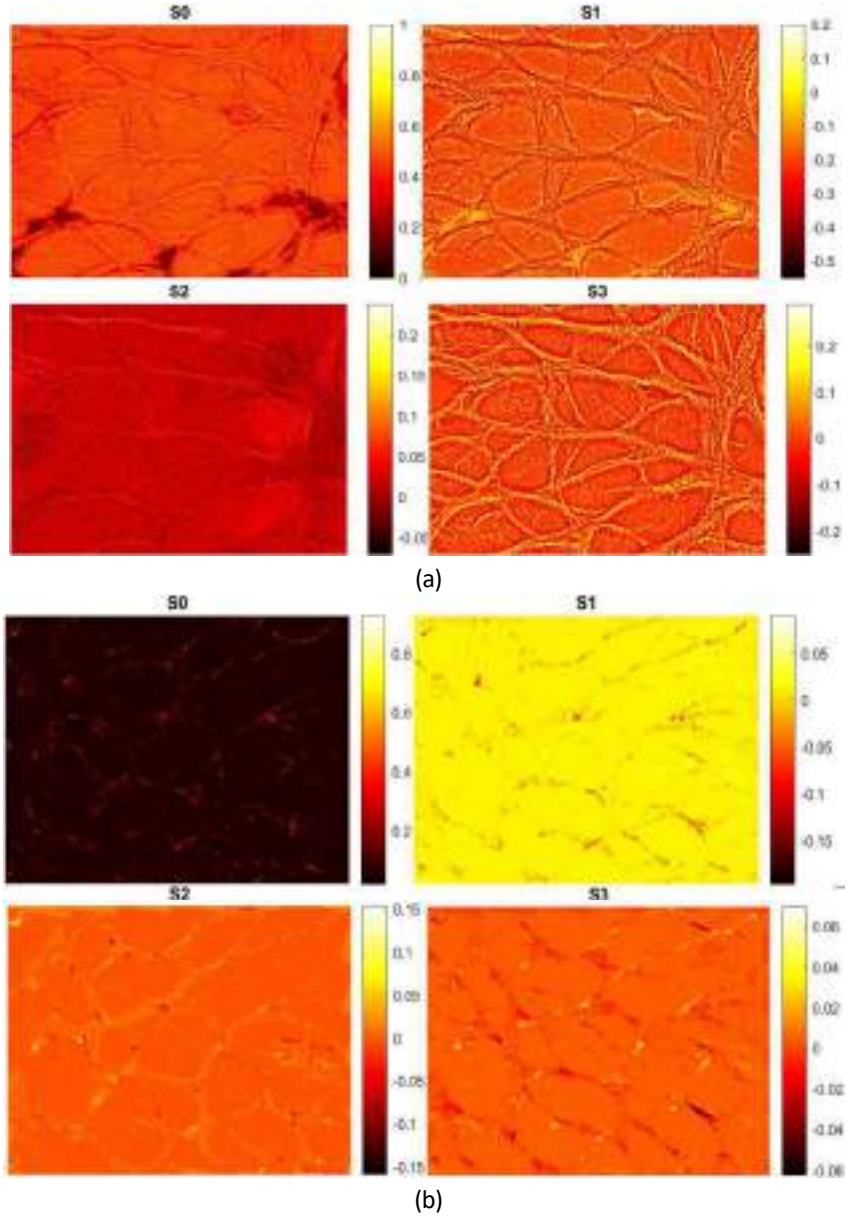

Figure 1: Stokes Vector derived from the images of LC captured using a) Widefield linear microscopy and b) SHG Microscopy, respectively.

ACKNOWLEDGEMENTS: We are grateful for financial support from the IOP Bell Burnell Graduate Scholarship Fund.

[1] I. A. Sigal, J.L. Grimm, N. Jan, K. Reid, D.S. Minckler and D.J. Brown; *Invest Ophthalmol Vis Sci,* **55**, 1-15, (2014).
[2]A.C. Babu, B. Vohnsen and I.A. Sigal; Frontiers in Optics, Optica Publishing Group, JW5A. 44, (2024).
[3]J. M. Bueno and B. Vohnsen, Vision Research, **45**, 3526–3534, (2005).

Improving a Multispectral Camera for Simultaneous Retinal Oximetry and Multispectral Image Acquisition

Armin Eskandarinasab[1], Laura Rey-Barroso[1], Francisco J. Burgos-Fernández[1], Meritxell Vilaseca[1]

[1] Center for Sensors, Instruments and Systems Development (CD6), Universitat Politècnica de Catalunya (Rambla Sant Nebridi 10, Terrassa, 08222, Spain)

Contact: armin.eskandarinasab@upc.edu

Retinal oximetry is a non-invasive, in-vivo technique that quantifies the oxygen saturation of hemoglobin within the retinal blood vessels. This measurement of retinal blood oxygenation plays a crucial role in the diagnosis and monitoring of various systemic and ocular conditions, including hypoxia, vascular endothelial growth factor, and diabetic retinopathy[1]. However, a significant limitation of existing retinal oximetry systems is their inability to provide spectral information about the retina, which could offer valuable insights into retinal health and disease.

Several methods have been developed to assess retinal oxygenation. One approach utilizes single-wavelength imaging to detect blood flow dynamics over a brief period, typically a few seconds. This technique allows for the observation and detection of heart pulse-related fluctuations in blood flow, capitalizing on the normal human heart rate of 60 to 120 beats per minute. Optical Coherence Tomography Angiography (OCT-A) offers a three-dimensional visualization of the retinal vasculature, providing detailed structural information. However, OCT-A's temporal resolution limitations necessitate alternative methods for capturing dynamic blood flow changes. Some techniques employ specialized cameras and laser light sources to analyze blood cell movement based on speckle patterns, enabling the assessment of blood flow velocity[2].

Another approach focuses on multi-wavelength imaging, where oxygen saturation is calculated from a single capture. These methods capture retinal images at oxygen-sensitive and non-oxygen-sensitive wavelengths simultaneously from the same retinal field of view. By applying the Beer-Lambert law, the oxygen saturation within the retinal vessels can be calculated[3]. A significant challenge in these methods is the potential influence of Retinal Pigment (RP) layer on the measurements. RP variations can significantly affect reflectance from retinal veins, although the effect on arterioles is generally considered negligible. Traditional methods of estimating RP levels based on patient ethnicity have been proven unreliable[3]. To overcome this, researchers are exploring deep learning techniques to predict oxygenation levels directly from retinal images, potentially mitigating the need for separate RP calibration.

Our research utilizes multispectral retinal imaging, a technique providing rich spectral information crucial for detecting subtle pathological changes and biomarkers often missed by traditional methods. The foundation of our work is a multispectral camera initially developed by Alterini et al.[4]

Building upon previous work conducted by our research group (Burgos-Fernández et al.[5], 2022), where the fundus reflectance was analyzed across various ocular conditions and retinal sections, we applied phasor analysis to extract notable features from the multispectral fundus images. Phasor analysis effectively reduces the dimensionality of data from numerous spectral bands (e.g., >12) into an intuitive 2D phasor plot (see Figure 1 for illustration), simplifying interpretation. Using features derived from this analysis, we successfully trained machine learning classifiers to differentiate between healthy and diseased retinas.

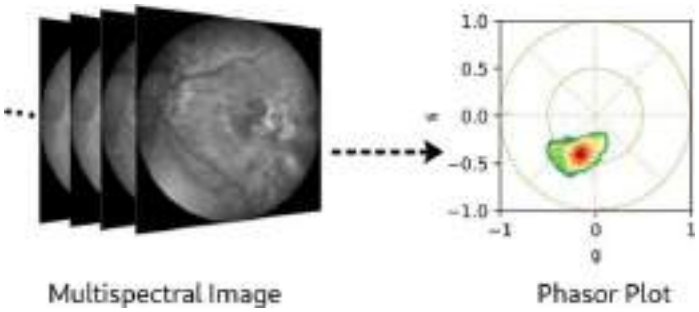

Figure 1: Every multispectral image consists of different bands, each representing a specific wavelength. By applying phasor analysis, the complex data from the multispectral image (known as a multispectral cube) can be simplified and converted into a 2D plot.

To further enhance the diagnostic potential of this approach, we are now reconfiguring the imaging system to incorporate retinal oximetry measurements. The device is capable of capturing images at multiple, distinct wavelengths necessary for this purpose. This modification will enable the acquisition of retinal vessel oxygen saturation data, allowing for the generation of oximetry maps. This oximetry information will then be fused with the multispectral retinal images. We hypothesize that the resulting fused 'multispectral-oximetry' data will provide more comprehensive information, significantly improving the ability to distinguish subtle disease-related biomarkers and spectral signatures that are difficult for the human eye to comprehend.

Generating retinal oximetry maps with this system encounters several key challenges. A primary concern arises from the sequential illumination of the retina using various LEDs, which introduces eye movement artifacts and a slight temporal delay in the acquisition of images at different wavelengths, potentially necessitating additional processing. Furthermore, retinal oximetry measurements, potentially lasting several seconds, necessitate specific wavelengths that might be in the visible spectrum leading to pupil's constriction. This, combined with the low reflectance of the retina, requires high-intensity LED illumination, which could lead to patient discomfort. To mitigate this issue while meeting oximetry requirements, we will prioritize the use of wavelengths at 620nm and above.

The multispectral-oximetry fusion process will be implemented using a two-step deep learning methodology. First, multiple oximetry related images will be fused into a single composite image. Second, this composite oximetry map will be fused with the multispectral retinal image to facilitate disease diagnosis.

ACKNOWLEDGEMENTS: Funded by European Union (HORIZON–MSCA–2022–DN, GA nº101119924–BE-LIGHT) and by MCIU/AEI/10.13039/501100011033 and FEDER, EU (Grant PID2023-147541OB-I00).

---

[1] E. Stefánsson, et al.; Retinal oximetry: metabolic imaging for diseases of the retina and brain. *Progress in retinal and eye research*, **70**, 1 (2019).

[2] K.A. Cho, et al.; Portable, non-invasive video imaging of retinal blood flow dynamics. *Scientific reports*, **10**, 20236 (2020).

[3] K. Hirsch, R. P. Cubbidge, and R. Heitmar; Dual wavelength retinal vessel oximetry–influence of fundus pigmentation. *Eye*, **37**, 2246 (2023).

[4] T. Alterini, et al.; Fast visible and extended near-infrared multispectral fundus camera. *Journal of biomedical optics*, **24**, 096007 (2019).

[5] F.J. Burgos-Fernández, et al.; Reflectance evaluation of eye fundus structures with a visible and near-infrared multispectral camera. *Biomedical optics express*, **13**, 3504 (2022).

A Hybrid Algorithm for Artifact Removal in Shack-Hartmann Sensor Images: Combining Correlation and Hough Transform

Sarvenaz Kalantarinejad, Aina Turull-Mallofré, Carlos E. García-Guerra, Mikel Aldaba

Centre for Sensors, Instruments and Systems Development (CD6), Universitat Politècnica de Catalunya, (Rambla Sant Nebridi 10, 08222, Terrassa, Spain)

Contact: sarvenaz.kalantarinejad@upc.edu

A Shack-Hartmann sensor is an optical system used to characterize wavefronts and detect ocular aberrations. Traditionally, Shack-Hartmann sensors relied on manual centering for single-shot image acquisition. In contrast, modern systems permit dynamic image acquisition, resulting in a set of images[1]. However, image artifacts can compromise the accuracy of aberration estimates, and these artifacts can be caused by factors such as eye blinking, laser reflections, or reflections from the cornea. In single-shot methods, this issue has usually been overcome by manually identifying and discarding images affected by artifacts. However, in continuous acquisitions (with hundreds or thousands of images per measurement), this becomes a challenge. The purpose of this work was to identify and exclude artifact-affected images as invalid from the aberration detection process. By doing so, the aim is to ensure the accuracy and reliability of aberration estimation, making it suitable for clinical applications.

A dataset of Hartmann-Shack images was created using images acquired in previous studies[1-2]. Images were categorized into four types: valid, blinking (invalid), laser reflex (invalid), and corneal reflex (invalid). The dataset was preprocessed to enhance clarity and centering, which improved the accuracy of the subsequent analysis. To analyze this dataset and identify invalid images, a correlation-based algorithm was developed[3]. This algorithm measured the similarity between each image and a reference, with a higher correlation indicating a higher similarity. To implement this, a reference image was generated by averaging a set of valid images. The correlation between the reference image and each image in the dataset was then calculated. A correlation threshold was defined to classify images as valid (high correlation) or invalid (low correlation). Besides the correlation method, an additional method was also implemented to improve the detection of corneal reflex images. Since corneal reflexes often occurred in the middle of the Shack-Hartmann images, the Hough transform was used[4-5]. The Hough transform detected bright circles in images, allowing corneal reflex images to be discarded as well.

The results were obtained using a dataset of 400 images, with each category containing 100 images selected manually to represent a range of artifacts. Figure 1 illustrates examples of each category. The images were labeled as valid or invalid based on the presence or absence of artifacts.

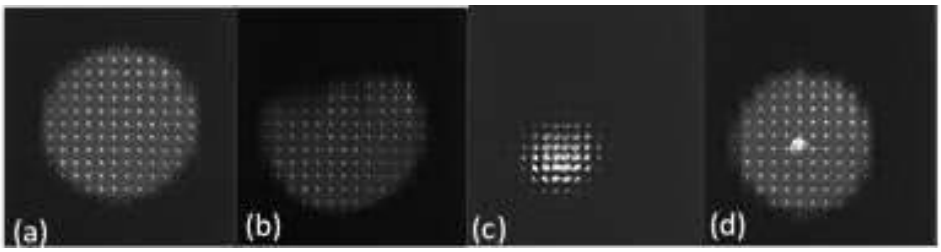

Figure 1: Representative images from each category. (a) Valid image, (b) Blinking, (c) Laser reflection, and (d) Corneal reflection.

First, a correlation threshold was defined, and images with a correlation threshold above this value were considered valid. Threshold values of 0.5, 0.6, and 0.7 were tested, with 0.7 giving the best results. This value was selected to maximize true negatives.

The performance of the algorithm is presented in Table 1, which shows the confusion matrix for each category. The confusion matrix is a summary of the algorithm's predictions, where the rows represent the actual labels (1 as valid and 0 as invalid) and the columns represent the predicted labels. The table shows the number of true positives (TP), true negatives (TN), false positives (FP), and false negatives (FN) for each category.

	Correlation						**Correlation+Hough**	
	Blink		**Laser**		**Corneal**			
class	**0**	**1**	**0**	**1**	**0**	**1**	**0**	**1**
0	85	15	100	0	67	33	91	9
1	40	60	40	60	40	60	44	56

Table 1: confusion matrix for each category.

The results indicate that the algorithm successfully discarded 85% of blink images and all laser reflection images as true negatives. However, the correlation-based approach alone was less effective (67%) for detecting corneal reflex images. By incorporating the Hough transform method, the results improved significantly, and the algorithm was able to correctly identify 91% corneal reflex images. The main limitation of the study is the high number of valid discarded images, which remains to be improved in future work.

ACKNOWLEDGEMENTS:
Grant PID2023-146101OB-I00 funded by MICIU/AEI/10.13039/501100011033 and by ERDF/EU.

[1]C. E. García-Guerra, J. A. Martínez-Roda, J. C. Ondategui-Parra, A. Turull-Mallofré, M. Aldaba, & M. Vilaseca. Translational vision science & technology, 12, 22, (2023).
[2]A. Turull-Mallofré, C. E. García-Guerra, C. Mestre, M. Vilaseca, J. Pujol, & M. Aldaba. Biomedical optics express, 14, 5488, (2023).
[3] M. Rais, J. M. Morel, C. Thiebaut, J. M. Delvit, & G. Facciolo. Applied optics, 55, 7836, (2016).
[4]D. Ioannou, W. Huda, & A. F Laine. Image and vision computing, 17, 15, (1999).
[5]H. Zhang, Y. Yang, Z. Zhang, C. Yin, S. Wang, K. Wei, H. Chen, and J. Zhao. Biomedical Optics Express, 15, 6531, (2024).

Reconstruction of the full Shape of the Crystalline Lens from Off-Axis OCT Images

Rodríguez-Sánchez, Javier[1]; de la Peña, Álvaro[1]; Vadillo, Estela[1]; de Castro, Alberto[1]; Talaván-González, Celia[1]; Carreño, Ester[2]; Marcos, Susana[3,4]; Martinez-Enriquez, Eduardo[1]

[1] Instituto de Óptica, Consejo Superior de Investigaciones Científicas, Madrid, Spain
[2] Hospital Universitario La Paz, Madrid, Spain.
[3] Flaum Eye Institute, University of Rochester, Rochester, NY, United States.
[4] Center for Visual Science. The Institute of Optics. Flaum Eye Institute., University of Rochester, Rochester, NY, United States.

Purpose:
We present, for the first time to our knowledge, the full-shape reconstruction of the crystalline lens—including its peripheral regions—using off-axis imaging of the eye with the commercial anterior segment Optical Coherence Tomography (OCT) system ANTERION.
Traditional on-axis OCT view of the crystalline lens is limited by the size of the pupil, since it is not possible to image through the iris. By acquiring images at multiple eccentric angles (including nasal, temporal, superior, and inferior orientations), we have successfully visualized the full shape of the crystalline lens including its periphery.

Methods:
Optical coherence tomography (OCT) images with a 14 mm lateral B-scan length were acquired from one eye of 4 subjects—two young adults (Y) and two early presbyopic individuals (EP)—using the ANTERION device (Heidelberg Engineering). All acquisitions were performed under pharmacologically induced mydriasis and paralyzed accommodation to enable clear visualization of the crystalline lens extent. To capture a comprehensive view of the lens geometry, imaging was conducted from eight different eye orientations: on-axis (normal incidence), 30° and 45° nasal, 30° and 45° temporal, 30° and 20° superior, and 45° inferior angles. For each of these orientations, sixty-five distinct meridional B-scans were acquired, allowing the reconstruction of a partial 3D model at each individual angle.

The acquired images underwent a series of custom-developed pre-processing steps, including the segmentation of the anterior and posterior surfaces of the cornea and the crystalline lens, conversion from pixels to millimetres, and correction of optical refraction distortions. Subsequently, the segmented and corrected data corresponding to the different imaging angles were registered into a common coordinate system using a robust pipeline based on 3D iris reconstruction for initial alignment, followed by iterative refinement using the iterative closest point (ICP) algorithm[1]. The registered point clouds were then projected onto a 6-term eigenlenses basis[2] to produce smooth, denoised and full lens reconstructions. From these, we extracted key morphological parameters: lens volume (VOL), lens surface area (LSA), equatorial diameter (DIA), and equatorial plane position (distance between the anterior lens surface and the equatorial plane, EPP).

Results:
VOL was 132/126 mm3 (Y) and 185/165 mm3 (EP). LSA was 149/141 mm2 (Y) and 176/164 mm2 (EP). DIA was 8.85/8.51 mm (Y) and 940/9.10 mm (EP). EPP was 0.79/0.70 mm (Y) and 0.99/1.12mm (EP). The first eigenlens coefficients (related with the general size of the lens) were 27.8/29.4 (Y), and -11/0 (EP). The second ones (related with the aspect ratio of the lens) were -23/-14 (Y) and -7/-6 (EP).

Conclusions:
The resulting metrics revealed consistent and quantifiable differences across the studied age groups, with eigenlenses coefficients providing additional insight into age-related changes in lens size and shape, particularly in terms of global curvature and aspect ratio. This novel reconstruction method of crystalline lens full shape opens new avenues for in vivo analysis and may improve biometric modelling and the understanding of age-related optical changes of the lens. Finally, visibility of the lens periphery and full quantification enables applications in the study of lens accommodation, myopia, presbyopia and IOL implants.

Figure 1: OCT off-axis view, including the periphery of the lens (blue ellipse)

ACKNOWLEDGEMENTS: Ministerio de Ciencia, Innovación y Universidades (PID2023-152641OA-I00, PREP2023-001467, PID2020-115191 RB-100); Comunidad de Madrid (TEC-2024/COM-322); 2023 Leonardo Grant for Researchers and Cultural Creators, BBVA Foundation; MCIN/AEI and FSE+ (RYC2022-038195-I).

[1] K. S. Arun, T. S. Huang and S. D. Blostein, "Least-Squares Fitting of Two 3-D Point Sets," in *IEEE Transactions on Pattern Analysis and Machine Intelligence*, vol. PAMI-9, no. 5, pp. 698-700, Sept. 1987, doi: 10.1109/TPAMI.1987.4767965.

[2] Martinez-Enriquez E, de Castro A, Marcos S. Eigenlenses: a new model for full crystalline lens shape representation and its applications. Biomed Opt Express. 2020 Sep 16;11(10):5633-5649. doi: 10.1364/BOE.397695. PMID: 33149976; PMCID: PMC7587276.

The Heidelberg FLIO and a Custom AOFLIO Show Consistent Fluorescent Lifetime Phasor Signatures

Michelle Peimann[1], Rosa M. Martínez-Ojeda[1], Marjan Mansourian[1], Sophia Piro[1], Jennifer J. Hunter[1]

[1] School of Optometry and Vision Science, University of Waterloo, 200 University Av. W, N2L 3G1, Waterloo, CAN

Contact: michelle.peimann@uwaterloo.ca

The purpose of this study is to compare the fluorescent lifetime signatures of expected endogenous fluorophores in the retina as measured using two different fluorescent lifetime ophthalmoscopes.

A custom adaptive optics scanning light ophthalmoscope (AOSLO)[1] was used for fluorescence lifetime imaging at 473 nm excitation (NKT Photonics). A model eye was designed with a lens (EFL = 100 mm) and a quartz cuvette placed in a custom cuvette mount at the focal plane of the lens. The emitted fluorescence was collected by a hybrid detector module (Becker & Hickl GmbH) with a bandpass filter (575-725 nm), the fluorescence lifetime was measured using time-correlated single-photon counting (Becker & Hickl GmbH). For comparison, a custom model eye with a lens (EFL = 24.5 mm) was attached to a Heidelberg Spectralis FLIO to measure the fluorescence lifetime of fluorophores in solution in a quartz cuvette. Fluorescence throughout the cuvette was excited at 473 nm and emitted photons were collected into long (560-720 nm) and short (498-560 nm) spectral channels. The collected data was analysed using exponential decay fitting in SPCImage (Becker and Hickl GmbH). Analysis in phasor space was performed using custom software. The phasor fingerprint is a map in phasor space of the coordinates for defined samples of individual fluorophores. Samples included rhodamine B, FAD, and carotenoids that were reconstituted and diluted in Dulbeccos PBS solution to simulate their natural environment in the eye. All samples were analysed at room temperature.

Solutions of individual fluorophores occupy unique confined locations in phasor space. In the current configuration, the Heidelberg FLIO captured more photons than the custom AOSLO resulting in tighter clusters of lifetime values. However, the Heidelberg FLIO and the custom AOSLO capture similar fluorescent lifetime signatures as represented in phasor space. The consistency of phasor fingerprints across devices is reassuring for comparisons of human data. Moving forward, a database for association of *in vivo* FLIO measurements to known fluorophores will provide a useful tool for gaining improved insight into the sources of fluorescence in the retina for both devices.

ACKNOWLEDGEMENTS: Funding from National Institutes of Health (NIH) R01 EY032116.

---

[1]S. Steven; Thesis (Ph. D.) University of Rochester. The Institute of Optics, 2020.

Multimeridional analysis of brightness artifacts in corneal densitometry and the role of eye color

Ana R. Arizcuren[1] and Alejandra Consejo[1]

[1] Aragon Institute of Engineering Research (I3A), University of Zaragoza, Zaragoza, Spain.
ana.arizcuren@unizar.es

Context and aim: Corneal densitometry (CD), calculated as the mean pixel intensity (MPI) of the cornea, is widely used to evaluate corneal transparency. However, CD is influenced by confounding factors such as age, [1] eye tilt,[2] and spurious brightness artifacts from reflections of the sclera, eyelids, and iris.[3] Our previous study showed that such brightness artifacts can account for up to 40% of the variability in CD measurements, [3] yet the analysis was based on a single image[3]. With current imaging systems routinely capturing multiple meridional images per eye (as in Scheimpflug or Optical Coherence Tomography), a key question arises: is a single meridian representative, or is a multimeridional analysis necessary to fully capture the extent of brightness artifacts on CD? Additionally, and motivated by the observation that light-colored irises appear more reflective in clinical images (Figure 1), we also explore here whether eye color contributes to increased brightness artifacts and artificially elevated CD measurements. In addition, we compare the presence of brightness artifacts between right (OD) and left (OS) eyes to assess the symmetry and consistency of these effects across both eyes.

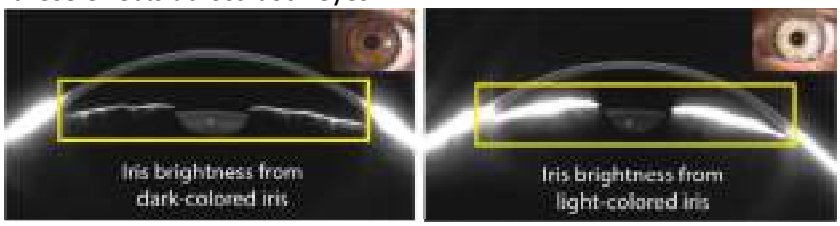

Figure 1: Example of brightness artifacts from iris reflections in a dark-colored iris (left) and a light-colored iris (right).

Methods: This study used Scheimpflug images acquired with the Pentacam HR tomographer. This device captures cross-sectional images along 25 meridians of the anterior segment. A total of 29 subjects were included in the study, and 1450 images from both eyes were analysed. Of the 29 subjects, 18 had light-colored eyes and 11 had dark-colored eyes. Image analysis was conducted across all 25 meridians. An automatic segmentation process was applied to identify the main ocular structures, including the cornea, the iris, and the peripheral scleral brightness artifacts (Figure 2). The MPI was calculated within the segmented full corneal region for each image. To quantify the presence of brightness artifacts, an intensity threshold specific to each image was defined. Pixels exceeding this threshold were considered to represent brightness artifacts.

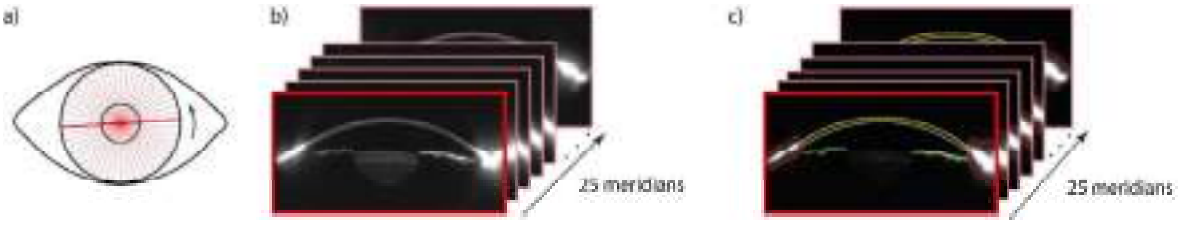

Figure 2: Schematic representation of the image acquisition and analysis process. a) The Pentacam HR captures Scheimpflug images along 25 meridians of the anterior segment. b) Example of raw Scheimpflug images. c) Automated segmentation of ocular structures including the cornea (yellow), iris (green), and lateral brightness artifacts (red), used for quantifying brightness presence in each region.

Results: Brightness artifacts were not uniformly distributed across the 25 meridians, with statistically significant differences observed ($p < 0.05$), Figure 3a. However, the magnitude of these differences was small—less than 2%—suggesting that while the variation is measurable, it is unlikely to have clinical relevance. In addition, significant differences were observed when comparing subjects with light-colored eyes and dark-colored eyes, Figure 3b. Those with light-colored eyes exhibited a higher prevalence of brightness artifacts and higher corneal MPI values compared to individuals with darker eyes ($p < 0.001$). This suggests that eye color may influence the degree of brightness artifact presence. Finally, no statistically significant differences were found between the left and right eyes in terms of brightness artifact presence or their impact on CD, Figure 3c. This indicates that the influence of brightness artifacts is consistent between eyes within the same subject.

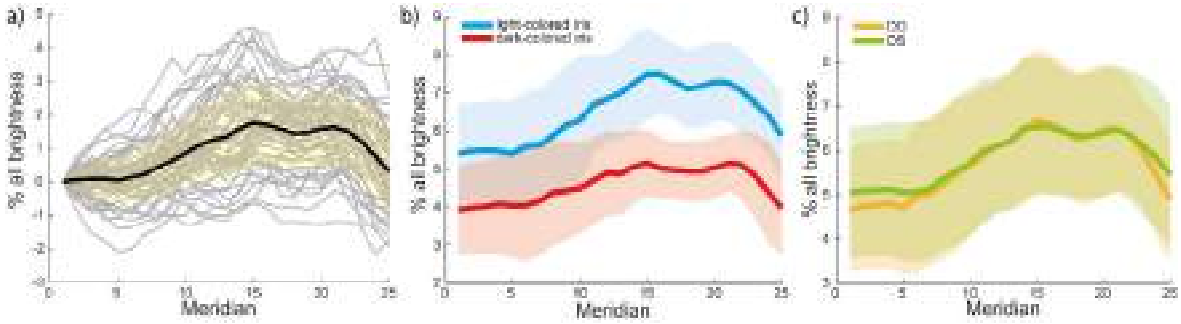

Figure 3: a) Percentage of brightness artifacts across all 25 meridians for each eye (gray lines) and group average (black line). b) Comparison of brightness artifact prevalence between subjects with light-colored eyes (blue) and dark-colored eyes (red), showing a significantly higher percentage in light-colored eyes ($p < 0.001$). c) Comparison of brightness artifact prevalence between OD (orange) and OS (green) eyes, showing no statistically significant differences ($p=0.26$).

Conclusions: These findings confirm that while brightness artifacts vary slightly between meridians, the overall variation within a given eye measurement is minor (<2%) and likely not clinically significant. However, eye color does influence the extent of brightness artifacts, underscoring the importance of considering pigmentation when interpreting CD. Accounting for these artifacts may be especially relevant in populations with lighter eyes. The consistency between right and left eyes suggests that bilateral comparisons are not biased by artifact distribution.

ACKNOWLEDGEMENTS: This work has been supported by European Research Council under the European Union's Horizon Europe research and innovation programme, StG 2024 call, Grant/Award Number: 101162733.

---

[1]M. Miażdżyk *et al*.; *Biomedical Optics Express*, **13**, 6258 (2022).
[2]A. Consejo *et al*.; *Ophthalmic and Physiological Optics*, **42**, 1032 (2022).
[3]A. Arizcuren *et al*.; *Ophthalmic and Physiological Optics*, **45**, 637 (2025).

Unorthodox parameters in machine learning-based keratoconus detection

Juan Casado-Moreno[1], Alejandra Consejo[1]

[1] Aragon Institute for Engineering Research (I3A), University of Zaragoza, Zaragoza, Spain (C/ María de Luna, 50018)

Contact: jcasado.moreno@unizar.es

INTRODUCTION

With the rising prevalence of myopia, accurately detecting preclinical keratoconus (KC) is essential to prevent iatrogenic complications associated with refractive surgery. Preclinical KC refers to the earliest stages of the disease, where topographic and tomographic signs are still subtle or absent, making its detection difficult. As artificial intelligence techniques gain traction, researchers have used traditional machine learning (ML) classifiers, employing clinical[1] or topographical modeling[2] parameters as inputs for models. These parameters are all related to the shape of the cornea, show little difference between healthy and preclinical KC eyes, limiting their discriminative power.

A more recent and promising area of research explores corneal densitometry, which quantifies light backscatter to objectively analyze corneal tissue as a marker for subtle changes associated with preclinical KC.[3] These image-derived parameters, which capture the pixel intensity distribution within the cornea, represent an unorthodox yet potentially valuable source of information. Image processing has been applied to raw corneal images. However, these parameters have not yet been tested in combination with ML algorithms. Consequently, the aim of this study is to use ML techniques to explore whether combining traditional shape-related tomographic parameters with unorthodox image-derived features can improve the detection of preclinical KC.

METHODOLOGY

Dataset: 9,250 Scheimpflug corneal images (Pentacam HR, Oculus) corresponding to 25 corneal meridians of 370 eyes were retrospectively collected at the West China Hospital (Chengdu, China). They were further divided into three groups: controls (C, 212 eyes), forme fruste keratoconus (FF, 62 eyes), and clinical keratoconus (KC, 96 eyes). FF is the contralateral, asymptomatic eye showing no clinical signs of keratoconus and is used as surrogate of preclinical stage of keratoconus. Only one eye per patient was included for analysis.

Image parameters: A total of 34 image-related parameters were extracted through image processing techniques. These primarily focus on specific measurements or ratios derived from them, including the mean pixel intensity (MPI) within the segmented 7-mm central corneal region, the image brightness—calculated as the average intensity of pixels exceeding a reference threshold relative to the corneal MPI—the MPI of the image background, and the MPI of the entire image.

Shape parameters: 16 traditional Pentacam HR parameters were extracted. These include six parameters associated with corneal thickness, such as *Thinnest Pachymetry* and *Maximum Pachymetry Progression*, three related to corneal curvature (*K Max*, *Front Km,* and *Back Km*), one parameter measuring anterior chamber size (*Corneal Volume*), and six combined indices, such as *Index of surface variance* (*ISV*) and *Keratoconus Index* (*KI*).

Architecture: The model is based on a Random Forest classifier, which was selected after outperforming other classifiers including XGBoost, Neural Networks (NN), Logistic Regression, and Support Vector Machines (SVM). Nested cross-validation was employed, with an outer Stratified K-Fold loop consisting of 6 folds for evaluating model performance and an inner Stratified K-Fold loop with 5 folds for hyperparameter tuning. This approach ensures that no data leakage occurs between the training and testing sets.

Model evaluation: The discriminative power of the method was analyzed using receiver operating characteristic area under the curve (ROC AUC), standard metrics (sensitivity, specificity, confusion matrix), and SHAP values to assess feature importance and model interpretability.

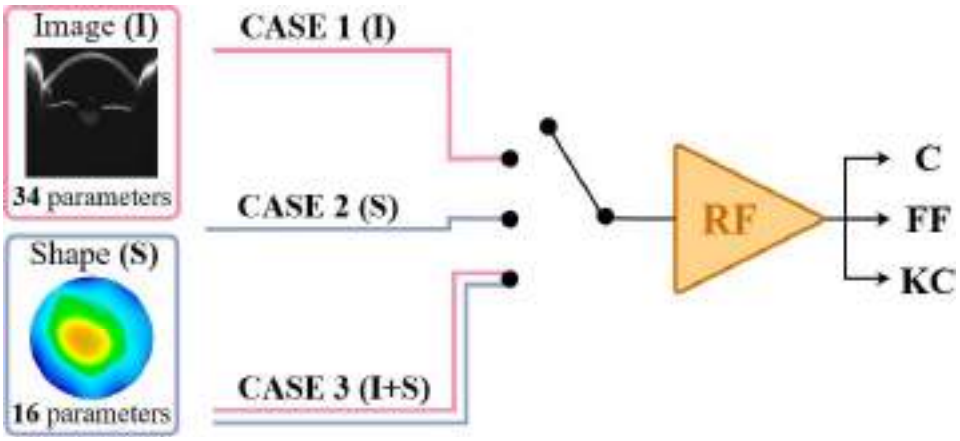

Figure 1: Diagram of the different input data cases selected for classifying the three classes using a random forest (RF) model. C: control; FF: forme fruste keratoconus; KC: clinical keratoconus.

RESULTS

The best results were obtained by combining corneal shape parameters with image-related features, leading to an overall accuracy of 86.40% and an AUC of 0.94, as shown in Table 1.

	Accuracy	Sensitivity	Specificity	AUC	AUC C	AUC FF	AUC KC
Case 1 (I)	69.80%	54.79%	82.37%	0.83	0.89	0.76	0.83
Case 2 (S)	81.09%	70.54%	87.54%	0.88	0.87	0.76	0.99
Case 3 (I+S)	**86.40%**	**78.72%**	**91.14%**	**0.94**	**0.94**	**0.89**	**0.99**

Table 1: Performance metrics for the different cases evaluated in this work. I, image; S: shape; AUC, area under the curve; C: control; FF: forme fruste keratoconus; KC: clinical keratoconus. Combination of image and shape parameters is marked in bold.

CONCLUSION

This study supports the integration of both shape and image-derived tissue features to enhance machine learning-based detection of keratoconus, particularly in its preclinical stages. The importance of image-based information is further underscored by our recent work, which demonstrated that deep learning models trained on raw Scheimpflug images can effectively distinguish keratoconus by implicitly capturing both morphological and tissue-related cues[4]. Together, these findings highlight the value of incorporating image-derived data—either through explicit feature extraction, as in the present work, or via end-to-end learning approaches[4]—for preclinical detection of keratoconus.

ACKNOWLEDGEMENTS: This work has been supported by European Research Council under the European Union's Horizon Europe research and innovation programme, StG 2024 call, Grant/Award Number: 101162733.

[1]R. Ambrósio Jr et al.; *Am. J. Ophth.*, **251**, 126 (2023).
[2]I. Issarti et al.; *Comput. Biol. Med.*, **109**, 33 (2019).
[3]A. Consejo et al.; *Trans. Vis. Sci. Tech.*, **10**, 32 (2021).
[4]J. Casado-Moreno et al.; (2025)

Changes in the Corneoscleral Profile Induced by Soft Contact Lens

Laura Remón[1], Ana R. Arizcuren[2], Claudia Raufast[1], Diana Gargallo[1] and Alejandra Consejo[2]

[1] Department of Applied Physics, University of Zaragoza, C/Pedro Cerbuna s/n, 50009, Zaragoza, Spain.

[2]Aragon Institute for Engineering Research (I3A), University of Zaragoza, Zaragoza, Spain

Contact: lauremar@unizar.es

Purpose:

An accurate understanding of the corneoscleral profile is essential for optimal contact lens (CL) fitting, particularly for scleral lenses.[1,2] Traditionally assessed subjectively using slit-lamp biomicroscopy and fluorescein, there is increasing interest in objective and robust measurement techniques in clinical settings. While most studies focus on the central cornea, research shows that evaluating the corneoscleral profile-including parameters like limbus position and corneoscleral junction (CSJ) angle-provides valuable insights for soft lens fitting.

The present study aims to objectively quantify how short-term soft contact lens wear affects corneoscleral parameters (limbus position and CSJ), and to determine whether these effects differ across lens materials and eye surface region.

Methodoloy:

The study, approved by the Ethics Committee for Clinical Research of Aragon (PI22/531), involved 22 healthy European Caucasian participants (mean age: 21.0 ± 1.0 years). Only the left eye of each participant was evaluated. All subjects had normal ocular health, no history of eye conditions or CL wear, and visual acuity better than logMAR 0.10. Written informed consent was obtained from all participants after the study's nature and potential consequences were thoroughly explained.

This study was conducted over two separate days, at least one week apart. Each day included two visits: one in the morning (baseline) and another 8 hours later, following CL wear. A -0.50 D soft CL was fitted to avoid affecting vision. Two commercially available soft CLs from the same manufacturer (CooperVision, coopervision.com) were selected: a silicone hydrogel (SiHy) lens (MyDay) and a hydrogel (Hy) lens (Biomedics 1 Day Extra). Three-dimensional corneoscleral topography maps were created using the Eye Surface Profiler (ESP, Eaglet Eye, eaglet-eye.com). Raw anterior eye height data were exported to construct the 3D maps. From these maps, two key corneoscleral parameters were calculated across 360 semi-meridians: limbus position and the CSJ.

Statistical analysis was performed using SPSS software (ibm.com). A two-way repeated measures ANOVA was conducted independently for limbus position and CSJ angle to examine differences across sessions (before and after lens wear) and lens material (Hy and SiHy). Assumptions of normality, sphericity, and homogeneity of variances were confirmed using the Shapiro-Wilk, Mauchly's, and Levene's tests, respectively. Statistical significance was set at 0.05, with Bonferroni correction applied for multiple comparisons.

Results:

Table 1 shows the mean values of limbus position and corneoscleral junction (CSJ) angle for the 22 eyes in different sectors at baseline (before CL fitting) and 8 hours later, that is, immediately after CL removal for each material (Hy, hydrogel; SiHy, Silicone hydrogel).

A significant change in limbus position was noted after short-term soft CL wear (two-way ANOVA, $F(1, 43) = 10.73$, $p = 0.002$). However, the CL material did not influence the change in limbus position between sessions (two-way ANOVA, $F(1, 87) = 0.004$, $p = 0.98$, < 0.001). A statistically significant change in CSJ angle was observed after short-term soft CL wear (two-way ANOVA, $F(1, 43) = 5.77$, $p = 0.02$). However, the CL material did not influence the change in CSJ angle between sessions (two-way ANOVA, $F(1, 87) = 0.003$, $p = 0.96$).

	Baseline		After CL wear	
	Limbus position (mm)	CSJ angle (°)	Limbus position (mm)	CSJ angle (°)
Hy				
Inferior	6.21 ± 0.21	177.1 ± 0.5	6.48 ± 0.29	177.6 ± 0.4
Temporal	5.62 ± 0.08	177.9 ± 0.3	5.70 ± 0.07	178.3 ± 0.2
Superior	5.73 ± 0.29	177.9 ± 0.4	5.85 ± 0.27	178.2 ± 0.3
Nasal	6.55 ± 0.41	176.6 ± 0.5	6.73 ± 0.11	177.0 ± 0.5
SiHy				
Inferior	6.27 ± 0.28	177.0 ± 0.6	6.43 ± 0.27	177.5 ± 0.5
Temporal	5.61 ± 0.06	177.9 ± 0.3	5.73 ± 0.06	178.2 ± 0.3
Superior	5.71 ± 0.28	177.8 ± 0.6	5.83 ± 0.23	178.3 ± 0.5
Nasal	6.59 ± 0.10	176.3 ± 0.6	6.71 ± 0.13	176.8 ± 0.5

Table 1: Mean values of limbus position and corneoscleral junction (CSJ) angle ± standard deviation in different sectors at the baseline session (before CL fitting) and 8 h later.

Conclusions:

After 8 hours of soft CL wear, significant changes in corneoscleral profile parameters were observed. These results indicate the importance of biocompatibility with CL materials. Although the clinical implication of these changes requires further experimentation, these findings may provide a useful additional metric to monitor subclinical anterior ocular changes due to CL wear.

ACKNOWLEDGEMENTS:
Grant TED2021-130723A-I00 funded by MCIN/AEI/10.13039/501100011033 and by European Union "NextGenerationEU"/PRTR

[1] D. Fadel; *Cont Lens Anterior Eye*, **41**,321 (2018).
[2]M. Ritzmann, PJ Caroline, R Börret, E Korszen; *Cont Lens Anterior Eye*, **41**, 205 (2018).

Analysis of changes in intraocular pressure and ocular perfusion pressure in young athletes: a preliminary study.

Aida Ramón-Campillo[1], Javier Gene-Morales[2,3], Ángel Saez-Berlanga[2], Alvaro Juesas[2], Inmaculada Bueno-Gimeno[1] and Andrés Gené-Sampedro[1,3]

[1] Department of Optics and Optometry and Vision Sciences, Faculty of Physics, University of Valencia, Dr Moliner, 50, 46100, Burjassot, Spain
[2] Group Prevention and Health in Exercise and Sport (PHES), Department of Physical Education and Sports, University of Valencia, Gascó Oliag, 3, 46010, Valencia, Spain
[3] Research Institute on Traffic and Road Safety (INTRAS), University of Valencia, Serpis, 29, 46022, Valencia, Spain

Contact: airacam@alumni.uv.es

Introduction: Intraocular pressure (IOP) is a key indicator of ocular health, influenced by age and various physiological changes.[1,2] Physical exercise can help regulate IOP, potentially reducing the risk of glaucoma,[3,4] although its effect vary depending on the type of exercise and the physical characteristics of the individual.[3]
Low-intensity aerobic or resistance exercise with light loads typically lower IOP, whereas high-load strength training may lead to an increase.[3] Commonly, the weight to be used during resistance training is calculated as % of one-repetition maximum (1RM), which is the weight with which an athlete can only perform one repetition. The load for 1RM can be calculated by different tests, e.g., performing one repetition with increasing loads until reaching the 1RM. Considering that IOP can be increased with maximal loads, the question arises as to whether evaluating the 1RM through repetitions to failure with submaximal loads could maintain stable IOP levels.
Therefore, this study aimed to evaluate IOP acute changes after a squat repetition-to-fatigue test with submaximal loads in young, trained, healthy individuals.

Methods: This study involved 12 volunteer participants (66.67% male) with a mean age of 25.36 ± 4.32 years, height: 1.72 ± 0.10 m, body mass: 71.30 ± 12.65 kg, body fat: 13.11 ± 4.91%, and relative strength (ratio 1RM load to body weight): 1.50 ± 0.30. These parameters indicated that the participants were in good physical condition.
The exercise selected was the parallel squat performed in a Smith Machine (Powerline PSM144X) performed at maximal concentric speed and two-second eccentric phase. Physiological variables including systolic blood pressure (SBP), diastolic blood pressure (DBP), mean blood pressure (MBP), heart rate (HR), IOP, and mean ocular perfusion pressure (MOPP) were recorded at baseline, after the general warmup (Measurement 1), after a submaximal effort (Measurement 2), and after each of the sets needed to calculate the 1RM (Measurements 3, 4, and 5). The test consisted of performing the maximum number of repetitions in a range from 8 to 15, if the weight was not enough or too much so that participants could perform more or less than 15 or 8 repetitions, another set was completed after a rest of 5 minutes. Most of participants completed the test in two sets (Measurements 3 and 4), only four participants performed a third set (Measurement 5). The IOP and BP measurements were conducted an average of 11.68 ± 2.75 and 43.78 ± 7.73 seconds after the end of the exercise, respectively.
A BP and HR monitor, and a rebound tonometer were used to measure BP and IOP, respectively. HR was collected immediately following exercise with a Polar chest strap. MBP and MOPP were calculated using the following formulae:

(1) $MOPP = \frac{2}{3}(MBP) - IOP$ (2) $MBP = DBP + \frac{1}{3}(SBP - DBP)$

Statistical analysis was performed with SPSS software, confirming a normal distribution using the Shapiro-Wilk test. An ANOVA was applied to assess the effects of the exercise on the dependent variables.

Results: A significant effect of time was found on all the variables studied ($p < .001 – .009$). Specifically, IOP did not significantly change from pre-exercise values, it only significantly decreased in Measurement 3 ($p = .002$) with tendencies of decreases in Measurements 1 and 4 ($p = .059 – .072$). All the cardiovascular parameters, including MOPP significantly increased compared to baseline ($p < .05$), with tendencies appearing in DBP. Figures 1 and 2 show the variation of IOP and MOPP.

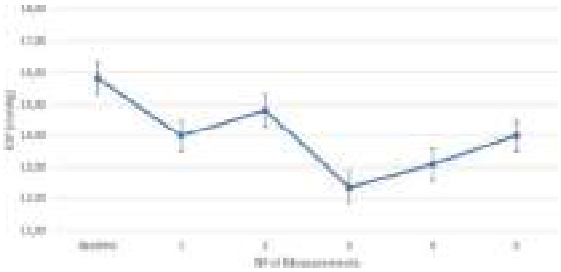

Graph 1. The mean and standard deviation of the IOP obtained in each of the measurements.

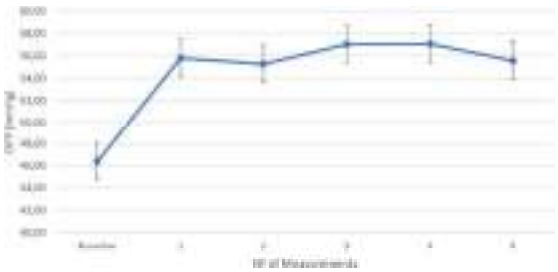

Graph 2. The mean and standard deviation of the MOPP obtained in each of the measurements.

Discussion: This study evaluated changes in IOP and MOPP in young athletes after performing squats. The analysis showed a decrease in IOP after exercise compared to baseline values, without clinical significance. As for MOPP, there was a significant increase when compared to baseline values, but not between exercise sets.

Although we did not measure the IOP during the exercise, the results are consistent with previous studies, confirming that IOP tends to return rapidly to baseline levels after potential increases during maximal squats.[3–5] Additionally, isometric exercises produce more increase than isokinetic ones.[6]

Conclusion: Our findings suggest that post-exercise IOP levels remain relatively stable after a repetition-to-failure test with submaximal loads in healthy young adults. However, caution should be applied since previous studies suggest that IOP may raise during the exercise. It is crucial to consider this effect, especially in glaucoma patients, and to encourage collaboration between exercise experts, ophthalmologists and optometrists to raise awareness of the risks to eye health.

1. Kawase K, Tomidokoro A, Araie M, et al. Ocular and systemic factors related to intraocular pressure in Japanese adults: the Tajimi study. *Br J Ophthalmol*. 2008;92(9):1175-1179. doi:10.1136/bjo.2007.128819
2. Schmidl D, Garhofer G, Schmetterer L. The complex interaction between ocular perfusion pressure and ocular blood flow – Relevance for glaucoma. *Exp Eye Res*. 2011;93(2):141-155. doi:10.1016/j.exer.2010.09.002
3. Vera J, Jiménez R, Redondo B, et al. Investigating the Immediate and Cumulative Effects of Isometric Squat Exercise for Different Weight Loads on Intraocular Pressure: A Pilot Study. *Sports Health Multidiscip Approach*. 2019;11(3):247-253. doi:10.1177/1941738119834985
4. Vera J, Raimundo J, García-Durán B, et al. Acute intraocular pressure changes during isometric exercise and recovery: The influence of exercise type and intensity, and participant´s sex. *J Sports Sci*. 2019;37(19):2213-2219. doi:10.1080/02640414.2019.1626072
5. Gene J, Colado JC, Perez-Castilla A, et al. Acute Intraocular Pressure Responses to Resistance Training in Combination with Blood Flow Restriction. *Research Quarterly for Exercise and Sport*. 2022;94(4):1110-1116. doi:10.1080/02701367.2022.2119197
6. Bakke EF, Hisdal J, Semb SO. Intraocular Pressure Increases in Parallel with Systemic Blood Pressure during Isometric Exercise. *Investig Opthalmology Vis Sci*. 2009;50(2):760. doi:10.1167/iovs.08-2508

Assessing Intraocular Pressure During Fenestrated Scleral Lens Wear: A Novel Methodology

Rita Seco[1], Joana Silva[1], José M. González-Méijome[1] and, Rute J. Macedo de Araújo[1]

[1] Ceorlab, Centre of Physics, University of Minho and Porto (CF-UM-UP), (Rua da Universidade, 4710-057, Braga, Portugal)

Contact: ritamariaseco@gmail.com

Purpose: Monitoring intraocular pressure (IOP) during scleral contact lens (ScCL) wear is particularly important for patients who must use these lenses for extended periods, either for therapeutic purposes or visual rehabilitation. However, conventional tonometry techniques are limited by the presence of the lens. This study aimed to evaluate IOP in healthy individuals while wearing fenestrated scleral lenses, without removing the lens, and to investigate whether peripheral measurements through a peripheral fenestration—avoiding the optic zone—offer a reliable alternative to central IOP measurements.

Methods: This experimental study included 14 adults (mean age 23.86 ± 3.39 years) with healthy corneas, evaluated across three visits. IOP was measured before, during, and 90 minutes after fenestrated ScCL wear using a rebound tonometer (iCare, Helsinki, Finland). All measurements were performed at a consistent morning time to reduce circadian variation, and visit order was randomized. In one visit, no lenses were worn, and IOP was measured on the central cornea to establish baseline values. In the second and third visits, all participants were fitted with Hexafocon A–fenestrated ScCLs (Senso MiniSclera, Procornea, Netherlands) with identical parameters: 16.4 mm diameter, 3.25 mm sagittal height, and the same haptic zone geometry. Each lens had a single 1 mm fenestration, located either centrally or temporally. Statistical analysis was performed using R software (v.4.4.2), with $p < 0.05$ considered statistically significant.

Results: In the visit without ScCL wear, a significant reduction in temporal IOP was observed after 90 minutes (−1.42 ± 2.2 mmHg, $p = 0.04$, Wilcoxon), while central IOP showed a slight but non-significant decrease. When participants wore the ScCL with a central fenestration, central IOP increased significantly after 90 minutes of lens wear (1.7 ± 2.1 mmHg, $p = 0.02$, Wilcoxon), returning to baseline after lens removal. In this condition, temporal IOP was only measured before and after lens wear, showing no significant change ($p = 0.93$, Wilcoxon), as no fenestration was present in that region.

Conversely, when the lens had a temporal fenestration, temporal IOP increased by 2.4 ± 2.9 mmHg after 90 minutes ($p = 0.07$, Wilcoxon), returning to baseline after removal ($p = 0.95$, Wilcoxon). In this case, central IOP was only assessed before and after lens wear, with no significant variation observed ($p = 0.83$, Wilcoxon), as the absence of a fenestration in the optical zone made it impossible to measure IOP centrally during lens wear.

Conclusion: The use of custom-fenestrated scleral lenses combined with a modified iCare probe enabled reliable IOP measurement without removing the lens. Peripheral measurements showed similar changes to central values, suggesting a potentially viable approach for continuous IOP monitoring in ScCL wearers in both clinical and research settings.

ACKNOWLEDGEMENTS: This work was supported by the Fundação para a Ciência e a Tecnologia (FCT))

Driving performance under the influence of visual distraction from smartwatch and navigation system use

Miriam Casares-López[1]. Álvaro García Gallardo and Sonia Ortiz-Peregrina[1]

[1] Laboratory of Vision Sciences and Applications. Department of Optics. Faculty of Science. University of Granada. Avenida Fuentenueva s/n. 18007 Granada. Spain

clmiriam@ugr.es

Introduction: In recent years, the use of smart devices while driving has increased exponentially, leading to greater driver distraction. These devices add visual demands on the driver, on top of the already significant visual requirements of driving.
Purpose: This study aimed to investigate the impact of visual distraction caused by the use of a smartwatch and a navigation tablet during driving, and to determine which visual functions and other factors most strongly influence driving performance.
Methods: The study included 26 regular drivers aged 21 to 47 years. Visual function was assessed through tests of central and peripheral static visual acuity (VA), central and peripheral contrast sensitivity (CS), Straylight, and stereopsis. Stereopsis, VA and CS were performed at a distance of 40 cm, with peripheral vision assessed at 30° eccentricity.[1,2] Driving performance was tested using a simulator in three different sessions: one with no visual distraction (baseline) and two with either a smartwatch or a tablet simulating a navigation system. In the smartwatch and navigation screen sessions, participants were required to perform three different tasks (secondary tasks) across two types of roads: dual carriageway and mountain road. An overall driving performance score (ODPS) was computed from several driving variables: higher ODPS values indicated better driving performance.[3,4] The influence of visual variables and other factors such as age, sex, and driving frequency on ODPS was analyzed using a generalized linear mixed model (GLMM).

Figure 1. Experimental setup of the driving task

Results: All participants demonstrated normal visual function. Driving performance significantly worsened with both the smartwatch and the navigation screen, as reflected by a reduced ODPS ($p<.001$ for both conditions compared to baseline), with no significant difference between the two

devices. On dual carriageway, the most affected parameters were related to speed, steering control, and lane positioning. On mountain roads. the most affected parameters were related to lane positioning. According to the GLMM (Table 1), in addition to the visual distraction condition (baseline, smartwatch and navigation tablet). both road type (p<.001) and biological sex (p=0.006) had significant effects on ODPS. Among the visual parameters, Straylight, CS, and peripheral VA were the most influential: participants with lower straylight, better CS, and better peripheral VA achieved higher ODPS values.

Table 1. Results of the GLMM. The ODPS was selected as dependent variable; visual distraction conditions, road type, age, biological sex, driving frequency, perceived driving difficulty, and the different visual variables) were selected as fixed factors; subjects was selected as random effect.

	coefficient	SE	t statistic	p-value	95% CI
Intercept	3.499	1.5206	2.301	0.023	[0.492, 6.505]
Visual distraction condition					
Baseline	0.412	0.1251	3.291	0.001	[0.164, 0.659]
Smartwatch	-0.061	0.0914	-0.672	0.503	[-0.242, 0.119]
Navigation screen	.	.	.	.	.
Road type					
Dual Carriageway	0.732	0.0726	10.076	0	[0.588, 0.875]
Mountain road	.	.	.	.	.
Age	0	0.0099	0.015	0.988	[-0.02, 0.02]
Biological sex					
Male	0.286	0.1026	2.788	0.006	[0.083, 0.489]
Female	.	.	.	.	.
Driving frequency	-0.032	0.0185	-1.736	0.085	[-0.069, 0.004]
Perceived driving difficulty	-0.035	0.0252	-1.398	0.164	[-0.085, 0.015]
VA	0.613	0.3158	1.941	0.054	[-0.012, 1.237]
Straylight (logS)	-2.322	0.5573	-4.165	<.001	[-3.424, -1.22]
CS	-0.027	0.0111	-2.437	0.016	[-0.049, -0.005]
Peripheral VA	8.338	1.6677	5.000	<.001	[5.041, 11.636]
Peripheral CS	-0.229	0.2978	-0.770	0.443	[-0.818, 0.360]
Stereopsis	0.002	0.0034	0.519	0.605	[-0.005, 0.008]

SD: standard error; AV: visual acuity; CS: contrast sensitivity; CI: confidence intervals

Conclusions: Driving performance significantly deteriorates when visual distraction from a smartwatch or navigation device is introduced. The most influential visual parameters were straylight, contrast sensitivity, and peripheral visual acuity. These findings contribute to a better understanding of the negative impact of visual distractions during driving, offering insights for improving road safety.

ACKNOWLEDGEMENTS: MCIN/AEI/10.13039/501100011033 (grant number PID2019-105684RB-I00); and FEDER/Junta de Andalucía-Consejería de Transformación Económica, Industria, Conocimiento y Universidades (grant number A-FQM-532-UGR20)

[1]M. Casares-López, S. Ortiz-Peregrina et al; *Scientific Reports.* **15***.* 1 (2025).
[2]S. Ortiz-Peregrina, M. Casares-López et al; *Biomedical Optics Express.* **13**. 10 (2022).
[3]C. Ortiz, S. Ortiz-Peregrina et al; *Accident Analysis and Pervention.* **117**. (2018).
[4]M. Casares-López, J.J. Castro-Torres et al; *Scientific Reports.* **10**. 1 (2020)

Colour Vision in Early Parkinson's Disease: MUC Test Assessment

Alba Herrero-Gracia[1], Rosa Hernández-Andrés[1], María José Luque[1] and M Amparo Díez-Ajenjo[1]

[1] Department of Optics and Optometry and Vision Sciences, Faculty of Physics, University of Valencia (C/ Doctor Moliner 50, 46100, Burjassot, Spain)

[2] Fundación de Oftalmología Médica de la Comunitat Valenciana (Av. Pío Baroja 12, 46015, Valencia, Spain)

Contact: alba.herrero@uv.es

Introduction: Parkinson's disease (PD) affects over 7 million people globally, with numbers expected to rise by 2030. It causes motor and non-motor symptoms, and while there is no cure, early treatment focuses on symptom relief.[1] PD is associated with a variety of visual symptoms, such as reduced visual acuity, impaired contrast sensitivity and colour perception, and changes in the visual field, which can have a significant impact on daily activities, social interaction and quality of life.[2] Previous studies have shown that colour vision is impaired in PD patients. These studies were performed with tests that do not correctly characterise colour vision (Ishihara) or with tests that are difficult for PD patients to use (Farnsworth Munsell 100 Hue).[3] The aim of the present study was to compare the colour vision of people with early PD with an age- and sex-matched control group (CG) using a colour vision test that correctly characterises colour vision and is easy for people with PD to use. This is the *Medida de Umbrales Cromáticos* (MUC) test, which is administered on a computer.[4]

Methodology: All participants provided informed consent for this descriptive, observational, prospective, and cross-sectional study, which followed ethical principles established by the Declaration of Helsinki. Inclusion criteria were ages 50-59, no eye or systemic diseases affecting vision, no neurodegenerative diseases other than Parkinson's, no vision-affecting medications, and ability to follow the test. Participants with Parkinson's had to be diagnosed by a neurologist and meet specific criteria. Control group participants were matched by age and gender and recruited from a university community. The study was approved by ethics committees and registered on clinicaltrials.gov. Participants took the monocular MUC test while seated in a dark room, using an HP PROBOOK 450G7 computer with colour calibration (1920x1080 resolution, 34.5x19.5 cm screen size) at full brightness and contrast, 80 cm away. The dominant eye was determined using a red filter dominance test, and participants wore their optimal optical correction. The test was completed in a single 15-minute session. The MUC test measures chromatic discrimination thresholds by recognising the orientation of a Landolt C letter, which differs in chromaticity from the background, using a psychophysical bisection method. A random luminance pattern minimizes acromantic interference, and the stimulus's spatial parameters, chromaticity, and luminance are user-configurable. The test explores equidistant directions in a constant response plane in the DeValois space, with results provided in the CIE1931 space. It is a modification of the classic Arden test, implemented in Matlab using the COLORLAB library.[5] Statistical analysis was performed using IBM SPSS Statistics 28.0.1. The variables analysed included age, sex, best corrected visual acuity (BCVA), major (a) and minor (b) semi-axes values, orientation (θ), and the area of the best-fitting ellipse for the colour discrimination threshold provided by the MUC test. Descriptive analysis of central tendency and dispersion was conducted, along with normality testing using the Shapiro-Wilk test. Differences between groups were compared using the Mann-Whitney U test, with statistical significance set at $p < 0.05$.

Results: A total of 14 healthy participants (9 females, average age 52 years, BCVA: -0.12) and 8 participants with PD (8 females, average age 52 years, BCVA: -0-08) were recruited. Figures 1 and 2 show the mean and standard deviation of the variables for both groups. The units for the different variables were age (years), orientation (degrees), semi-axes (not specified), and BCVA (Log Unit, LogMAR scale). The SW test results indicated that none of the variables followed a normal distribution ($p<0.05$). Statistically significant differences were found between the groups using the MW test for the variables a ($p=0.003$) and b ($p=0.002$), with higher values in the Parkinson's group. However, no significant differences were found for age ($p=0.53$), sex ($p=0.22$), BCVA ($p=0.37$), and orientation ($p=0.57$).

Discussion: Patients with PD show impairments in colour vision, affecting both the red-green and blue-yellow pathways. This study found that, in Parkinson's patients, the ellipse generated by the MUC programme is larger, both in the major axis (red-green pathway) and minor axis (blue-yellow pathway), compared to healthy subjects. In line with previous studies, Silva et al. (2005) concluded that only the red-green pathway was affected in PD patients, but this study extends the finding to include the blue-yellow pathway, as shown in other studies using the Farnsworth-Munsell 100 Hue test.[6–8] This research enhances the understanding of visual deficits in Parkinson's patients, potentially influencing the development of diagnostic tools, progression monitoring, and clinical management strategies in early stages.

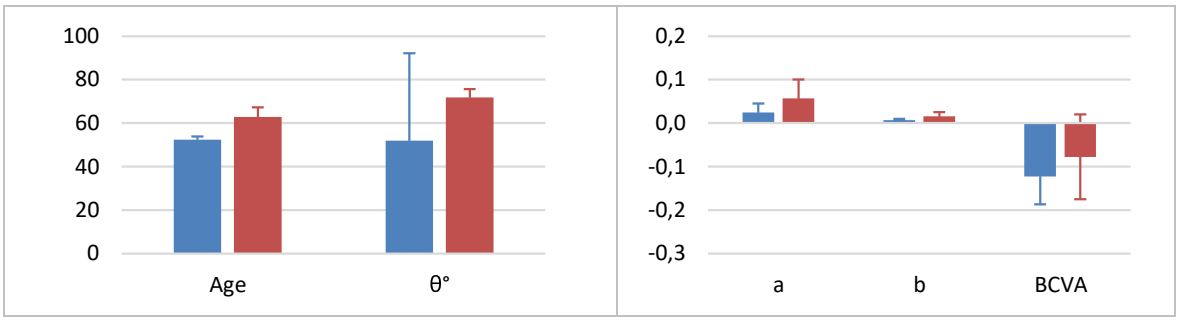

Figure 1: Mean and standard deviation for the variables of the CG (blue) and PG (red) groups.

ACKNOWLEDGEMENTS: A big thank you to the Neurology Service of the Hospital Arnau de Vilanova and the Asociación Parkinson Valencia for helping us to recruit for this study. Their support was key to making this research possible. This work was supported by the University of Valencia through the Predoctoral Research Training Contract awarded to the first author [Atracción de Talento 2022, UV-INV_PREDOC22-2153229].

[1]SG. Reich and JM. Savitt; *Med Clin North Am*, **103**, 337 (2019).
[2]Borm, F. Visser, M. Werkmann et al; *Neurology,* **94**, E1539 (2020).
[3]YS. Oh, JS. Kim, SW. Chung et al; *Eur J Neurol,* **18**, 577 (2011).
[4]MJ. Luque, D. De Fez and MC. Domene; MUC Medida de Umbrales Cromáticos Manual de instalación y uso.
[5]J. Malo and MJ. Luque; COLORLAB: a colour processing toolbox for Matlab.
[6]MF. Silva, P. Farja, FS. Regateiro et al; *Brain,* **128**, 2260 (2005).
[7]NI. Bohnen, J. Haugen, A. Ridder et al; *Mov Disord Clin Pract*, **4**, 864 (2017).
[8]L. Kertelge, N. Brüggemann, A. Schmidt et al; *Movement Disorders,* **25**, 2665 (2010).

Does cannabidiol use affect visual function and optical quality?

Francesco Martino[1], Sonia Ortiz-Peregrina, Miriam Casares-López, Pilar Granados-Delgado, José Juan Castro-Torres and Rosario G. Anera

[1] Laboratory of Vision Sciences and Applications, Department of Optics, Faculty of Sciences, University of Granada (Prof. Adolfo Rancaño, s/n 18071, Granada, Spain)

francesco@ugr.es

Introduction: Cannabidiol (CBD) is the main non-psychotropic constituent of cannabis. The use of CBD has increased significantly[1]. Several studies have found numerous beneficial and therapeutic effects of CBD, such as neuroprotective, anxiolytic, anti-epileptic and antioxidant properties[2]. Regarding ocular health, it has been reported that CBD may reduce intraocular pressure (IOP), which could be useful in the treatment of glaucoma[3]. In diabetic retinopathy, CBD could reduce retinal cell death and blood retinal barrier breakdown[4]. Endocannabinoid receptors, mainly the CB1, play an important role in maintaining ocular homeostasis. These receptors are located in important locations at the visual system such as the ciliary body or the retina[5]. However, no studies have yet assessed the effects of isolated CBD use on visual function and optical quality.
Purpose: To study and compare the effect of different concentrations of CBD on vision using objective and subjective tests to assess optical quality and visual function.
Methods: A randomized, double-blind, placebo-controlled, experimental study was conducted. Thirty participants with a mean age of 26.0 ± 6.3 years were enrolled. Placebo (0 mg of CBD), 15% (16 mg of CBD), and 30% (32 mg of CBD) concentrations of CBD were employed. Visual function was evaluated through different tests: pupil size, static and dynamic visual acuity, contrast sensitivity, dot motion detection, Visual Disturbance Index (VDI) and stereoacuity, and optical quality was assessed by log(s), MTF-cutoff, Objective Scatter Index (OSI), and Strehl ratio (SR).
Results: No changes in pupil size were found after CBD use (scotopic: P=0.31; low mesopic: P=0.21; high mesopic: P=0.27). There was no significant impairment of static and dynamic visual acuity (P>0.05). Contrast sensitivity was not affected by CBD use (P>0.05). No deterioration in stereoacuity was observed at distance (P=0.08) or near (P=0.58). Mean dot motion detection showed no differences between the three concentrations. For optical quality, none of the parameters worsened with CBD use (P>0.05). No changes were observed for VDI.
Conclusion: The study revealed that vaporized CBD did not result in any short-term deterioration in optical quality or visual function. This non-psychotropic cannabinoid (CBD) did not appear to adversely affect vision and seems to be a safe substance in the short term for the concentrations assessed. The results of this study could be useful and helpful for evidence-based decision making for public health policy regarding its use.

	CBD 0% mean (SD)	CBD 15% mean (SD)	CBD 30% mean (SD)	Statistic (χ^2/F*)	*P* -value
log(s)	0.81 ± 0.11	0.83 ± 0.17	0.84 ± 0.11	1.299	0.52
MTF-cutoff (cpd)	37.23 ± 9.31	36.46 ± 8.69	37.40 ± 9.21	0.200	0.91
OSI	0.62 ± 0.50	0.61 ± 0.40	0.59 ± 0.43	0.055	0.97
Strehl ratio	0.26 ± 0.05	0.21 ± 0.05	0.21 ± 0.05	0.180*	0.84

logarithm of straylight, log(s); Modulation Transfer Function cutoff, MTF-cutoff; Objective Scatter Index, OSI.

Table 1: Comparison of the optical quality parameters under the three CBD conditions (0%, 15% and 30%).

		CBD 0% Mean ± SD	CBD 15% Mean ± SD	CBD 30% Mean ± SD	*P*-value
Pupil size (mm)	Scotopic	6.53 ± 0.80	6.36 ± 0.77	6.30 ± 0.79	0.31
	Low mesopic	5.21 ± 1.05	5.25 ± 0.95	4.95 ± 0.97	0.21
	High mesopic	4.70 ± 0.99	4.62 ± 0.92	4.45 ± 0.91	0.27
SVA	Monocular	1.12 ± 0.20	1.07 ± 0.15	1.11 ± 0.17	0.68
	Binocular	1.25 ± 0.17	1.23 ± 0.12	1.28 ± 0.14	0.35
Mean DVA	Monocular	0.57 ± 0.11	0.57 ± 0.09	0.58 ± 0.12	0.93
	Binocular	0.69 ± 0.11	0.68 ± 0.09	0.68 ± 0.08	0.31
VDI	Monocular	0.22 ± 0.16	0.22 ± 0.18	0.25 ± 0.22	0.48
	Binocular	0.15 ± 0.10	0.14 ± 0.07	0.19 ± 0.17	0.06
Stereoacuity (arcsec)	Distance	61.67 ± 61.14	56.33 ± 56.84	70.00 ± 58.66	0.08
	Near	28.83 ± 14.67	31.67 ± 15.88	30.67 ± 15.08	0.58

Static and dynamic visual acuity (SVA, DVA); Visual Disturbance index, VDI.

Table 2: Comparison of visual function test results under the three CBD conditions (0%, 15% and 30%).

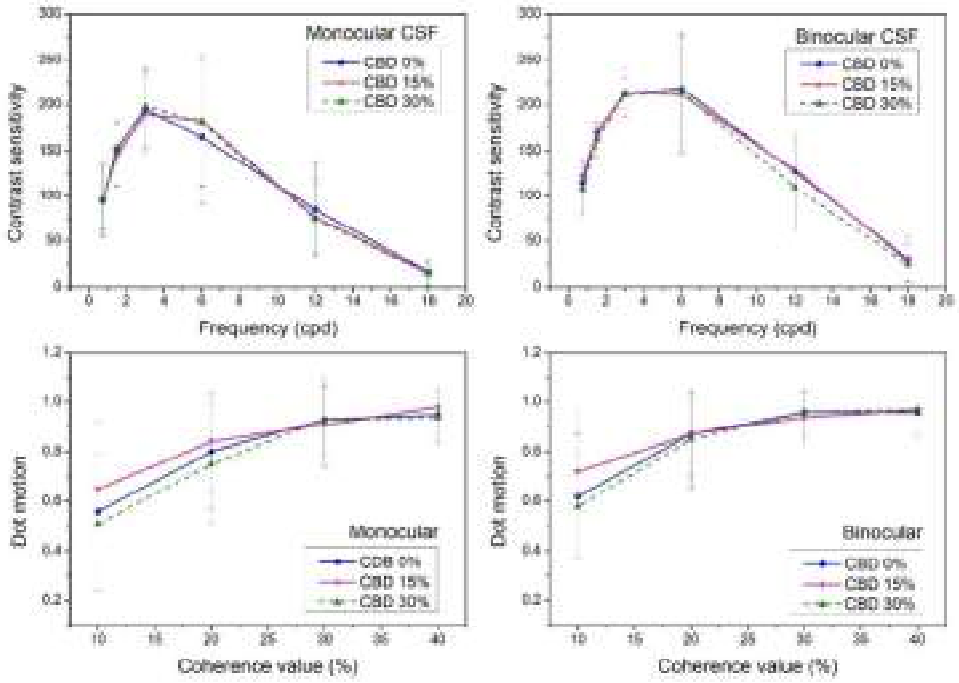

Figure 1: Contrast sensitivity and dot motion detection under different CBD conditions (0%, 15% and 30%).

ACKNOWLEDGEMENTS: We thank Dräger Hispania S.A.U. (Madrid, Spain) and LABOGRAN (Granada, Spain) for lending us the drug analyser. Grants C-EXP-194-UGR23 funded by Consejería de Universidad, Investigación e Innovación and by ERDF Andalusia Program 2021-2027 and PID2020-115184RB-I00, funded by MCIN/ AEI/10.13039/501100011033.

[1] Goodman S, Wadsworth E, et al; Cannabis and Cannabinoid Research, **7**,3 (2022).
[2] Campos AC, Fogaça MV, et al; Pharmacological Research, **112**,119 (2016).
[3] Wang MTM and Danesh-Meyer HV; Survey of Ophthalmology, **66**,2 (2021).
[4] Su EN, Kelly ME, et al; Investigative Ophthalmology & Visual Science, **56**,6 (2015).
[5] Yazulla S; Progress in Retinal and Eye Research, **27**,5 (2008).

Age-related changes of the foveal neural contrast sensitivity function

Sara Silva-Leite[1], Jonas Müller[2], Siegfried Wahl[1,2] and Niklas Domdei[1]

[1]Carl Zeiss Vision International GmbH. (Aalen, Germany)
[2]Institute for Ophthalmic Research, Eberhard Karls University Tübingen. (Tübingen, Germany)

Contact: sara.silva@zeiss.com

Purpose: Determine whether the known decline in visual function of older adults[1] is solely due to optical factors or involves neural alterations.

Methods: We conducted an observational, monocentric, cross-sectional study to measure the foveal neural contrast sensitivity function (NCSF). Before the NCSF measurements, all participants underwent a comprehensive optometric examination to confirm their refractive status and ensure compliance with the eligibility criteria, specifically the exclusion of macular diseases. The measurements were performed using an interferometric setup[2] allowing to bypass the eye's optics. Horizontal interference fringe stimuli ($\lambda = 550 \pm 5$ nm; 1.5° field-of-view) were projected directly on the retina. We used a psychophysical adaptive staircase algorithm (QUEST) in a two-interval forced choice (2IFC) paradigm to determine the contrast thresholds, with a minimum of 30 and a maximum of 50 trials per measurement. Thresholds were measured three times for each spatial frequency (3, 6, 9, 12, 18, 24, and 30 cpd) in a randomised sequence. The area under the curve (AUC) was calculated as the numerical integration (Matlab: trapz).

Results: We evaluated the dominant eyes of 90 healthy participants aged between 20 to 80 years old (minimum of 10 participants per decade). All age groups show the typical shape of the neural contrast sensitivity curve, with peak sensitivity at 9 cpd (Figure 1A). The overall magnitude of contrast sensitivity is reduced in older participants, where the 70-79 age group shows the most prominent reduction across all spatial frequencies tested. The analysis of the area under the NCSF as a function of age reveals a highly significant correlation (p-value < 0.001, F-test; Figure 1B).

Conclusion: In this study, we show that NCSF decreases with increasing age, with more pronounced changes observed in participants over 70 years old. While optical degradation is well-documented in the literature, our results suggest that neural components—both the retina and the brain—contribute to the decline of visual function with age, too. This is important for estimating potential improvements in visual function, for example due to cataract surgery.

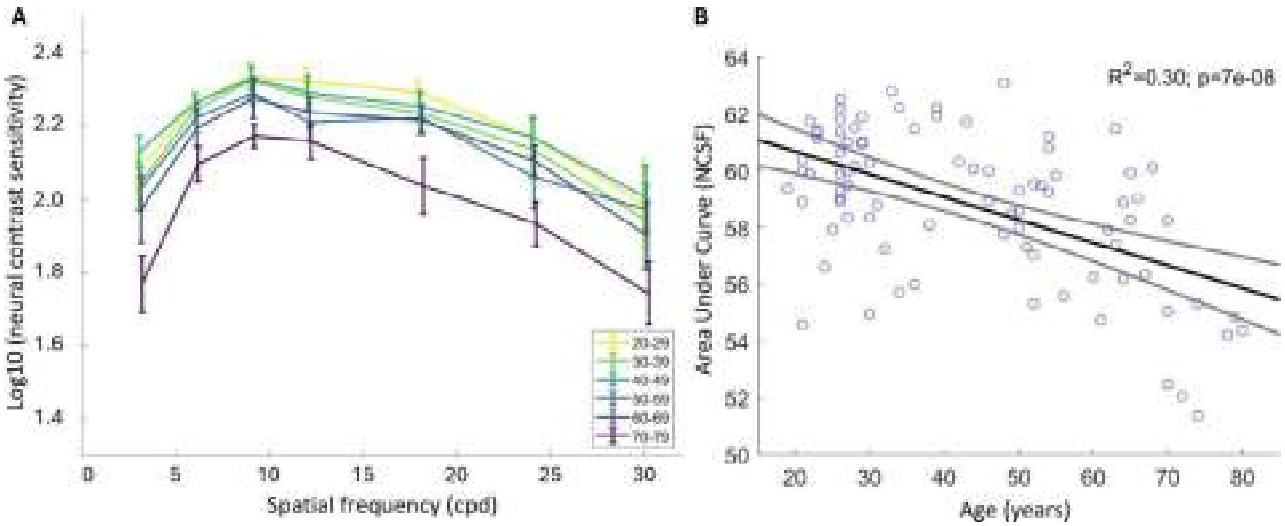

Figure 1: Changes of the neural contrast sensitivity function (NCSF) with age. A) NCS as a function of spatial frequency (cycles per degree, cpd) across different age groups. Each curve represents the mean log10 (NCSF) of each age decade, with error bars indicating the standard deviation. N ≥ 10 participants per decade. B) Correlation between the area under the NCSF curve and the age in years for all spatial frequencies analysed. The correlation coefficient and the *p*-value are represented in the figure (*p*-value calculated using a linear regression model).

ACKNOWLEDGEMENTS: This work was supported by the European Union's Horizon 2022 research and innovation programme under the Marie Sklodowska-Curie grant agreement [ACTIVA No 101119695]. The authors thank Jenny Lorén Witten, Antonia Roth, Dr. Med. Jan-Philipp Bodenbender and Dr. Med. Laura Kühlewein for their support during the measurements.

---

[1]C. Owsley; *Annual Review of Vision Science*, **2**, 255 (2016).
[2]N. Suchkov, T. Kurian, C. Schwarz, A. Leube and S. Wahl; *Biomedical Optics Express*, **12**, 6040 (2021).

Clinical implications of high-order aberrations for accommodation measurement in subjective refraction

Aina Turull-Mallofré, Carlos E. García-Guerra and Mikel Aldaba

Center for Sensors, Instruments and Systems Development, Universitat Politècnica de Catalunya, Rambla Sant Nebridi 10, 08222, Terrassa, Spain
Contact: aina.turull@upc.edu

Higher-order aberrations (HOAs), including 4th and 6th order spherical aberration, are known to have an impact on refractive error computation[1] and to change with accommodation, especially with higher accommodation stimuli.[2,3] However, practical limitations, such as pupil size, often restrict the measurement of higher-order aberrations in clinical settings. Although some studies recommend including these terms when studying accommodation, they typically examine wide defocus ranges (up to 5 D in 1 D steps) and suggest that their impact around 1 D is minimal; moreover, they do not explore changes with positive defocus, which is used as a method to relax accommodation in the fogging technique.[2,3] This narrower defocus range, however, is relevant to procedures like subjective refraction. This work aims to study the impact of 4th and 6th-order spherical aberration for estimating accommodative responses within a clinically relevant range of ±1 D using 0.25 D steps by analyzing responses using Zernike polynomials up to 6th order for a 4-mm fixed pupil.

In this study, the consensual through-focus accommodative response of healthy young adults was measured using a custom-developed Hartmann-Shack (HS) aberrometer coupled to a phoropter.[4] First, the subjective refraction endpoint, previously determined by an optometrist, was placed in the phoropter. Then, lenses ranging from +1.00 D to -1.00 D in 0.25 D steps were introduced in front of the non-measured eye while viewing a visual acuity chart placed at 5 m.

The spherical equivalent was calculated using three approaches: (1) least-squares fitting using the 2nd-order Zernike coefficients (LS), (2) paraxial curvature matching with up to the 4th-order Zernike coefficients (PC4), and (3) paraxial curvature matching using up to 6th-order Zernike coefficients (PC6).[1] Relative accommodation was derived for each method by referencing the most hyperopic point in the through-focus response. The three methods were compared by analysing differences in spherical equivalent and relative accommodation across the three methods at each stimulus level using ANOVA or a non-parametric equivalent if normality assumptions were not met.

Thirty-six participants took part in the study, with a mean age of 22.06 ± 3.70 years, ranging from 18 to 31 years. The mean spherical equivalent subjective refraction ± SD of the sample was -0.81 ± 1.45 D. The median spherical equivalent and accommodation for the through-focus response are represented in Figure 1.

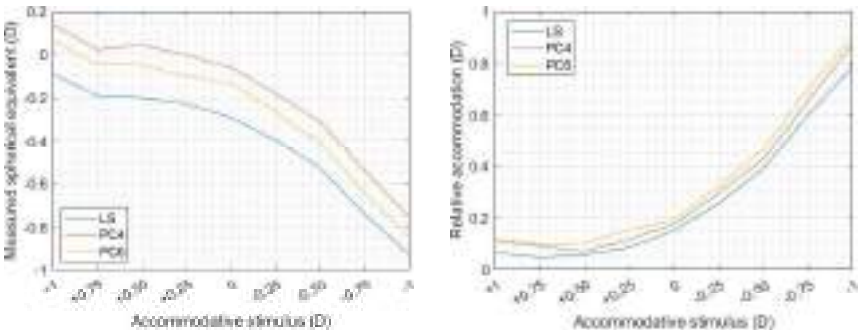

Figure 1. Left: Mean spherical equivalent across all subjects at each step of the through-focus response, computed using the three described methods from Zernike coefficients. Right: Mean relative accommodation across all subjects at each defocus step, calculated from the spherical equivalent using the three described methods from Zernike coefficients.

The computed mean differences between methods are described in Figure 2. No statistically significant differences were found between methodologies across any step of the through-focus response.

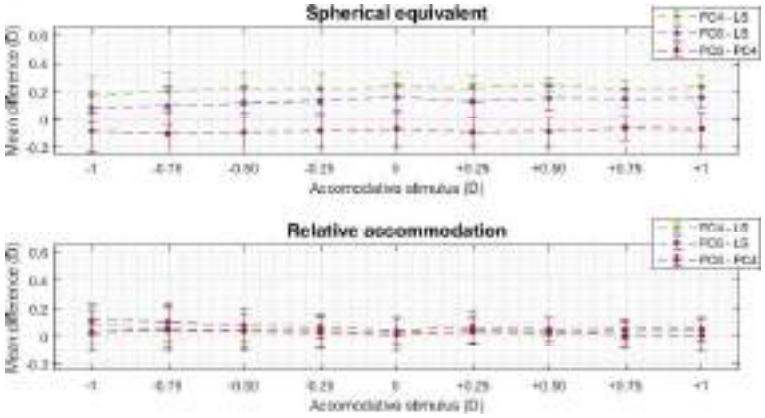

Figure 2. Mean difference in spherical equivalent error (up) and relative accommodation (down) between the computational methods, with standard deviation represented by error bars.

This study shows that including up to 6th-order spherical aberration terms has a minimal effect on the estimation of refractive error and accommodative responses within the ±1.00 D range using a fixed 4 mm pupil. Therefore, for clinical applications like monitoring accommodation during subjective refraction or refraction procedures based on the accommodative response,[5] including these higher-order terms, might not be essential for computing the accommodative response, simplifying the wavefront analysis and data acquisition procedure.

ACKNOWLEDGEMENTS: Grant PID2023-146101OB-I00 funded by MICIU/AEI/10.13039/501100011033 and by ERDF/EU.

[1] L. N. Thibos, H. Xin, A. Bradley and R. A. Applegate, *Journal of Vision*, **4**, 329 (2004).
[2] N. López-Gil and V. Fernández-Sánchez, *Journal of Vision*, **10**, 1 (2010).
[3] T. Buehren and M. J. Collins, *Vision Research*, **46**, 1633 (2006).
[4] C. E. García-Guerra, J. A. Martínez-Roda, J. C. Ondategui-Parra, A. Turull-Mallofré, M. Aldaba and M. Vilaseca, *Translational Vision Science & Technology*, **12**, 22 (2023).
[5] A. Turull-Mallofré, C. E. García-Guerra, M. Aldaba, M. Vilaseca and J. Pujol, *Investigative Ophthalmology & Visual Science*, **64**, 4987 (2023).

Visual field assessment using an automatic eye tracking perimetry

Eduardo Esteban-Ibáñez [1,2], Sara Guillén[1], Marina Vilella [1,2], Marta Lacort [1,2], Adrián Alejandre[1], Carmen Bilbao [2,3] and Marta Ortín[1]

[1] DIVE-Medical SL, Zaragoza, Spain
[2] Aragón Health Research Institute (IIS Aragón), Zaragoza, Spain
[3]Ophthalmology Department, Miguel Servet University Hospital, Zaragoza, Spain

Contact: eduardo.esteban@dive-medical.com

Purpose:
To develop and validate a visual field test that minimizes dependence on motor and cognitive skills, utilizing saccadic responses to visual stimuli measured through eye-tracking technology.

Methods:
The visual field test was implemented on a DIVE device (Device for an Integral Visual Examination, DIVE Medical SL, Spain).[1,2] The performance of the DIVE visual field test was compared to standard automated perimetry (SAP) in patients older than 6 years and to confrontation visual field testing in younger children. Visual fields were classified as normal and abnormal. Visual field defects were categorized as hemianopia, quadrantanopia, arcuate defect or unclassifiable defect. We quantified the agreement between both visual field assessments.

Results:
The age range of the participants was 3 to 83 years. The DIVE visual field test was successfully completed by all patients older than 6 years, and only 3 children younger than 6 years did not cooperate to finish the DIVE visual field exam. Sixty-eight paired exams from 35 participants were finally included in this study, with 18 exhibiting visual field defects on SAP and 50 having normal fields either on SAP or on confrontation tests. Compared to SAP, the DIVE visual field test demonstrated a sensitivity of 100% and a specificity of 96.9% for identifying normal versus abnormal visual fields. Agreement between DIVE and SAP defect categorization was observed in 66.7% of the cases. Additionally, all children younger than 6 years were classified as normal by both DIVE and confrontation methods.

Conclusions:
The DIVE visual field test demonstrates feasibility in patients older than 3 years of age and offers a promising alternative to traditional perimetry methods. Eye-tracking-based perimetry reduces patient demands while maintaining high diagnostic performance and reliability when compared to SAP.

References:
[1]E. Esteban-Ibañez et al.; *International Ophthalmology*, **42**, 747 (2022).
[2]V. Pueyo et al.; *Journal of Vision*, **22**, 4 (2022).

ACKNOWLEDGEMENTS: NEOTEC SNEO-20221063

Validation of a Laptop-Webcam-Based Eye Tracking System for Saccade Measurement

Lorenzo Fratini[1], Jaume Pujol[2], José Luis Güell[1] and Clara Mestre[2]

[1] Instituto de Microcirugía Ocular (IMO) Barcelona Grupo Miranza, Carrer de Josep Maria Lladó, 3, 08035 Barcelona, Spain

[2] Centre for Sensors, Instruments and Systems Development, Universitat Politècnica de Catalunya, Rambla Sant Nebridi 10, Terrassa 08222 (Barcelona), Spain

Contact: Lorenzo.fratini@imo.es

In recent decades, video oculography (VOG) has become the most popular eye tracking technique due to its performance, versatility, and minimal intrusiveness. Currently, most commercial video-based eye trackers utilise the pupil-corneal reflection technique, which is based on the detection of the pupil and one or more corneal reflections from an IR light source.[1] VOG has become essential in many fields such as psychology, marketing, or vision science and clinical diagnostics, enabling analysis of eye movements such as saccades, fixations, and smooth pursuits. High-performance commercial eye trackers offer precise measurements; however, their high-cost limits widespread accessibility, particularly for clinical and home-based applications.[2] Recently, deep learning has revolutionised conventional eye-tracking methods based on regressing gaze from the human eye appearance.[3] Deep learning-based eye tracking offers several advantages such as low hardware requirements, increased robustness to head movements, and reduced need for individual calibration procedures. The goal of this study was to compare the performance of a laptop-webcam-based eye tracking system to detect and distinguish between saccades and fixations with a research-grade eye tracker.

Binocular eye movements of 8 healthy adults with normal binocular vision (28.12±3.04 years) were recorded using the Tobii Pro Spectrum and a laptop webcam (Lenovo Thinkbook 14 G7 IML) simultaneously. Head movements were limited with a chinrest. The Tobii Pro Spectrum eye tracker was placed at the recommended distance of 70 cm and captured gaze data at 1200 Hz, while the webcam system was placed at 50 cm from the participants and captured data at 30 Hz. Stimuli were presented on the native Tobii Pro Spectrum screen with a resolution of 1920 x 1080 pixels (52.8 x 29.7 cm). Participants were instructed to follow a red dot (6 mm) on a white background that appeared for 1 to 3 s at the centre of the screen and at eccentricities of ±5, 15, 20 cm. Several Python scripts were developed to synchronize the stimulus presentation with the Tobii Pro Spectrum and laptop's webcam devices. For the webcam, we employed Google's MediaPipe Face Landmarker, a deep learning framework designed for real-time face landmark detection. MediaPipe estimates 3D facial landmarks from live video streams, facilitating the estimation of iris location and eye movements.[4] For the Tobii Pro Spectrum, raw data were exported. First, all data were normalised between [0,1] with respect to the display pixels and then, a Savitsky–Golay filter was used for smoothing raw signals. Eye velocity was computed by differentiation of the position signals, and saccades were detected using an adaptive velocity threshold algorithm. [5]

Figure 1 shows a representative example of horizontal eye position data obtained with the webcam system and the Tobii Pro Spectrum. For this analysis, the amplitudes of saccades made in response to the first 3 stimulus' position changes [from the center of the screen (0.5 in normalised units, norm-units) to +15cm (0.78 norm-units), -15cm (0.22 norm-units) and +5cm (0.59 norm-units)] were included. To study the agreement between the two systems, a Bland-Altman analysis with the

data across the eight participants was performed. For the smallest (0.28 norm-units), intermediate (0.37 norm-units) and largest saccadic amplitudes (0.56 norm-units), the mean ± SD of the differences in measured amplitude with the two systems were 0.05 ± 0.04 norm-units, 0.09 ± 0.07 norm-units, and 0.07 ± 0.04 norm-units, respectively. Pooling all saccades together, Bland-Altman analysis showed a bias of +0.017 norm-units with 95% limits of agreement from −0.175 to +0.208 norm-units, indicating the webcam agrees with the Tobii Pro Spectrum within ±0.19 norm-units in amplitude measurement for 95% of individual saccades, and there is no significant bias between the two systems (Figure 2).

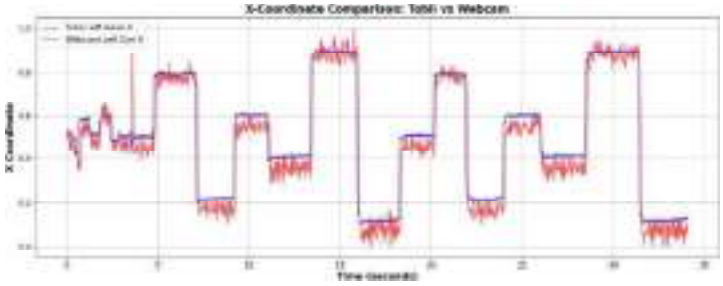

Figure 1: Raw horizontal left eye position data in normalized units obtained with the webcam (red) and the Tobii Pro Spectrum (blue).

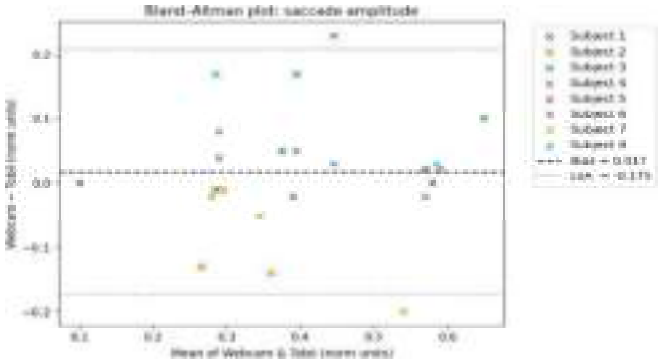

Figure 2: Bland–Altman plot comparing saccadic amplitudes obtained with the webcam and the Tobii Pro Spectrum.

This preliminary study allowed us to first validate this innovative deep learning-based eye tracking system for detecting saccades. Although, on average, the measured amplitudes agreed with those obtained with a high-performance eye tracker, considerable inter-subject variability was found. Future work will deepen the study of the sources of this variability, expand the number of data available, and include different metrics to assess the spatial accuracy, precision and resolution of the system.

ACKNOWLEDGEMENTS: HORIZON–MSCA–2022–DN, *Improving BiomEdical diagnosis through LIGHT-based technologies and machine learning* "BE-LIGHT" (GA nº 101119924 – BE-LIGHT).

---

[1] Mestre, C., Gautier, J., & Pujol, J; Journal *of biomedical optics*, *23*(3), 035001-035001 (2018).

[2] Holmqvist, K., Nyström, M., Andersson, R., Dewhurst, R., Jarodzka, H., & J. Van de Weijer; Oxford University Press (2011).

[3] Cheng, Y., Wang, H., Bao, Y., & Lu, F.; *IEEE Transactions on Pattern Analysis and Machine Intelligence* (2024).

[4] Lugaresi, C., Tang, J., Nash, H., McClanahan, C., Uboweja, E., Hays, M., ... & Grundmann, M.; In *Third workshop on computer vision for AR/VR at IEEE computer vision and pattern recognition (CVPR)* (Vol. 2019).

[5] Nyström, M., & Holmqvist, K.; *Behavior research methods*, *42*(1), 188-204 (2010).

Impact of Bangerter foils on non-strabismic binocular anomalies and fine motor skills analysed using eye-tracker and motion-capture camera

Pilar Granados-Delgado[1], Miriam Casares López [1], José Juan Castro-Torres [1] and Ewa Niechwiej-Szwedo[2]

[1] Laboratory of Vision Sciences and Applications, Department of Optics, Faculty of Science, University of Granada, Avenida Fuentenueva s/n, 18007 Granada, Spain
[2] Developmental Visuomotor Neuroscience Lab, Department of Kinesiology and Health Sciences, Faculty of Health, University of Waterloo, 200 University Avenue West Waterloo, ON, Canada N2L 3G

pilargrd@ugr.es

Introduction: The binocular visual system (BVS) is susceptible to being affected by ocular pathologies such as cataract in one eye. This results in interocular differences that affect visual performance.[1] Previous studies have examined the relationship between the BVS and fine motor skills (FMS),[2,3] providing insights into the association between grasping duration and stereopsis, as well as between reaching speeds and the vergence system, particularly in children engaged in a bead threading task.[3] However, the influence of increased straylight on unstable BVS showing alterations in vergence visual function, and their impact on FMS has not been previously assessed.
Purpose: To study the influence of Bangerter 0.4 foils (BF) on visual functions (visual acuity (VA), contrast sensitivity (CS), phoria, near point of convergence (NPC), positive and negative horizontal fusional vergences (FV) and stereopsis), and manual skills in participants with non-strabismic binocular anomalies (NSBVA) but without symptoms.
Methods: To evaluate visual performance, VA, CS, phoria, NPC, PFV, NFV and stereopsis were assessed. FMS was evaluated using a threading task[3,4] that involved reaching, grasping and placing. Hand and eye kinematics were recorded using an eye-tracker and a motion capture system (Figure 1). Fifteen trials were recorded for each viewing condition. Two different groups (NSBVA and control) of young participants were evaluated. The impairment was induced using a BF 0.4 in the dominant eye (FDE). Both groups had similar BCVA (at least 0.0 logMAR) but the NSBVA group did not satisfy the Sheard criterion[5]. The influence of impairment binocular function and their impact on the beads task, was also assessed. Finally, the correlation between visual function and hand-eye kinematic variables was investigated.

Figure 1: Experimental set up for the bead threading task using two infrared markers and eye-tracker.

Results: A total of 12 participants (mean age 24.3 ± 5.7 years) was part of this study, 6 per group. In the NSBVA group, five participants were found to have PFV reduced (lower than the double of their foria), and the other one displayed the NPC that was impaired by repetition. Table 1 shows a summary of the visual functions and kinematic measures recorded during the bead threading task for the control and the NSBVA groups, in the two viewing conditions. For all the visual and kinematic variables analysed, there was only significant differences for phorias values between the control

and NSBVA groups in both viewing conditions (U = -2.751; p = 0.004 and t = 4.494; p = 0.001, without BF and FDE respectively). The BF was significantly impaired for mean CS and stereoacuity (t = 2.502; p = 0.029 and W = 2.994; p = 0.003, respectively). It was found that higher PFVs were correlated with shorter total task execution times (r = - 0.635; p= 0.026).

Visual functions		Viewing condition		Kinematics values		Viewing condition	
		Without BF	FDE			Without BF	FDE
Mean near Visual Acuity VA (logMAR)	Control	- 0.10 (-0.1 – -0.06)	-0.09 (- 0.10 – - 0.02)	**Reach duration** (milliseconds, ms)	Control	483.74 (± 34.33)	482.82 (± 39.20)
	NSBVA	-0.10 (-0.10 – -0.10)	-0.10 (- 0.10 – - 0.03)		NSBVA	497.40 (± 54.75)	507.62 (± 72.24)
Mean Contrast Sensitivity	Control	137.07 (± 9.58)	112.43 (± 16.53)	**Grasp duration** (ms)	Control	263.42 (± 81.68)	254.13 (± 106.97)
	NSBVA	124.10 (± 20.15)	120.21 (± 24.19)		NSBVA	208.88 (± 109.31)	247.68 (± 87.15)
Phoria (Δ)	Control	-2.33* (± 1.75)	- 2.75* (± 1.71)	**Thread duration** (ms)	Control	409.55 (± 102.55)	377.83 (± 28.93)
	NSBVA	-11.33* (± 5.85)	- 11.60* (± 5.22)		NSBVA	378.46 (± 67.55)	401.95 (± 99.33)
Near Point of Convergence NPC (cm)	Control	7.75 (± 2.14)	7.13 (± 2.53)	**Peak reach velocity** (mm/s)	Control	- 687.31 (± 71.42)	- 674.78 (± 52.50)
	NSBVA	9.54 (± 2.06)	9.10 (± 1.75)		NSBVA	- 648.67 (± 96.25)	- 649.70 (± 47.84)
Positive fusional vergence PFV (Δ)	Control	16.00 (14.00 – 24.75)	16.50 (12.25 – 35.00)	**Hand Reaction time** (ms)	Control	1123.30 (± 82.39)	1122.86 (± 93.59)
	NSBVA	17.00 (14.00 – 24.75)	16.00 (7.00 – 17.00)		NSBVA	1145.84 (± 65.52)	1166.68 (± 181.83)
Negative fusional vergence NFV (Δ)	Control	15.83 (± 5.31)	13.50 (± 2.52)	**Eye Reaction time** (ms)	Control	761.68 (± 79.50)	778.08 (± 79.68)
	NSBVA	16.17 (± 1.67)	14.80 (± 3.03)		NSBVA	766.68 (± 100.16)	739.38 (± 170.22)
Stereoacuity (Frisby) (arcsec.)	Control	7.50 (5.00 – 12.50)	57.50 (40.00 – 75.00)	**Total time** (ms)	Control	1620.88 (± 171.18)	1575.02 (± 127.33)
	NSBVA	5.00 (5.00 – 27.50)	55.00 (40.00 – 97.50)		NSBVA	1592.31 (± 134.40)	1666.71 (± 155.57)

Table 1. Mean (± SD) and median (IQR= Q3-Q1) values in the two experimental viewing conditions: without, and with the filter on the dominant eye (FDE), for the two groups (control and NSBVA). *Statistically significant differences (p < 0.05) between the control and NSBVA groups. Δ: Prism dioptres.

Conclusion: The study found that BF 0.4 had a negative effect on mean CS and stereoacuity in both groups, but that their impaired values were already at a level considered normal. The visual function that exhibited disparities between the control and NSBVA groups was the phoria. Higher phoria and superior FV system were related to the performance of bead threading task, but there was no significant effect when they were analysed separately. Considering these findings, it can be concluded that NSBVA in the absence of symptomatology does not exert a significant impact on hand and eye motion variables. In future research, the impact of binocular vision impairment in both eyes, as seen in bilateral cataracts, could be assessed to ascertain the implications of binocular straylight in both eyes in NSBVA.

ACKNOWLEDGEMENTS: Grants PID2020-115184RB-I00, funded by MCIN/ AEI/10.13039/501100011033, and grants A-FQM-532-UGR20 and C-EXP-194-UGR23, funded by Junta de Andalucía.

[1]F. Martino, JJ. Castro-Torres, et al; *Ophthalmic and Physiological Optics,* **14**, 1 (2022).
[2]P. Granados-Delgado, M. Casares-López, et al; *Life-Basel,* **14**, 1 (2024).
[3]E. Niechwiej-Szwedo, G. Thai, et al; *Human Movement Science,* **72***,* 10 (2020).
[4]E, Niechwiej-Szwedo, M. Nouredanesh, et al; *Human Movement Science,* **75**, 9 (2021).
[5]M, Sheiman, B. Wick. *Clinical Management of Binocular Vision* (2019).

Eye movements and visual performance from eye-tracking in table tennis players

Alejandro Guiseris Santaflorentina[1], Ana Sánchez Cano[1,2], Elvira Orduna Hospital[1,2]

[1] Departamento de Física Aplicada, Facultad de Ciencias, Universidad de Zaragoza (Pedro Cerbuna, 12, 50009, Zaragoza, España)

[2] Instituto de Investigación Sanitaria de Aragón (IIS Aragón) (San Juan Bosco, 13, 50009, Zaragoza, España)

Contact: 736596@unizar.es

Introduction: Table tennis is one of the fastest ball sports, requiring a dynamic interaction between vision and movement[1,2]. Players must process visual information such as convergence, speed assessment, and trajectory prediction[3], relying on eye movements more than head movements[4]. Gaze behaviour includes saccades and smooth tracking, with saccades becoming essential at high speeds[5]. Dynamic visual acuity and peripheral vision play key roles, allowing athletes to anticipate opponents and react swiftly to stimuli in both central and peripheral fields[6123,4556786910113].

Purpose: This study aims to analyse eye movements, accuracy, and visual efficiency during specific training sessions in table tennis across three groups: experienced athletes, individuals with intellectual disabilities, and individuals with Down syndrome. By comparing these groups, we aim to identify ocular differences and explore benefits of visual training for skill enhancement.

Methods: This prospective study was approved by the Research Ethics Committee of the Community of Aragon (CEICA) (PI24/483) and conducted in accordance with the Declaration of Helsinki. Written informed consent was obtained from all participants. After a comprehensive optometric examination, inclusion criteria required a spherical equivalent within ±4.00 D, age-normal vergence, and oculomotor function skills, normal binocular function, best-corrected visual acuity (BCVA) of at least 0.8 (20/25) in each eye, and absence of strabismus or visual pathologies. A total of 27 subjects, aged 9 to 58 years, were recruited from various organizations, including 12 experienced athletes from A.D. School Zaragoza Table Tennis (Group 1), 8 individuals with Down syndrome from the Special Olympics of Aragon (Group 2), and 7 individuals with intellectual disabilities from the ATADES organization (Group 3). The study was conducted in a controlled environment using standard table tennis tables. Participants performed the same exercise designed to analyze their eye movement patterns during gameplay. Eye-tracking data were collected using a Neon technology-based sports eye-tracker (Pupil Labs, Berlin, Germany), consisting of infrared binocular cameras (850 nm LEDs), an IMU system for motion tracking at 200Hz, and a scene camera capturing a 100° × 80° field of view. Data collection focused on key visual parameters analysed included gaze accuracy, fixations, saccades, blinks, and pupil diameter. Data were pre-processed using Pupil Cloud, with events manually marked for precise segmentation of eye movement data to be analysed with custom-built software in Python.

Results: The results represented in Table 1 and Figure 1 show that Group 1 exhibited the largest pupil diameter, followed by Group 2 and Group 3, indicating a possible correlation between expertise and pupil size. Blink duration was relatively consistent across groups, with only minor variations. However, both fixation and saccade duration showed greater differences, with Group 3 displaying the longest fixations, potentially reflecting slower information processing, while Group 1 had the shortest, suggesting more efficient visual strategies. Regarding saccades, Group 1 exhibited shorter amplitudes and higher velocities, indicating quicker and more precise eye movements, which may reflect a more efficient ability to shift attention. In contrast, Group 3 had

larger amplitudes and slower velocities, suggesting a less coordinated and slower process of reallocating visual attention. Interestingly, Group 2, individuals with Down syndrome, demonstrated better performance than Group 3, people having intellectual disabilities. This suggests that the visual processing abilities of individuals with Down syndrome may be less impacted by cognitive challenges, allowing for more efficient attention shifting and better overall visual performance compared to individuals with intellectual disabilities. These patterns highlight how differences in both fixation and saccade characteristics can influence overall visual performance and underscore the importance of considering the varied impacts of cognitive abilities on visual behavior.

Conclusion: These findings emphasize differences in visual behavior that may impact performance and could be improved with targeted visual training. Experienced athletes, in particular, exhibited more efficient eye movement patterns, suggesting the potential advantages of such training for performance enhancement.

	n	Pupil diameter OD/OI (mm)	Blink duration (ms)	Fixation duration (ms)	Saccade duration (ms)	Saccade amplitude (°)	Saccade velocity (px/s)
Group 1	12	5.04±0.74/ 5.21±0.77	242.22±17.10	295.23±62.99	68.41±11.72	7.61±1.69	3969.54±711.06
Group 2	8	4.18±0.59/ 4.29±0.50	243.31±28.69	304.60±49.61	68.44±12.59	9.45±2.53	3872.82±671.63
Group 3	7	3.99±0.63/ 4.02±0.63	251.41±21.00	324.17±63.38	77.23±22.83	11.08±3.79	4468.12±979.17

Table 1. Sample characteristics, including the number of subjects (n), mean ± standard deviation of pupil diameter, blink duration, fixation duration, saccade duration, amplitude, and velocity across the three groups.

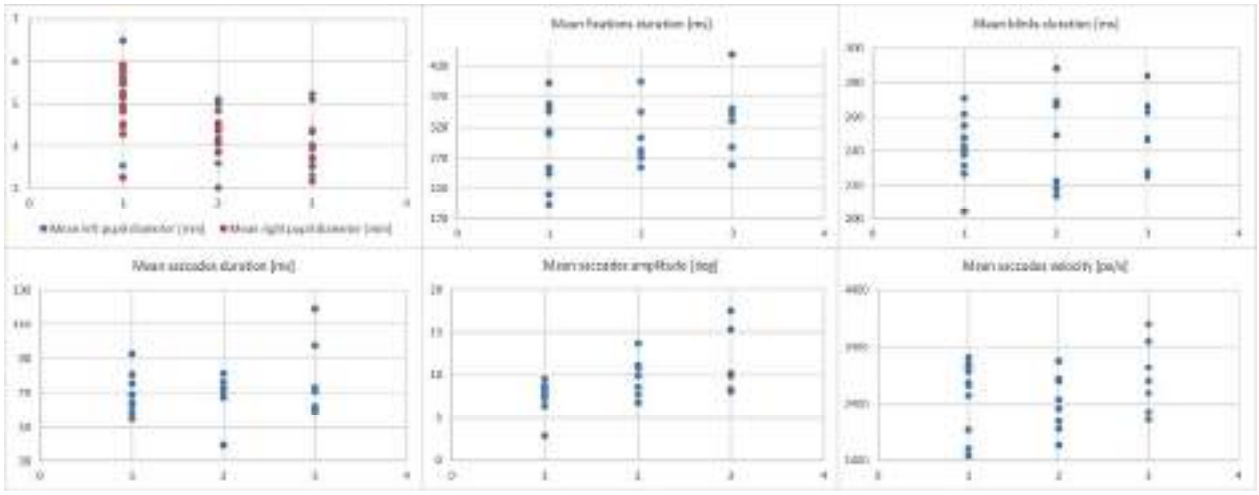

Figure 1: Plots showing the difference between groups in each evaluated parameter.

ACKNOWLEDGEMENTS: Special thanks to A.D. School Zaragoza Table Tennis, ATADES, and Special Olympics for their support, providing space, players, and invaluable cooperation.

[1] Kondrič, M., Zagatto, A. M., Sekulić, D.; Journal of Sports Science and Medicine, **12** (2013).
[2] Fuchs, M. *et al*.; *J Sports Sci,* **36**, 2653 (2018).
[3] Paul, B., Biswas, K., Sandhu, S.; Brazilian Journal of Biomotricity, **5**, 106 (2011).
[4] Higuchi, T., Nagami, T., Nakata, H., Kanosue, K.; PLoS One, **7**, 13 (2018).
[5] Nakazato, R., Aoyama, C., Komiyama, T., Himo, R., Shimegi, S.; Front Sports Act Living, **6** (2024).
[6] Quevedo, L., Antonio Aznar-Casanova, J., Da Silva, J. A.; Sociedade Brasileira de Psicologia, **26**, 1283 (2018).

Video-ophthalmoscope to measure retinal reflectance changes to flickering light

Radim Kolar[1], Ralf P. Tornow

[1] Department of Biomedical Engineering, Faculty of Electrical Engineering and Communication, Brno University of Technology, (Technicka 12, 61600, Brno, Czech Republic)
[2] Department of Ophthalmology, Friedrich-Alexander-University Erlangen–Nürnberg (Schwabachanlage 6, 91054, Erlangen, Germany)

Contact: kolarr@vut.cz

This paper presents a compact, monocular video-ophthalmoscope designed for real-time measurement of retinal reflectance changes in response to flickering light stimuli. The device is a result of our continues research[1,2] and it integrates an OLED display for flicker light stimulation and a fiber-optic LED light source for imaging, enabling high-frame-rate video acquisition at low retinal irradiance (12 µW/cm²) while ensuring patient comfort. Unlike conventional fundus cameras that use a ring of light for illumination in the pupil plane, this setup employs an inverted pupil illumination approach, where the central pupil area is used for illumination and the periphery for imaging. This eliminates the need for complex optics while maintaining high-quality retinal imaging. The optical system includes a 40D Volk ophthalmic lens for intermediate retinal imaging, two achromatic lenses (100 mm focal length), and a CMOS camera (1224×970 pixels) for capturing retinal video sequences. A bandpass filter is placed in front of the camera to block the flickering light from the detector, ensuring accurate reflectance measurements.

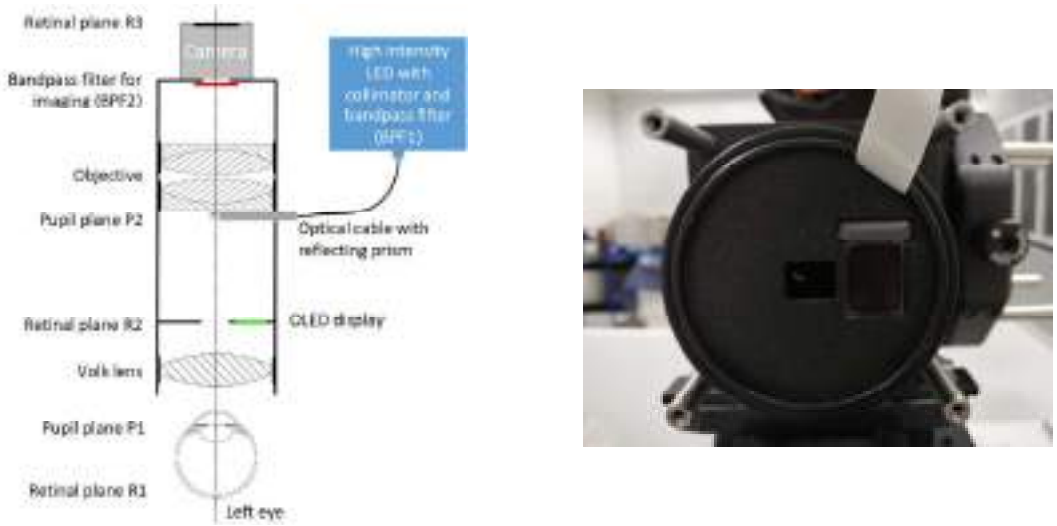

Figure 1: Schematic layout of the video-ophthalmoscope with depicted retinal (R) and pupil (P) planes is shown (left). External light source with bandpass filter BPF1 (blue), OLED display (green), and bandpass filter BPF2 (red) to eliminate the flicker light from the camera. The image on the right shows the front view of retinal plane R2 (Volk lens removed) with OLED display (right rectangle) and the field aperture (left rectangle).

The study evaluated the device's performance by assessing flicker-induced retinal reflectance changes in 10 healthy subjects. Participants underwent flicker stimulation at 12 Hz, with retinal irradiance set to 2 µW/cm². The acquisition protocol consisted of three phases: a pre-flickering baseline phase (20 seconds), a flickering phase (30 seconds), and a post-flickering recovery phase

(20 seconds). Image sequences were continuously recorded, and reflectance changes were analysed offline across different retinal regions.

Results demonstrated a consistent decrease in optic nerve head (ONH) reflectance during flicker exposure, attributed to increased blood volume and metabolic activity. The average reflectance reduction was 7.16%, with a recovery to 1.94% in the post-flickering phase. Temporal analysis confirmed the device's ability to capture dynamic retinal reflectance variations, which align with blood velocity and volume changes already published[3,4].

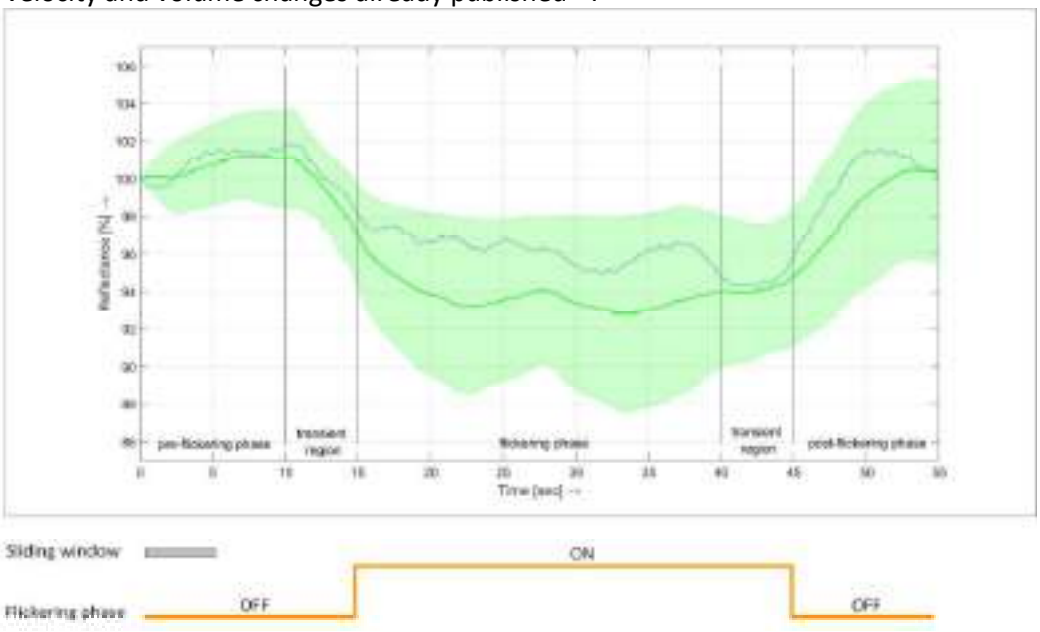

Figure 2. The time course of average reflectance changes. The green line represents the average value of all 10 subjects, while the border of the greenish region corresponds to standard deviation. The blue dotted curve represents an example of one subject. The curves are normalized to 100% with respect to the first sample. The curves were calculated using a sliding average (5 s) shown as a grey rectangle. This results in the marked transient region, during which the window overlaps both phases – flickering and no flickering. The small red rectangle inside the sliding window corresponds to the position of the new averaged sample to clarify the transient regions.

This portable video-ophthalmoscope provides a novel, non-invasive method for assessing neurovascular coupling in the retina. By allowing spatial and temporal analysis of flicker-induced changes, it holds promise for diagnosing and monitoring conditions such as glaucoma, diabetic retinopathy, and neurodegenerative diseases affecting retinal circulation. Future work will focus on optimizing flicker light parameters, expanding clinical validation, and exploring simultaneous bilateral measurements using synchronized devices to enhance diagnostic accuracy.

References

[1]R. P. Tornow, J. Odstrcilik, and R. Kolar; *Biomedical Optics Express*, **9**, 6237 (2018).
[2]R. Kolar et al.; *Journal of Biophotonics*, **15**, e202200094 (2022).
[3]C. E. Riva, E. Logean and B. Falsini; *Neuroscience Letters*, **356**, 75 (2004).
[4]M. Crittin and C. E. Riva; *Optics and Lasers in Engineering*, **43**, 583 (2005).

Comparison of eye movements in a Head-mounted and a Table-top implementations of the visual simulator SimVis Gekko2

Pilar Urizar[1], Alejandra Varea[1,2], Ricardo Mera[1], Yassine Marrakchi[1], Eduardo Lage[3,4], Enrique Gambra[1] and Carlos Dorronsoro[1]

[1] 2EyesVision S.L. (Madrid, Spain)
[2] Institute of Optics, IO-CSIC (Madrid, Spain)
[3] PlenOptika, Inc. (Boston, MA, United States)
[4] Department of Electronics and Communications Technology, UAM (Madrid, Spain)

Contact: purizar@2eyesvision.com

Purpose:

To evaluate the eye movements during a preoperative clinical visual simulation of different multifocal corrections and assess the potential impact on alignment stability. To compare gaze dynamics and transient eye decentration between two configurations of SimVis Gekko2 (SVG2) see-through visual simulator, both incorporating an Eye Monitoring System: (1) head-mounted (HM) and (2) table-top (TT).

Methods:

SimVis Gekko is a see-through and binocular head-mounted visual simulator of presbyopic corrections, that allows patients to try different intraocular lenses and provide feedback of their visual experience before surgical implantation[1,2]. To ensure a precise preoperative visual evaluation with SimVis technology, an accurate eye centration of the patient is required. However, eye movements occur naturally when exploring the wide field of view of SVG2 (20 deg) as well as convergence when focusing on targets at different distances[3]. The Eye Monitoring System incorporated into the SVG2 uses two near-infrared (NIR) Purkinje eye trackers, one per optical channel of the binocular device, combined with a processing unit and software for guiding and verifying eye centration. During this study, the eye position of the patient has been continuously tracked in two implementations of SVG2: (1) head-mounted (HM), allowing free head movement; and (2) table-top (TT), preventing them.

In this study, a research version of the Eye Monitoring System recorded the eye position at 10 Hz during conventional preoperative clinical evaluations. 16 patients were recorded for 90 seconds while scoring image quality at far and near distances for three different corrections (plano-monofocal, trifocal, and EDOF). Each patient repeated the experiments 3 times with each of the system implementations (SVG2-HM and SVG2-TT).

Results:

The mean difference in eye position between the HM and TT configurations was less than 0.1 mm in both vertical and horizontal directions, with no statistically significant difference. During the visual experiment, eye decentration while exploring the FoV or switching viewing distances was less than 0.29 mm 50% of the time and less than 1.12 mm 95% of the time with the HM (and with the TT: <0.36 mm and <1.71 mm, respectively). The maximum light reduction due to vignetting, occurring less than 20% of the time of the experiment, was approximately 17% for HM and 25% for TT. The range of eye movements was smaller with the HM (horizontal: 0.26 mm; vertical: 0.18 mm) compared to the TT (horizontal: 0.40 mm; vertical: 0.38 mm). The corresponding FoV covered was 6.77° horizontally and 4.86° vertically for HM, and 10.13° and 9.58° for TT.

Conclusions:

Both SVG2 implementations (HM and TT) provided similar eye centration. Greater eye movements were observed with the TT configuration, likely compensating for the restriction of head movements. Even though the eye movement during the exploration of the FoV of the SVG2, no significant mean difference in eye decentration was measured.

ACKNOWLEDGEMENTS:

Funding:
Comunidad de Madrid - Doctorado Industrial (IND2023/BMD-27723) to AV;
Ministerio de Ciencia e Innovación, Ayudas a proyectos de colaboración público-privada (Retos CPP2021-008388) to CD, EG and PU.

---

[1]L Sawides, A de Castro, CM Lago, X Barcala, A Zaytouny, S Marcos, & C Dorronsoro. *SimVis simulations of multifocal IOL designs based on public-literature data*. Optical Design and Engineering VIII. SPIE (2021).
[2]M Vinas, S Aissati, M Romero, C Benedi-Garcia, N Garzon, F Poyales, C Dorronsoro, & S Marcos. *Pre-operative simulation of post-operative multifocal vision*. Biomedical Optics Express 10(11), 5801-5817 (2019).
[3]L González-Vides, JL Hernández-Verdejo, & P Cañadas-Suárez. *Eye Tracking in Optometry: A Systematic Review*. Journal of Eye Movement Research 16(3):3 (2023).

A novel approach to assess oculomotor behaviour in amblyopia

Maite Valentino, Clara Mestre, Marc Argilés, Luis Pérez-Mañá and Jaume Pujol

Centre for Sensors, Instruments and Systems Development, Universitat Politècnica de Catalunya, Rambla Sant Nebridi 10, Terrassa 08222 (Barcelona), Spain

Contact: maite.valentino@upc.edu

Amblyopia is a neurodevelopmental disorder affecting up to 2–4% of the population. Although amblyopia is traditionally defined by reduced best-corrected visual acuity, it is increasingly recognised as a condition involving impairments in visuospatial processing, stereopsis, contrast sensitivity, and oculomotor control[1-3]. Oculomotor studies in amblyopia have typically been conducted in controlled laboratory settings, using remote eye trackers and unrealistic visual stimuli on a monitor. This approach, while valuable for understanding basic oculomotor mechanisms, lacks ecological validity and may not accurately reflect the impact of amblyopia on visual behaviour in real-world contexts. To address this limitation, the main objective of this study was to characterise the oculomotor behaviour of children with amblyopia during the performance of tasks that simulate everyday activities. A protocol consisting of a battery of naturalistic tasks inspired by common childhood scenarios and previously developed and validated in an adult population was employed. These tasks included gross motor activities involving postural control and spatial exploration, as well as fine motor tasks requiring precise eye-hand coordination, and they required oculomotor control in both dynamic and static situations.

Binocular eye movements were recorded using the portable Pupil Core (Pupil Labs) head-mounted eye tracker, which allows for free and natural head and body movements. The study included 10 children with strabismic or anisometropic amblyopia (aged 8 ± 3 years), 14 age-matched controls (6.5 ± 2.5 years), and 10 healthy adults with normal binocular vision (aged 28.3 ± 3.3 years). All participants completed the same battery of tasks under free viewing conditions.

Fixation stability, quantified using the 68% Bivariate Contour Ellipse Area (BCEA), was assessed during a gross motor task requiring participants to stand on one foot while fixating on a target. The amblyopic group showed significantly reduced fixation stability [median (IQR) of 107.03 (123.81) deg²] compared to 59.79 (55.35) deg² in the control group and 3.90 (2.36) deg² in adults ($p < 0.001$), highlighting reduced gaze stability when postural and attentional demands are combined (Figure 1).

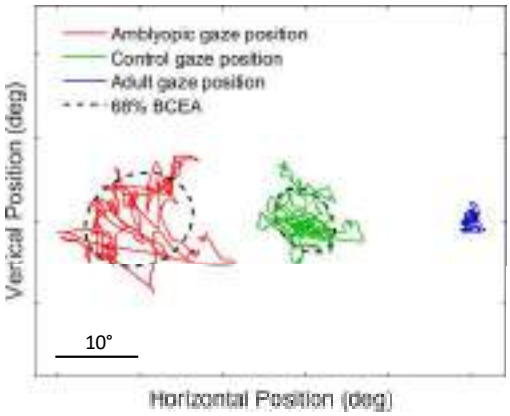

Figure 1: Fixation stability comparison of the 68% BCEA for one amblyopic (114.41 deg²), one control (41.72 deg²), and one adult eye (3.07 deg²) during the balance task.

When instructed to follow a sinusoidal pattern with the eyes, the amblyopic group exhibited a significantly lower saccade rate [0.55 (0.66) saccades/s] compared to controls [1.23 (0.69) saccades/s] and adults [2.26 (0.82) saccades/s] (p=0.004). In addition, saccades peak velocity also differed significantly between groups, with the amblyopic group showing the lowest values [35.48 (29.71) deg/s], followed by controls [53.03 (27.42) deg/s] and adults [69.46 (35.32) deg/s] ($p < 0.001$). These results suggest a reduced ability to compensate for tracking errors and diminished responsiveness during smooth pursuit in amblyopia.

During a visual search task, the saccades exhibited by all groups followed the expected main sequence relationship between saccade amplitude and peak velocity[5]. No significant differences were found in the slope in the three groups (p=0.405), suggesting that saccadic dynamics are largely preserved, at least within the current sample. Figure 2 shows the main sequence obtained from all the saccades performed by the participants in the different tasks. Although some group differences were observed in individual parameters such as saccade frequency or the coefficient of determination of the main sequence, not all saccadic parameters consistently distinguished the amblyopic group from both controls and adults. As in other tasks, a high degree of inter-individual variability was present, likely reflecting differences in attentional deployment or execution strategies. Further data will be necessary to clarify whether consistent group-level patterns emerge.

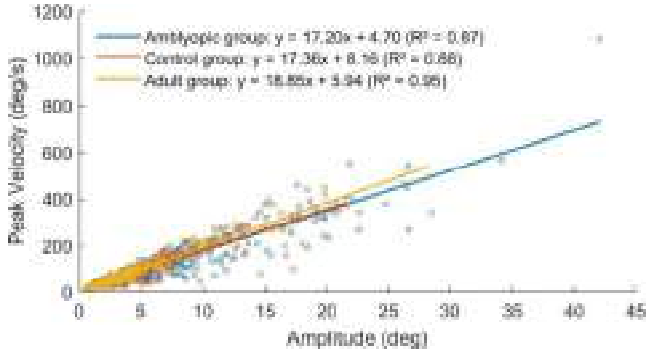

Figure 2: Main sequence including all saccades performed by the participants during all tasks, where the colours of the dots represent different groups.

This study takes a pioneering approach by employing portable eye tracking to characterise the oculomotor performance of children with amblyopia during naturalistic tasks. By assessing behaviour across tasks, we identified group differences in fixation control and pursuit dynamics, as well as high inter-individual variability in visual search behaviour. These findings underscore the value of assessing oculomotor function in real-world settings to better understand how amblyopia impacts visual performance. This approach may contribute to a more complete characterisation of visual capacity and offers promising avenues for refining diagnostic tools and treatment strategies.

ACKNOWLEDGEMENTS: This publication is part of the project PID2023-146101OB-I00 funded by MCIN/AEI/ 10.13039/501100011033 and ERDF, EU. The authors gratefully acknowledge the support of Pere Pujol (Parc de Salut Mar), Laura Asensio (Hospital Universitari MútuaTerrassa), and Ana Wert (Instituto de Microcirugía Ocular IMO Grupo Miranza) for facilitating data collection at their respective institutions.

[1]S.P. McKee, D.M. Levi and J.A. Movshon; *Journal of Vision*, **3**, 380 (2003).
[2]A.L. Webber; *Clinical and Experimental Optometry*, **101**, 443 (2018).
[3]E.E. Birch and K.R. Kelly; *Progress in Retinal and Eye Research*, **93**, 101168 (2023).
[4]K.R. Kelly, S.E. Morale, C.L. Beauchamp, L.M. Dao, B.A. Luu and E.E. Birch; *Investigative Ophthalmology & Visual Science*, **61**, 43 (2020).
[5]A.T. Bahill, M.R. Clark and L. Stark; *Mathematical Biosciences*, **24**, 191 (1975).

Application of optofluidic tunable lens for dioptric power measurement in ophthalmic lenses

Sara Ferrer-Altabás[1], Daniel Sauter[2], Hans Zappe[2] and Vicente Micó[1]

[1] Department of Optics and Optometry and Vision Sciences, Faculty of Physics, University of Valencia, Street Dr. Moliner, 50, 46100 Burjassot, Valencia (Spain)
[2] Gisela and Erwin Sick Chair of Micro-Optics, Department of Microsystems Engineering—IMTEK, University of Freiburg, Georges-Köhler-Allee 101, 79110 Freiburg, Germany

Contact: Sara.Ferrer@uv.es

Introduction: Several techniques have been developed throughout the years to determine dioptric power in ophthalmic lenses, with non-contact methods being preferred to prevent potential surface damage. Among these, extensive research has focused on interferometric and deflectometric approaches, Hartmann-Shack sensing, and focimetry, among others[1]. In recent years the field of variable optics has gained increasing attention, particularly liquid-based variable optics, which provide remarkable advantages in terms of focal length tunability and higher-order aberrations control within a compact element[2]. Due to their versatility, these elements have been widely adopted across various applications. However, their use in focal length or dioptric power measurement in optical elements remains limited, generally playing a secondary role in the implementation of other measurement techniques[3–5].

Aim: The aim of this work is to present preliminary results of the use of an electrowetting-driven tunable lens (EDTL) as the key element in dioptric power measurement in ophthalmic lenses.[6]

Methods: We present a device containing a EDTL with 32 independent electrodes which can generate sphero-cylindrical dioptric power. The EDTL is previously characterized with a Hartmann-Shack sensor to relate applied voltages with generated dioptric power. The optical setup was vertically arranged to prevent gravity effects on the EDTL, and it consisted of a green LED light source (Thorlabs LED505L), a condenser lens close to a target (Max Levy AA058,), the EDTL including a support for ophthalmic lenses in the measurement plane (Figure 1), an objective lens and a CMOS sensor (IDS UI-3582LE-C). The introduction of a sample lens in the measurement plane displaces the image from the sensor, which is refocused by actuating over the EDTL guided by sensor feedback. The measured dioptric power is calculated from the applied voltage distribution regarding the Hartmann-Shack calibration and combined with magnification information from the recorded image of the target. A preliminary validation is performed by measuring nine sphero-cylindrical ophthalmic lenses and comparing the results with a lensmeter Topcon CL-300®.

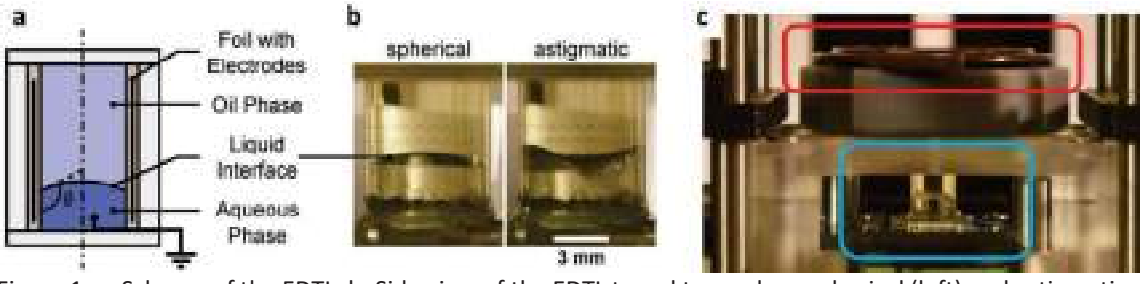

Figure 1: a. Scheme of the EDTL; b. Side view of the EDTL tuned to produce spherical (left) and astigmatic (right) dioptric power; c. Side view of the EDTL (blue) in its final place on the setup while a spherical negative lens is placed in the measurement plane (red)

Results: Each of the nine lenses was measured three times, and mean and standard deviation were calculated using rectangular Fourier notation[7] and are represented in Figure 2. The average results and standard deviation values for each component are -0.09 D $\pm$ 0.20 D for the M component, -0.003 $\pm$ 0.149 D for the J_0 component, and 0.07 $\pm$ 0.17 D for the J_{45} component.

Discussion: The comparison with a commercial automatic lensmeter shows good agreement, with each component remaining within $\pm$0.25 D on average, aligning with typical clinical criteria. The M component exhibits the largest error and dispersion, primarily due to variability in the voltage required to generate a given dioptric power and the dispersion introduced by image magnification, yielding values of 0.18 $\pm$ 0.36 D and -0.36 $\pm$ 0.19 D, respectively. Conversely, J_0 and J_{45} demonstrate higher accuracy, though some outliers are observed, which can be attributed to the aforementioned error sources. In addition, a trend in the M component is noticeable (Figure 2a), likely due to the thin lens assumption used in our calculations. Despite these factors, the system achieves results close to international standards ($\pm$ 0.06 D) even with a limited set of nine lenses. Further optimization could not only reduce these errors but also expand the measuring capabilities to prismatic effects and higher order aberrations[8]. Future studies should consider a larger dataset to further validate these findings and assess the robustness of the system across a wider range of conditions.

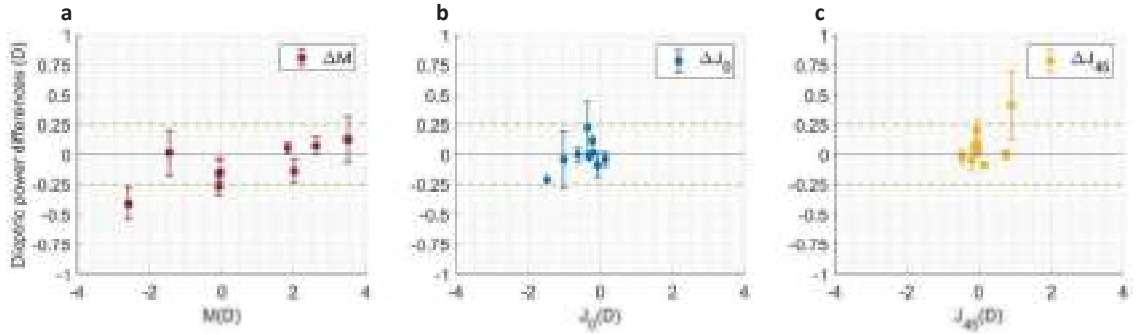

Figure 2: Dioptric power differences between the measurements with the proposed device and automatic lensmeter Topcon CL-300® expressed in rectangular Fourier notation. The x-axis represents the measured values with the automatic lensmeter. The components M, J_0 and J_{45} are separated in a, b and c plots, respectively. Green dashed lines mark a $\pm$0.25 D threshold.

Conclusions: This experimental validation provides proof-of-concept results supporting the use of an optofluidic tunable lens as the core in dioptric power measurement for both spherical and astigmatic cases. Although there are still challenges to address, the combination of the EDTL and image processing data has showed promising results in a small sample of uncut ophthalmic lenses.

ACKNOWLEDGEMENTS: This research has been funded by Grant PID2023-153363NB-C21 from MCIN/AEI/10.13039/501100011033 and FPU21/00985 by the Spanish Ministerio de Ciencia, Innovación y Universidades; and partially funded by the German Research Foundation (DFG) through the project "TOFU2re". The device presented is protected by patent application at OEPM n. P202430098.

[1]P.G. Mendoza-Villegas, G. Trujillo-Schiaffino, et al. *Optica Pura y Aplicada*, **47**, 145 (2014).
[2]L. Chen, M. Ghilardi, et al. *Frontiers in Robotics and AI*, **8**, 1 (2021).
[3]N. Barak, V. Kumari, et al. *Journal of Optics*, **24**, 125603 (2022).
[4]A. Arias Gallego, A. Ohlendorf, et al. *Ophthalmic Technologies XXXIII*, 81 (2023).
[5]R. Oliva-García, C. Cairós, et al. *Sensors*, **23**, 6651 (2023).
[6]S. Ferrer-Altabás, D. Sauter, et al. *Optics and Laser Technology*, (2025).
[7]L.N. Thibos, W. Wheeler, et al. *Optometry and Vision Science*, **74**, 367 (1997).
[8]P. Zhao, D. Sauter, et al. *Applied Optics*, **60**, 5302 (2021).

Validation of a Novel Computerized Contrast Sensitivity Test: Comparison with the F.A.C.T.

Paula García Balaguer[1], Mª Josefa Luque Cobija[1] and Mª del Carmen García Domene[1]

1 Research Group on Applied Psychophysics, Department of Optics and Optometry and Vision Sciences, Physics Faculty, University of Valencia (Carrer del Dr. Moliner, 50, 46100 Burjassot, Valencia)

Contact: paula.garcia-balaguer@uv.es

Aim: The contrast sensitivity function (CSF) is useful for evaluating visual pathway integrity, but traditional tests often fail in populations with attentional challenges, such as attention deficit hyperactivity disorder (ADHD), due to demands for sustained focus and prolonged testing. To address these limitations, a novel computerized CSF test that employs engaging stimuli and adaptive algorithms was developed to enhance compliance and efficiency. This study validates the test by evaluating its agreement with the commercial Near Functional Acuity Contrast Test (F.A.C.T.), as prior step for testing in the target ADHD population.

Experimental Method: The custom test was developed on a colorimetrically characterized 16-inch MacBook Pro (Apple, California, USA). Stimuli were sinusoidal gratings along the cardinal achromatic (A), red-green (RG) and blue-yellow (BY) axes of the Derrington-Krauskopf-Lennie (DKL) color space. To enhance engagement, a "bee" shape was used to mask the gratings. This study analyzes only the achromatic gratings for comparison with F.A.C.T. Stimuli were generated using MATLAB (MathWorks, Massachusetts, USA) and Colorlab Toolbox [1], then presented at a mean luminance of 50 cd/m². Five spatial frequencies (1.5, 3, 6, 12 and 18 cpd) were evaluated, each with 50 logarithmically spaced amplitude levels.

Testing was conducted monocularly in a single session with healthy controls (n = 10, age: 25.5 ± 1.9 years). Participants were seated 1 meter from the screen, with optical correction applied and head stabilized using a chin rest. After a 3-minute dark adaptation period, the test began. Participants identified the quadrant containing the "bee" stimulus, while the other quadrants displayed "fly" stimuli composed of achromatic noise (Figure 1A). Responses were recorded via a keypad mirroring the screen's spatial layout, which included a "no stimulus/I don't know" option. Contrast thresholds were determined using a Modified Binary Search (MOBS) algorithm and expressed in cone contrast units, to employ the same metric all cardinal directions.

Subsequently, the F.A.C.T. was administered under photopic conditions (1200 lx). After a 5-minute light adaptation period, participants were positioned 40 cm from the chart, which was uniformly illuminated by a D65 illuminant in a lighting cabin (Gretag Macbeth, X-Rite, Michigan, USA). For each row (A–E, corresponding to spatial frequencies of 1.5–18 cpd) and column (1–9, with contrast decreasing by 0.15 log units per patch) [2], participants reported the orientation of the grating. Thresholds were defined as the last correctly identified contrast level using a descending method of limits.

Results: To study the agreement between devices, cone contrast data were transformed into Michelson contrasts. Spearman's rank correlation coefficients (Rho) were computed for each spatial frequency. The results showed moderate to low positive correlations across spatial frequencies, none of which reached statistical significance: 1.5 cpd (Rho = 0.590, p = 0.073), 3 cpd (Rho = 0.551, p = 0.099), 12 cpd (Rho = 0.504, p = 0.138) and 18 cpd (Rho = 0.284, p = 0.427). At 6 cpd, the correlation dropped to Rho = 0 (p = 1), indicating a complete lack of association.

Bland-Altman tests systematically show larger values in FACT than in the Bee test, as was to be expected from the lower mean luminance, the inclusion of random noise and the presence of the bee mask. To compare both techniques accounting for these differences, the Contrast Sensitivity Index (ICS) [3] defined in Eq. 1 was used. Bland-Altman analysis based on ICS scores

(Figure 1B) revealed agreement between both techniques, with a mean discrepancy of 0.854 (95% CI: -0.244 to 1.951), with a 95% prediction interval from -2.787 to 4.495. The positive mean difference indicates that the F.A.C.T. tends to produce larger ICS values than the custom test, the trend is inverted at higher sensitivities, where the ceiling effect in FACT appears.

$$A.\ Dynamic\ CS\ function\ (dCSF) = \log CSF\ (f) - \log median\ CSF\ (f)$$

$$B.\ ICS = 1dCSF(1.5\ cpd) + 2dCSF\ (3\ cpd) + 3dCSF\ (6\ cpd) + 2dCSF\ (12\ cpd) + 1dCSF\ (18\ cpd)$$

Equation 1

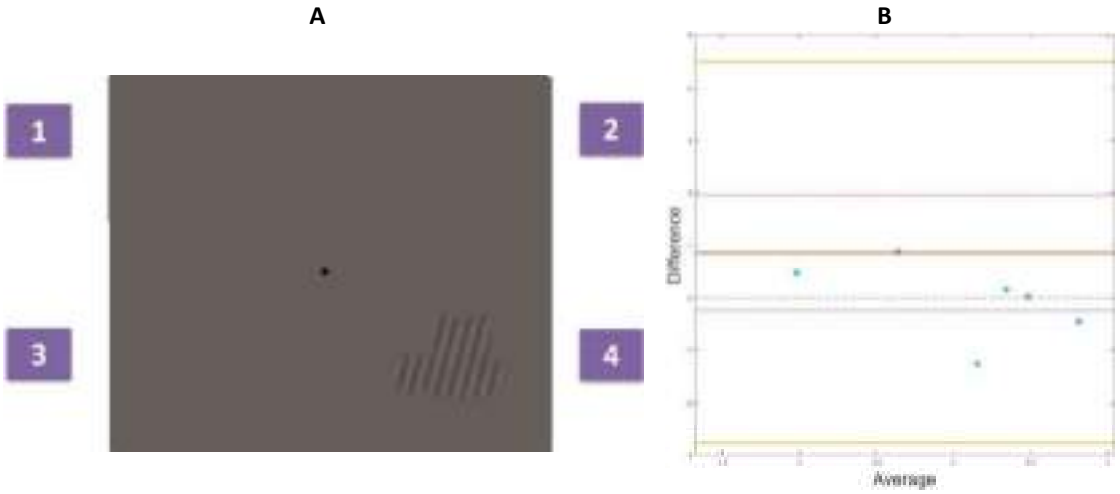

Figure 1: A. Crafted test display B. Bland Altman plot: data (blue dots), mean difference (orange line) and its CI (purple dotted lines), limits of agreement (yellow lines) and zero reference (gray dotted line).

Discussion: The results demonstrate that F.A.C.T. exhibits limitations in grading sensitivity, particularly at 6 cpd—a frequency associated with peak contrast sensitivity due to a well-documented *ceiling effect* [4]. The ICS shows that the custom test allows for a finer and more differentiated gradation of sensitivity at this frequency, which allows the detection of subtle variations among patients that are assigned the same sensitivity with F.A.C.T..

Nonetheless, it is observed that the inclusion of achromatic noise in the stimuli could introduce variability in threshold determination. Moreover, it is important to note that, compared to the F.A.C.T., the task posed by our test can be more demanding or difficult to perform, potentially affecting efficiency in clinical evaluation. Therefore, future modifications of the test should explore strategies to optimize the spectral amplitude of the noise, minimizing its interference without compromising the method's ability to detect subtle differences in sensitivity.

Acknowledgements: *FPU22 - Grants for University Teaching Personnel Training (State Plan for Scientific and Technical Research and Innovation (PEICTI) - Ministry of Science, Innovation and Universities)*

---

[1]Malo J, Luque MJ. COLORLAB: a color processing toolbox for Matlab.
[2]Hitchcock EM, Dick RB, Krieg EF. Visual contrast sensitivity testing: a comparison of two FACT test types. Neurotoxicology and teratology. 2004;26(2):271-7.
[3]Altinbay D, Sahli E, Idil A. Comparison of two different contrast sensitivity testing methods in patients with low vision. Journal of Current Ophthalmology. 2022;34(1):60-6.
[4]Pesudovs K, Hazel CA, Doran RM, Elliott DB. The usefulness of Vistech and FACT contrast sensitivity charts for cataract and refractive surgery outcomes research. British Journal of Ophthalmology. 2004;88(1):11-6.

Macroscopic modelling of absorption in the retina and its relation to the Stiles-Crawford effects

Amy Fitzpatrick[1] and Brian Vohnsen[1]

[1] Department of Physics, University College Dublin, Beech Hill Rd, D04 P7W1, Dublin 4, Ireland.

Contact: amy.fitzpatrick1@ucdconnect.ie

Introduction: There are several theories seeking to provide a complete and comprehensive explanation of the Stiles-Crawford Effects of the first and second kind (SCE-I and SCE-II). The aim of this study is to validate the hypothesis that both effects can be attributed to self-screening and leakage of light[1]. In this interpretation, we assume crosstalk between adjacent cone photoreceptors. This consequently explains the lack of a Stiles-Crawford effect in scotopic conditions as leaked light emerging from one rod, is captured by opsins in a neighbouring rod, yielding a flattened angular response[2].

Methods: A macroscopic model, or phantom (approximate scale of $1{:}10^4$), is used to simulate the absorption process in the foveal photoreceptor outer segments. It consists of a hexagonal arrangement of liquid filled test-tubes, containing red, blue and green food dye solutions, in proportions approximating the visual pigments responsible for absorption in the eye. An image of this retinal phantom can be seen in Figure 1. The array is illuminated using a green laser-diode or bandwidth limited light from a white tungsten-halogen source. The visibility distribution and the resulting directionality is determined using a colour CCD camera (Thorlabs^{TM}) that records the scattering of light at various incident angles.

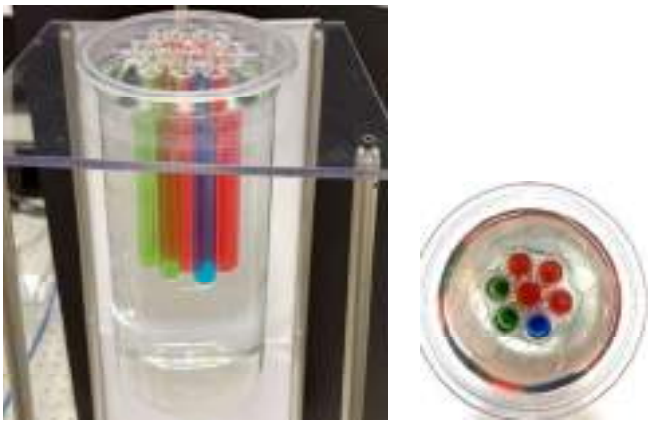

Figure 1: Macroscopic model of the foveal photoreceptor mosaic that can hold up to 19 test tubes. The tubes and water-dissolved food dyes emulate the light absorption characteristics of the S, M and L cones.

Results: The experimental directionality parameter found using the macroscopic model can be related to those obtained from the right eye of human emmetropic subjects. These human directionality measurements are derived using a uniaxial flicker system, featuring a digital micromirror device[3]. The system has been optimised for improved accuracy. We conclude that this absorption model is consistent with the data obtained using the SCE characterisation flicker system, as well as analytical simulations carried out using COMSOL™. Directionality parameters in the range 0.03/mm^2 to 0.10/mm^2 were found, when rescaled to a schematic eye of axial length 22.2mm in the case of the macroscopic measurements and simulations. These approximate that of human subjects determined psychophysically. The SCE-II is then determined by identifying shifts in the spectral peaks at off-axis incident angles.

Conclusion: Alternative hypotheses, such as waveguiding, have failed to explain all aspects of the SCE phenomenon[1,4]. This research seeks to expand our understanding of these effects. Our findings support the theory of leakage as an underlying cause and verifies that the SCE-I and SCE-II can be modelled effectively at the macroscopic level using an array of absorbers to represent the visual pigments in ocular cones.

ACKNOWLEDGEMENTS:

This research is funded by the SIRAT (Scholarship in Research and Teaching) scheme, issued by the School of Physics, University College Dublin.

---

[1] B. Vohnsen, A. Carmichael, N. Sharmin, S. Qaysi and D. Valente; *Journal of Vision*, **17(12):18**, 1 (2017).

[2] A. Fitzpatrick and B. Vohnsen; *Journal of Optics*, (submitted, 2024).

[3] A. Carmichael and B. Vohnsen; *Ophthalmic and Physiological Optics*, **38(3)**, 273 (2018).

[4] V. Nilagiri, M. Suheimat, A. Lambert, A. Turpin, B. Vohnsen and D. Atchison; *Biomedical Optics Express*, **12(8)**, 4969 (2021).

Development and evaluation of a holographic stereo-acuity test

Jorge Lasarte Sanz[1,2], Jorge Ares[3], Mª Victoria Collados[3] and Jesús Atencia[3]

[1] Centre for Industrial and Engineering Optics, Physical to Life Sciences Research Hub, Technological University Dublin, Ireland.
[2] School of Physics, Clinical and Optometric Sciences, Faculty of Sciences and Health, Technological University Dublin, Ireland.
[3] Engineering Research Institute of Aragon (I3A), Faculty of Science, Universidad de Zaragoza, Zaragoza, Spain

Contact: vcollado@unizar.es

Stereoacuity testing, a fundamental clinical tool for assessing binocular depth perception, has remained largely unchanged for decades, with commonly used tests such as the Random Dot Stereogram, Titmus Wirt, best known as "The fly test", Howard-Dolman and TNO, dating back to the mid-20th century[1]. Despite their widespread use, these methods present significant limitations[2]: they depend on coarse disparity steps that hinder precise threshold detection, and they often require external visual aids such as polarized or red-green glasses, which may not be suitable for individuals with certain optical pathologies or conditions. To address these limitations, a novel holographic approach to stereoacuity testing that leverages the intrinsic ability of holography to produce true three-dimensional images perceptible without auxiliary equipment is proposed. This method eliminates dependence on external filters, unlocking the possibility to test individuals with optical conditions that were unable with the conventional tests. Furthermore, a unique spatial stimulus arrangement that places test objects both in front of and behind the fixation plane with customizable disparity increments is introduced. This enables a continuous and finely tunable evaluation of stereoacuity across a broader range of depth levels. The proposed system offers a refined and accessible alternative for clinical and research applications, potentially setting a new standard in stereoscopic vision assessment.
To assess the performance of the proposed method, a comparative evaluation was conducted between the holographic test and conventional stereoacuity tests in a sample of participants shown in Table 1.

	Holographic test (")		**TNO (")**	**TITMUS (")**	**FRISBY (")**	**HOWARD-DOLMAN (")**
	BACK	**FRONT**				
Children	86 (±39)	85 (±37)	55 (±11)	36 (±10)	73 (±43)	-
Young	103 (±47)	92 (±46)	64 (±28)	37 (±20)	55 (±0)	132 (±91)
Adult	108 (±22)	62 (±33)	51 (±20)	30 (±5)	101 (±63)	134 (±77)

Table 1: Comparison of stereoacuity measurements between the conventional and holographic test methods.

ACKNOWLEDGEMENTS:
This publication has emanated from research conducted in Universidad de Zaragoza, with the financial support of Science Foundation Ireland under Grant number 20/FFP-P/8851 and by the "Diputación General de Aragón-Fondo Social Europeo" (TOL research group, E44-23R).

---

[1]K.R. Brooks; *i-Perception*, **8**, 2041669516680114 (2017).
[2]S.P. McKee, D.M. Levi, and S.F. Bowne; *Vision Research*, **30**, 1763 (1990).

Direct comparison between an LED monitor and DMD projection in creating shades of grey for visual stimuli

Chiara Maria Mariani [1] and Brian Vohnsen [1]

[1] Optics Group, School of Physics, University College Dublin, L.M.I. Building, Beech Hill Road, Dublin, D04 P7W1, Ireland

Contact: chiara.mariani@ucdconnect.ie

As the European population ages, vision-related diseases become increasingly prevalent. While cataracts and glaucoma are treatable, age-related macular degeneration (AMD) remains a leading cause of vision loss with no cure[1].

Contrast sensitivity (CS) is among the first visual functions affected by retinal degeneration, providing a way to detect AMD in its early stages through objective patient testing. To make the exam more participatory, accurate CS measurement with electronic devices relies on precise grayscale rendering, which is limited in standard 8-bit displays but significantly enhanced in Digital Micromirror Devices (DMDs), which can exceed 14-bit depth.

We compared a standard LED monitor (Dell) and an in-house built DMD projector (Vialux V-7001) for monocular CS measurement in five healthy participants (ages 23–56 years). Testing involved optotypes, Snellen E as per Figure 1, presented as black-on-white background and white-on-black background. Both configurations were studied as perception processes the two stimuli differently[4]. Individuals with AMD may experience greater difficulty with certain polarities. This is due to impaired retinal function, especially in the central retina, and vision's reliance on the peripheral retina, which is less sensitive to contrast changes. As a result, we expect differences in contrast sensitivity between black-on-white and white-on-black stimuli in people with AMD.

(a) (b)

Figure 1: Example of a Snellen E optotype projected onto a semi-transparent diffuser glass after being reflected by the DMD, illustrating the precision of contrast rendering at (a) maximum contrast and (b) lower contrast.

A telescope was integrated with the DMD to expand the visual field to match the LED display. Participants wore their habitual refractive correction, and contrast sensitivity was assessed at different retinal eccentricities. Differences in luminance reproduction directly impact contrast sensitivity, as contrast depends on the maximum and minimum luminance of a stimulus. Variability in device-specific luminance parameters leads to inconsistencies in results across different devices. Although contrast variations may be clinically insignificant, changes in luminance can influence visual adaptation, thereby highlighting the importance of display calibration for accurate visual testing[3].

Our findings show that the DMD outperforms the LED display in CS testing, likely due to superior luminance precision. While contrast variations across devices may be clinically insignificant, differences in luminance reproduction can influence visual adaptation, emphasizing the importance of display

calibration, in line with current literature[2]. These results support the integration of high-bit-depth DMD technology for advanced vision assessments, with potential applications in clinical diagnostics.

References.

[1] Li, J. Q., Welchowski, T., Schmid, M., Mauschitz, M. M., Holz, F. G., & Finger, R. P.; *British Journal of Ophthalmology*, **104**, 1077 (2020).

[2] Molina-Martín, A., Piñero, D. P., Coco-Martín, M. B., Leal-Vega, L., & de Fez, D.; *Technologies*, **9**, 68 (2021).

[3] To, L., Woods, R. L., Goldstein, R. B., & Peli, E. (2013). Psychophysical contrast calibration. *Vision research*, **90**, 15-24.

[4] Lu, Z. L., & Sperling, G. Black–white asymmetry in visual perception. *Journal of Vision*, ***12*(10):8**, 1-21. (2012).

ACKNOWLEDGMENTS: Financial support from Horizon MSCA 2022-DN-01 “ACTIVA”; Project 101119695.

Retinal Image Quality Assessment of Myopia Control Lenses in a Synthetic Accommodative Wavefront Model

María Mechó-García[1], Paulo Fernandes[1], José Manuel González Méijome[1] and Miguel Faria-Ribeiro[1]

[1] *Clinical & Experimental Optometry Research Lab, Physics Center of Minho and Porto Universities (CF-UM-UP), School of Sciences, University of Minho, 4710-057, Braga, Portugal.*

Contact: mmechogarcia@fisica.uminho.pt

There are several commercially available options for managing myopia progression, including ophthalmic lenses and contact lenses (CLs). These specials CLs are based on multifocality designs and have a drawback of limiting the retinal image quality (RIQ) [1-4].
This study uses a wavefront model[5,6] to evaluate the effects of CLs on retinal image quality (RIQ) as a function of an accommodative demand.

300 synthetic eyes were generated using an accommodative wavefront model to simulate the changes in RIQ with accommodation.
After correcting each wavefront map with its best spherical-cylindrical correction (using just the 2nd order terms), the maximum RIQ [ranged between 0 and 1], for each eye obtained after through-focus, was calculated, with the naked eye, and with both CLs, one with +2.00D treatment zones dual-focus (DF) design (MiSight) and the other with an extended-depth-of-focus (EDOF) design (Mylo), implemented in custom Matlab R2022b (The MathWorks, MA, USA) scripts. The simulation was performed virtually, by positioning the target at 0 D and -2.5 D, representing an object in the infinity and at 40 cm (Accommodative demand = -2.5 D) (Figure 1).

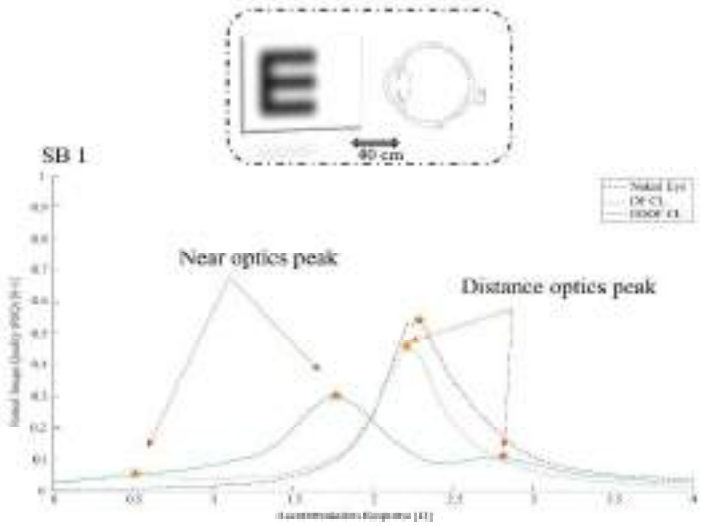

Figure 1: Schematic change in image quality for a wavefront-generated eye viewing a target at 40 cm (Accommodative demand = 2.50 D). The green and blue curves represent the through-focus image quality for myopia control contact lenses: Dual Focus design (DL) and Extended Depth of Focus design (EDOF), respectively. The dashed line corresponds to the accommodative through-focus image quality of the naked eye. The asterisk indicates the local maxima identified by the algorithm.

The theoretical Accommodative Response (AR), change in the RIQ as a function of the TV, that maximizes RIQ was calculated obtaining the maximum point in the through-focus, which is not always the peak correspondent to the distance focus. The predicted accommodation lag was calculated as the difference between the maximum peak and the expected response, -2.5D, for the naked eye and the two myopia CLs designs (DL and EDOF).

The mean RIQ for the relaxed eye was 0.42 ± 0.10 in the naked eye. It decreased to 0.26 ± 0.05 with the DF and threefold to 0.15 ± 0.04 with the EDOF. For an accommodative demand of -2.5D, the RIQ was 0.34 ± 0.09 in the naked eye condition, 0.24 ± 0.07 with the DF, and 0.19 ± 0.03 with the EDOF. For the -2.5 D the CL's effective add power, the accommodative RIQ showed a secondary peak, with RIQs of 0.08 ± 0.03 (DF) and 0.12 ± 0.04 (EDOF).
Both myopia control CLs reduced RIQ at 0 D. At -2.5D, both lenses caused a secondary peak in the RIQ through focus. With EDOF, the secondary peak was less than 0.1 D from the maximum peak, likely due to its EDOF design. The theoretical AR was reduced with both myopia control CLs, 0.27 D for DF CLs, and 0.75 D for EDOF CLs.

These results indicate that both lenses impose significant limitations on RIQ and theoretical AR, align with findings from previous studies on subjective optical performance, and validate the model as a useful testing tool.

ACKNOWLEDGEMENTS: Funding from the European Union's Horizon 2020 research and innovation programme under the Marie Skłodowska Curie Grant Agreement No. 956720.

[1]J. Huang, D. Wen, Q. Wang, C. McAlinden, I. Flitcroft, H. Chen, S. M. Saw, H. Chen, F. Bao, Y. Zhao, L. Hu, X. Li, R. Gao, W. Lu, Y. Du, Z. Jinag, A. Yu, H. Lian, Q. Jiang, Y. Yu, and J. Qu, "Efficacy Comparison of 16 Interventions for Myopia Control in Children: A Network Meta-analysis". *Ophthalmology* **123(4)**, 697–708 (2016).
[2]M. A. Bullimore and K. Richdale, "Myopia Control 2020: Where are we and where are we heading?". *Ophthalmic Physiol Opt* **40(3)**, 254–270 (2020).
[3]J. M. González-Méijome, S. C. Peixoto-de-Matos, M. Faria-Ribeiro, D. P. Lopes-Ferreira, J. Jorge, J. Legerton, and A. Queiros, "Strategies to Regulate Myopia Progression with Contact Lenses: A Review". *Eye & Contact Lens* **42(1)**, 24 (2016).
[4]P. Sankaridurg, "Contact lenses to slow progression of myopia". *Clin Exp Optom* **100(5)**, 432–437 (2017).
[5]M. Mechó-García, M. Arcas-Carbonell, E. Orduna-Hospital, A. Sánchez-Cano, N. López-Gil, R. J. Macedo-de-Araújo, M. Faria-Ribeiro, P. Fernandes, J. M. González-Méijome, and J. Rozema, "Statistical Model of Ocular Wavefronts with Accommodation". *Investigative Ophthalmology & Visual Science* **65(12)**, 12 (2024).
[6]M. Mechó-García, M. Arcas-Carbonell, E. Orduna-Hospital, A. Sánchez-Cano, V. Fernández-Sánchez, R. J. Macedo-de-Araújo, P. Fernandes, J. M. González-Méijome, and J. J. Rozema, "Change in monochromatic aberrations with accommodation in a large adult population". *BMC Ophthalmol* **25(1)**, 104 (2025).

Chromatic Temporal Defocus Sensitivity

Victor, Rodriguez-Lopez[1]

[1] Institute of Optics, Spanish National Research Council (IO-CSIC), (Serrano 121, 28006, Madrid, Spain)

Contact: victor.rl@csic.es

Programmable lenses have emerged as a powerful tool for assessing dynamic changes in optical power with high temporal precision. In a previous study[1], we introduced the *temporal defocus sensitivity function* (TDSF), a function that quantifies the minimum noticeable defocus variation as a function of temporal frequency, using achromatic visual stimuli. Given the increasing relevance of chromatic content in displays and optical systems, as well as its importance as a cue in the development of novel refraction techniques based on chromatic flicker (the Direct Subjective Refraction—DSR method—[2]), in the present work we extend this characterization to stimuli of different chromatic composition.

A tunable lens (Optotune) was used to induce sinusoidal temporal modulations of defocus. Stimuli were presented on an AMOLED display (Waveshare), allowing for precise control for the red, green, and blue light components, with narrow spectral bandwidths (full width at half maximum of 35 nm) and well-separated peak wavelengths (625 nm for red, 530 nm for green, and 460 nm for blue). An achromatic stimulus (white-on-black) was also included for comparison. All chromatic components were carefully adjusted to be equiluminant. Observers (n=3, young adults) performed a 2-alternative forced-choice task using a Gabor patch of 4 cycles-per-degree. A staircase method was used to determine the just noticeable defocus change (JND) over a range of temporal frequencies (0.5 to 35 Hz). The data were fit to a model of temporal defocus perception, from which two key parameters were extracted: the maximum sensitivity (i.e., the inverse of the smallest detectable defocus) and the *Defocus Critical Fusion Frequency* (DCFF), defined as the temporal frequency beyond which defocus variations are no longer perceptible.

Across all chromatic conditions, the maximum sensitivity was consistently below 0.1 D, indicating a high temporal resolution for defocus detection. Notably, DCFF values varied with chromaticity: blue stimuli showed a lower DCFF (22 Hz), followed by red (26 Hz), while green (35 Hz) and achromatic (36 Hz) stimuli showed the highest fusion frequencies. These results suggest a differential temporal integration of defocus cues across the visible spectrum. Correlation analysis revealed strong associations between the red and blue conditions ($r^2 = 0.71$) and an even higher correlation between green and white stimuli ($r^2 = 0.99$).

These findings provide novel insights into the chromatic dependencies of dynamic defocus perception and are particularly relevant for the design of optical systems that rely on rapid, temporally varying control of optical power. Understanding the limits of defocus detectability at different wavelengths can help optimize visual technologies to match the temporal and spectral sensitivities of the human visual system.

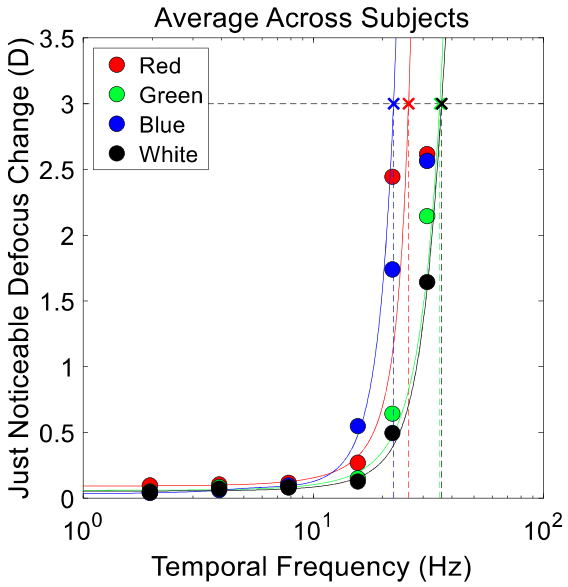

Figure 1. Chromatic spatiotemporal defocus sensitivity function.

References

1. Victor Rodriguez-Lopez, Wilson Geisler, Carlos Dorronsoro. The spatiotemporal defocus sensitivity function. Biomedical Optics Express 14, 3654-3670 (2023). https://doi.org/10.1364/BOE.486242.
2. Victor Rodriguez-Lopez, Alfonso Hernandez, Carlos Dorronsoro. Defocus flicker deactivates accommodation. Biomedical Optics Express, 14, 3671-3688 (2023). https://doi.org/10.1364/BOE.486466.

Exploring the clinical potential of a manual tunable lens in amplitude of accommodation assessment

Raquel Salvador-Roger[1], José J. Esteve-Taboada[1]; Abinaya Priya Venkataraman[2] and Alberto Domínguez-Vicent[2]

[1] Department of Optics, Optometry and Vision Sciences, Faculty of Physics, University of Valencia, Burjassot, Spain
[2] Unit of Optometry, Division of Eye and Vision, Department of Clinical Neuroscience, Karolinska Institute, Stockholm, Sweden

Contact: raquel.salvador@uv.es

Introduction: Accommodation is the physiological mechanism by which the dioptric power of the eye increases to maintain sharp retinal image of near objects. The amplitude of accommodation (AA) is defined as the interval between the minimum and maximum accommodative effort. One of the most common methods to measure the AA is the minus lens technique which is performed with a phoropter.[1] The emergence of tunable lenses in optometry opens the door to test whether AA may be studied using tunable lenses.

Objectives: To assess the repeatability and agreement of the minus lens technique for measuring the AA when performed with a manual tunable lens (MLTL) versus a conventional phoropter (MLPh). The study aims to determine whether the MLTL provides comparable accuracy and consistency to the established phoropter-based method.[1]

Methods: A total of 101 participants (mean age ± SD: 25 ± 5 years) underwent AA measurements using both MLTL and MLPh techniques. For each method, three repeated measurements were taken to assess repeatability. The repeatability limit (CoR) was calculated as 1.96 times the within-subject standard deviation. The agreement between methods was analyzed using non-parametric Bland-Altman plots the median difference, and with the limits of agreement (LoA) determined using the 2.5th and 97.5th percentiles.

Results: The CoR was ±0.39 D for MLTL and ±0.75 D for MLPh, indicating superior consistency with the tunable lens. Normality was not followed according to the Kolmogorov-Smirnov test. The non-parametric Bland-Altman analysis revealed a median difference of 0.50 D (LoA: -0.03 to 1.52 D) between the two methods (see Figure 1). Although MLTL and MLPh yielded similar median AA values, MLTL measurements were faster (median time: 16.8 s, IQR: 12.0–21.3 s) compared to MLPh (median time: 56.3 s, IQR: 38.7–68.3 s), reducing testing time by more than 3.5 times.

Conclusions: The MLTL method demonstrates better repeatability and reduced testing time compared to the traditional MLPh technique. While the agreement analysis between methods suggests that they provide comparable AA estimations, the efficiency and compact nature of tunable lenses could make them a viable alternative for clinical optometry settings.

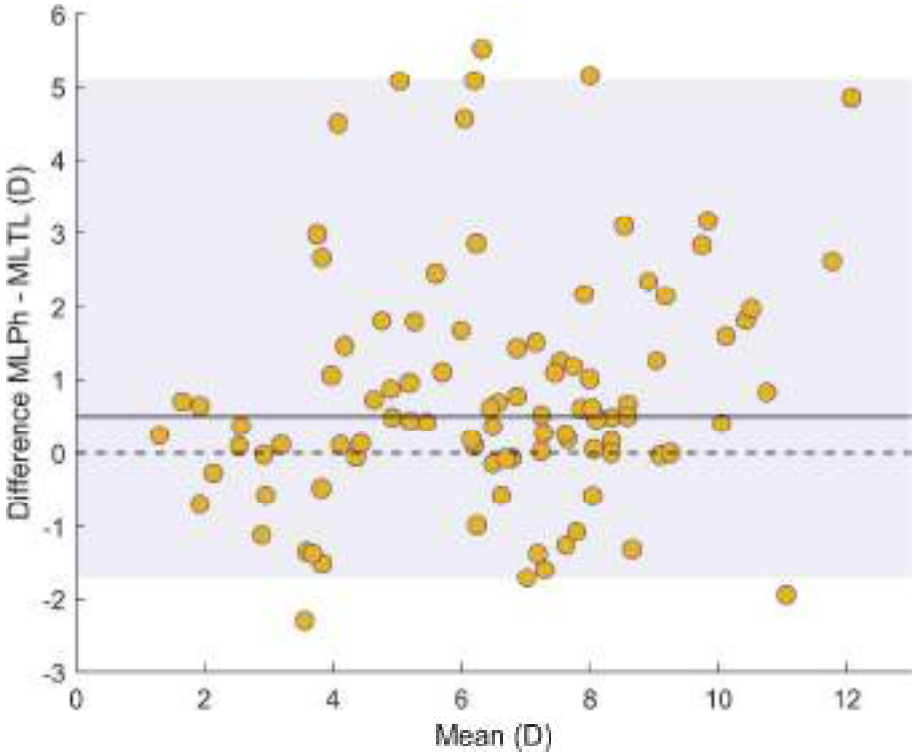

Figure 1: Bland-Altman non-parametric plot showing the agreement between the conventional minus lens method and the new minus lens method with a tunable lens. Continuous line represents the median, dashed line represents the 0 D value and shadow grey area represents the limits of agreement.

ACKNOWLEDGEMENTS: Spanish Ministerio de Universidades FPU20/05624 and EST24/00228

[1] M. Rosenfield and N. Chiu; *Optometry and Vision Science,* **72**, 577 (1995).

Statistical Shape Modelling of Eyes with Eigeneyes

Vadillo, Estela[1]; de la Peña, Álvaro[1]; Rodriguez-Sanchez, Javier[1]; de Castro, Alberto[1]; Marcos, Susana[2,3]; Martinez-Enriquez, Eduardo[1]

[1] Instituto de Óptica, Consejo Superior de Investigaciones Científicas, Madrid, Madrid, Spain
[2] Flaum Eye Institute, University of Rochester, Rochester, NY, United States.
[3] Center for Visual Science. The Institute of Optics. Flaum Eye Institute., University of Rochester, Rochester, NY, United States.

Contact: estela.vadillo@io.cfmac.csic.es

Purpose: Quantification of the eye's geometry is crucial for developing personalized eye models, with specific applications in the study of myopia and presbyopia and their corrections (contact and intraocular lenses design and selection). We propose a novel approach for the compact representation of the geometry of the eye, applying dimensionality reduction techniques to describe complex anatomical variability with minimal parameters.

Methods: We analyzed anterior segment Optical Coherence Tomography (OCT) data from 400 eyes with pupils larger than 3 mm of 290 patients (mean age 66 ± 16 years), acquired using the IOLMaster 700 system (Zeiss). For each eye, six radial meridional cross-sectional images (6 mm width) were collected, evenly spaced around the visual axis. Custom developed deep-learning-based algorithms[1] were used to automatically segment the anterior and posterior surfaces of the cornea, the crystalline lens, and the retina. These segmentations were registered to a common coordinate system to construct individual 3-D eye models[1]. In eyes where the visible area of the crystalline lens was less than 6 mm (because the iris blocks the incident light), extrapolation up to 6 mm was performed using Zernike polynomial fitting.

All 3-D models were registered so that the retina was placed at coordinate Z=0. For each model, a residual elevation data was computed by subtracting the shape of the average eye from each individual eye. Principal Component Analysis (PCA) was then applied to these residuals to identify a new orthogonal basis (eigeneyes) which captures the principal modes of variation in ocular geometry across the dataset[2]. Each eye's full 3-D geometry can then be approximated as a linear combination of a small number of eigeneyes. The reconstruction error (root mean square error, RMSE) of this representation was calculated and compared to a conventional 8-parameter (8-P) model based on spherical fits to the cornea and lens, and axial distances between surfaces. We used a 6-eigeneyes representation to model realistic eyes of a given age. Assuming a multivariate normal distribution, we estimated the conditional probability $P(a_1, \ldots, a_6 \mid age = A)$, where a_k represents the *k* eigeneye coefficient, and used it to generate realistic random eyes via sampling.

Results: Six eigeneyes were sufficient to explain 99% of the total variance in the dataset, and with the first two eigeneyes we already captured 98% of the variability. The first eigeneye captured large-scale changes in axial length and curvature of the anterior and posterior cornea. The second eigeneye reflected second-order deformations in corneal shape and thickness. The third component modified lens thickness, curvature, and anterior chamber depth, while the fourth, fifth, and sixth eigeneyes described finer details such as tilt, lens asymmetry, and higher-order curvature

variations.
The mean RMSE of the eigeneye-based reconstruction was 0.036 ± 0.016 mm, significantly lower (paired t-test, $p << 0.05$) than the RMSE obtained with the 8-P model (0.085 ± 0.026 mm). This indicates that the eigeneye representation provides a more accurate and flexible description of ocular geometry than a standard parametric representation, using fewer effective parameters. Finally, a statistical analysis revealed significant correlations between each eigeneyen and different biometric parameters: the first eigeneye showed a negative correlation with both age (r = -0.24) and spherical refraction (r = -0.56), while the second and third eigeneyes were moderately correlated with age (r = 0.40 and r = -0.27, respectively).

Conclusions: We proposed a new, compact, and data-driven method for representing 3-D eye geometries using a small number of orthogonal basis functions derived from anatomical variability. This approach enables the construction of realistic and individualized ocular models with high accuracy and minimal information loss. In addition to its potential use in personalized IOL design and surgical planning, the eigeneye framework provides a mathematical foundation for exploring the interdependence of anatomical features, age-related changes, and refractive error. The method is inherently extensible and can accommodate further anatomical details or be adapted to other imaging modalities, offering a promising tool for both clinical research and computational modelling of the human visual system.

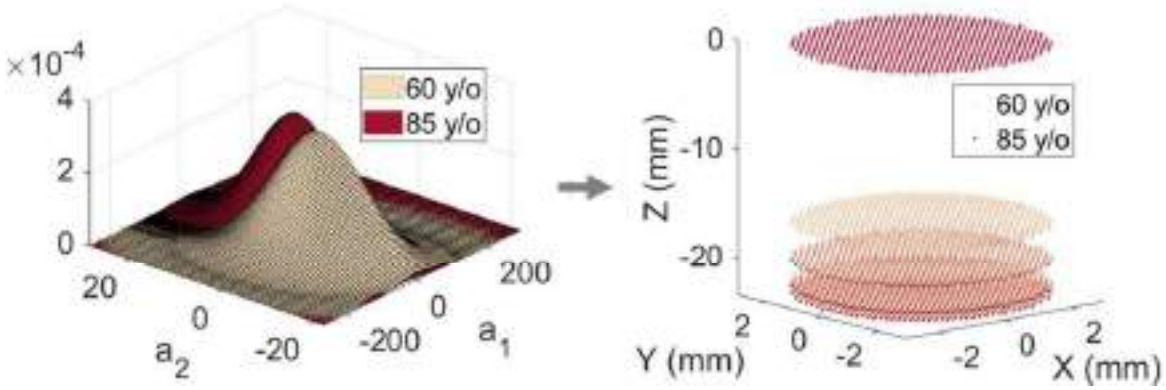

Figure 1: Distributions of the first two coefficients for ages 60 and 85 y/o.

Acknowledgements: Ministerio de Ciencia, Innovación y Universidades (PID2023-152641OA-I00, PID2020-115191 RB-100); Comunidad de Madrid (TEC-2024/COM-322); 2023 Leonardo Grant for Researchers and Cultural Creators, BBVA Foundation; MCIN/AEI and FSE+ (RYC2022-038195-I).

[1] Eduardo Martinez-Enriquez, Pablo Pérez-Merino, Miriam Velasco-Ocana, and Susana Marcos, "OCT-based full crystalline lens shape change during accommodation in vivo," Biomed. Opt. Express 8, 918-933 (2017)
[2] Eduardo Martinez-Enriquez, Alberto de Castro, and Susana Marcos, "Eigenlenses: a new model for full crystalline lens shape representation and its applications," Biomed. Opt. Express 11, 5633-5649 (2020)

Comparative Analysis of three different implementations of SimVis Gekko in Clinical Workflow

A. Varea [1,2], P. Urizar[1], P. Papadogiannis [1], E. Lage[3], R. Mera[1], Y. Marrakchi[1], E. Gambra[1], C. Dorronsoro[1,2]

[1] *2EyesVision, Madrid, Spain*

[2] *Institute of Optics, Spanish National Research Council (IO-CSIC), Madrid, Spain*

[3] *Department of Electronics and Communications Technology, Universidad Autónoma de Madrid, Madrid, Spain.*

*E-mail: avarea@2eyesvision.com

Purpose:
To assess alignment time, alignment stability, visual perception, comfort, and experience, we evaluated the integration of three different SimVis Gekko implementations into standard clinical workflow: 1) Head Mounted (HM), 2) Head Mounted with Eye Monitoring System (HM-EMS), and 3) Table Top with EMS (TT-EMS).

Methods:
SimVis Gekko is a see-through visual simulator that provides pre-surgery visual experience of various intraocular lens models available on the market, including full range, partial range, and any monovision combination[1]. This scientifically validated technology comes with multiple implementation options [2,3]. The HM version enables head movements and provides a natural visual experience. The HM-EMS version facilitates eye movement tracking and offers easier and faster eye alignment. The TT-EMS version allows quicker alignment but requires larger eye movements to explore the visual scene, leading to transient misalignments.

Nine presbyopic (47-63 yo) and ten non-presbyopic (21-42 yo) subjects scored the image quality (Perceptual Score [PS] from 1 to 5, being: 5 great and 1 poor) through three simulations (Plano-monofocal, PanOptix-Alcon [Full range] and Vivity-Alcon [Partial Range]) at far and near with the three implementations (HM, HM-EMS and TT-EMS). The alignment time was measured before the exams, and the alignment stability was registered during the exam in EMS devices. All trials were repeated three times by the same operator. An analysis of the impact of the refractive error on the perceptual score for five emmetropic/ low myopic (with spherical equivalent [SE] between 0.00D and -2.00D, [mean -0.50±0.75D]) and five mild/high myopic subjects (SE between -3.00D and -7.00D, [mean -4.50±1.50D]) was conducted for non-presbyopic subjects on the three devices. Also, the impact of subjects´ age (under and over 30 yo, [mean 27±4 and 35±4 yo, respectively]) on the perceptual score was evaluated in non-presbyopic subjects (five subjects per group). A survey was conducted to determine the level of comfort, satisfaction of the experience and clinical feasibility of each device.

The Wilcoxon Signed-Rank test and the Mann-Whitney test were used to evaluate the difference in measurement times. The Friedman's test was conducted to assess the difference in perceptual scores among the three devices, and the Kruskal-Wallis test was applied to evaluate the impact of refractive error and age on perceptual scores.

Results:

The alignment time was less than one minute in all devices. The alignment time with TT-EMS was 52% shorter compared to HM, while HM-EMS also showed a shorter alignment time, being 14% quicker than HM. A significant learning effect was found across repetitions in all devices, being lower for TT-EMS. Alignment was maintained for all measurements and subjects, with only transient misalignment less than 10% of the time for HM-EMS (13% for TT-EMS) for 16 of the subjects, suggesting a good alignment stability during the whole test. Presbyopes, unable to accommodate the near tests, used a larger range of perceptual scores across distances and simulations than non-presbyopes (4.96 to 2.40 vs 5.00 to 3.19, [being a range of 1.81 vs 2.56], respectively). Also, presbyopes were more tolerant to full range (+1.03 perceptual points) and partial range (+0.20) than non-presbyopes. Intrasubject variability was like interdevice variability (±0.21), suggesting high repeatability in all simulations. Additionally, there was no significant difference in PS between devices for simulations. Regarding the impact of refraction or age on the perceptual score, no significant differences were found between groups, suggesting that neither refraction nor age has an impact on the final vision perception. Finally, subjects preferred the HM experience, although they all found it equally comfortable. All subjects found all devices suitable for clinical use.

Conclusions:

The study identified variations in alignment time, with EMS devices showing faster results. TT-EMS achieved the shortest alignment times but experienced more transient misalignments due to eye movements, which were not clinically relevant. Additionally, subject experience was superior with HM across the three SimVis Gekko implementations. These findings highlight the clinical potential of the three SimVis Gekko implementations and their suitability for integration into standard clinical workflows, indicating that these devices can be effectively used across a diverse patient population.

References:

[1] X. Barcala, M. Vinas, M. Romero, E. Gambra, J.L. Mendez-Gonzalez, S. Marcos & C. Dorronsoro; Multifocal acceptance score to evaluate vision: MAS-2EV, *Scientific Reports,* **11,** 1397 (2021).

[2] L. Sawides, A. de Castro, CM Lago, X. Barcala, A. Zaytouny, S. Marcos; SimVis simulations of multifocal IOL designs based on public-literature data. *SPIE - The International Society for Optical Engineering* 11871: 0 (2021).

[3] V. M. Vinas, S. Aissati, M Romero, C. Benedi-Garcia, N. Garzon, F. Poyales, C. Dorronsoro, S. Marcos. Pre-operative simulation of post-operative multifocal vision. *Biomedical Optics Express, **10**, 5801 (2019).*

Acknowledgements:

Comunidad de Madrid - Doctorado Industrial (IND2023/BMD-27723) to AV; Ministerio de Ciencia e Innovación, Ayudas a proyectos de colaboración público-privada (CPP2021-008388) to CD, PP, PU and EG.

TRAVEL GRANTS AWARDEES | SPIE

1	Nathaniel Norberg
2	Oliwia Kaczkoś
3	Jorge Lasarte Sanz
4	Sunil Kumar Chaubey
5	Marina Bou Marin
6	Chiara Maria Mariani
7	Aishwarya Chanady Babu

TRAVEL GRANTS AWARDEES | OPTICA

1	Rosa Maria Martinez Ojeda
2	Daniel Romero Ruiz
3	Inas Baoud Ould Haddi
4	Aina Turull Mallofré
5	Júlia Hernàndez
6	Rosa Vila Andrés
7	Alba Herrero Gracia
8	Aida Ramón-Campillo
9	Anabel Martínez Espert
10	Paula García Balaguer
11	Sara Ferrer Altabás
12	Eduardo Esteban-Ibañez
13	Sara Silva-Leite
14	María Mechó García
15	Raquel Salvador Roger
16	Maite Valentino Herrera
17	André Rino Amorim
18	Juan Casado Moreno
19	Ana Ramos Arizcuren
20	María Arcas Carbonell
21	Alejandro Guiseris Santaflorentina
22	Rita Seco
23	Fátima Cuéllar Santiago
24	Alejandra Varea
25	Michelle Peimann

AWARDS | BER2025

BEST POSTER AWARDS

1	Rosa Vila Andrés
2	Petros Papadogiannis

BEST TALK AWARD

1	Nathaniel Norberg

BER2025 ATTENDEES

1	José Juan	Castro Torres	University of Granada	Spain
2	Mikel	Aldaba Arévalo	Polytechnic University of Catalonia · BarcelonaTech	Spain
3	Sonia	Ortiz Peregrina	University of Granada	Spain
4	Francesco	Martino	University of Granada	Spain
5	Luis	Jiménez del Barco Jaldo	University of Granada	Spain
6	Rosario	González Anera	University of Granada	Spain
7	José Ramón	Jiménez Cuesta	University of Granada	Spain
8	Pilar	Granados-Delgado	University of Granada	Spain
9	Miriam	Casares López	University of Granada	Spain
10	Joan	Goset Maldonado	Polytechnic University of Catalonia · BarcelonaTech	Spain
11	María	Viñas Peña	Spanish National Research Council	Spain
12	Simone	Mortal	ICFO - The Institute of Photonic Sciences	Spain
13	Elvira	Orduna Hospital	University of Zaragoza	Spain
14	Patrick	Kolsch	NKT Photonics	US
15	Brian	Vohnsen	University College Dublin	Ireland
16	Amy	Fitzpatrick	University College Dublin	Ireland
17	Aishwarya	Chanady Babu	University College Dublin	Ireland
18	Sunil Kumar	Chaubey	University College Dublin	Ireland
19	Consuelo	Robles García	Voptica SL	Spanish
20	Antonio	Castelo Porta	European Photonics Industry Cluster (EPIC)	Spanish
21	Alejandro	Guiseris Santaflorentina	University of Zaragoza	Spain
22	María	Arcas Carbonell	University of Zaragoza	Spain
23	Carlos F.	Dorronsoro Fernández	2EyesVision	Spain
24	Petros	Papadogiannis	2EyesVision	Spain
25	María Pilar	Urizar Ursua	2EyesVIsion	Spain
26	Alejandra	Varea Béjar	2EyesVision	Spain
27	Rita Maria	Serra Seco	University of Minho	Portugal
28	Enrique Josua	Fernández Martínez	University of Murcia	Spain
29	Clara	Mestre Ferrer	Polytechnic University of Catalonia · BarcelonaTech	Spain
30	Marta	Ayala Martínez	University of Seville	Spain
31	Chiara Maria	Mariani	University College Dublin	Ireland
32	Justo	Arines Piferrer	University of Santiago de Compostela	Spain
33	Eva María	Acosta Plaza	University of Santiago de Compostela	Spain
34	Rafael	Huertas Roa	University of Granada	Spain
35	Juan Luis	Aragon Alcaraz	University of Murcia	Spain
36	Juan de la Cruz	Cardona Pérez	University of Granada	Spain
37	Luis	Gómez-Robledo	University of Granada	Spain
38	Aina	Turull Mallofre	Polytechnic University of Catalonia · BarcelonaTech	Spain
39	Marina	Bou Marin	Polytechnic University of Catalonia · BarcelonaTech	Spain
40	Sarvenaz	Kalantarinejad	Polytechnic University of Catalonia · BarcelonaTech	Spain
41	Maite	Valentino Herrera	Polytechnic University of Catalonia · BarcelonaTech	Spain
42	Armin	Eskandarinasab	Polytechnic University of Catalonia · BarcelonaTech	Spain
43	Lorenzo	Fratini	Polytechnic University of Catalonia · BarcelonaTech	Spain
44	Victor	Rodríguez López	Spanish National Research Council	Spain
45	Raquel	Salvador Roger	Universitat de València	Spain
46	Alba	Herrero Gracia	University of Valencia	Spain
47	María Sagrario	Millán	Polytechnic University of Catalonia · BarcelonaTech	Spain
48	Laura	Clavé Cerezo	Polytechnic University of Catalonia · BarcelonaTech	Spain
49	Fátima	Cuéllar Santiago	Polytechnic University of Catalonia · BarcelonaTech	Spain
50	Paula	García Balaguer	Universidad de Valencia	Spain
51	Sara	Ferrer Altabás	Universitat de València	Spain
52	Eduardo	Esteban Ibáñez	DIVE-Medical SL / Aragon Health Research Institute	Spain

53	Alan	Montero Herrera	Grupo GOAPI	Spain
54	Alberto	de Castro	Spanish National Research Council	Spain
55	Paulina	Dotor Goytia	Spanish National Research Council	Spain
56	Diego	Chorrero Labrador	Spanish National Research Council	Spain
57	Javier	Rodríguez Sánchez	Spanish National Research Council	Spain
58	Aixa	Alarcón Heredia	Johnson and Johnson Vision	Spain
59	Estela	Vadillo Polo	Spanish National Research Council	Spain
60	Inas	Baoud Ould Haddi	University complutense of Madrid	Spain
61	Júlia	Hernàndez Ris	Polytechnic University of Catalonia · BarcelonaTech	Spain
62	Gloria	Bueno García	University of Castilla-La Mancha	Spain
63	Aida	Ramón-Campillo	University of Valencia	Spain
64	María	Mechó-García	University of Minho	Portugal
65	Kate	Grieve	Institut de la Vision	France
66	Rosa	Vila Andres	Universitat de València	Spain
67	Nathaniel	Norberg	Institut de la Vision	France
68	Elena	Gofas	Institut de la Vision	France
69	Oliwia	Kaczkoś	International Centre for Translational Eye Research	Poland
70	Laura	Remon Martín	University of Zaragoza	Spain
71	Juan	Casado Moreno	University of Zaragoza	Spain
72	Ana	Ramos Arizcuren	University of Zaragoza	Spain
73	Sara	Silva-Leite	Zeiss Vision Science Lab	Germany
74	Anabel	Martínez Espert	Universitat de València	Spain
75	Jorge	Lasarte Sanz	Technological University Dublin	France
76	Lucie	Sawides	Spanish National Research Council	Spain
77	André	Amorim	University of Minho	Polish
78	Katarzyna	Komar	Institute of Physical Chemistry PAS	Spanish
79	Rosa	Martínez Ojeda	University of Waterloo	Canadian
80	Michelle	Peimann	University of Waterloo	SPANISH
81	José Manuel	González Méijome	University of Minho	Czech Republic
82	Radim	Kolar	Brno University of Technology	Español
83	Daniel	Romero Ruiz	Spanish National Research Council	Spain
84	Juan Manuel	Bueno García	University of Murcia	Spain
85	Pablo	Perez Merino	Spanish National Research Council	Spain
86	Walter	Furlan	University of Valencia	Spain
87	Wojciech	Mojsiejuk	LUT University	Española
88	Francisco	Pérez Ocón	University of Granada	Spain
89	Samuel Felipe	Serna Otálvaro	OPTICA Ambassador - Bridgewater University-MIT	US
90	Felipe	Beltran-Mejia	OPTICA Ambassador - Universidade Federal do ABC	Brasil
91	Harilaos	Ginis	DIESTIA	Greece
92	Eduardo	Martínez Enríquez	Spanish National Research Council	Spain
93	Andreas	Börner	NKT Photonics	Germany
94	María José	Bautista Llamas	University of Seville	Spain
95	Vanessa	Morcillo	Wooptix	Spain
96	Pablo	Artal Soriano	University of Murcia	Spain
97	Susana	Marcos Celestino	University of Rochester, USA	US
98	Mayra	Arroyaga Crespo	Tobii	Spain
99	Esther	Fernández Muñoz	INDO	Spain
100	Javier	Bello Fernández	Servilens	Spain
101	Lourdes	Bello Jiménez	Servilens	Spain

SOME BER2025 MOMENTS

WEDNESDAY, 4TH JUNE 2025


Biophotonics for Eye Research
II Soltetina 2025 Granada

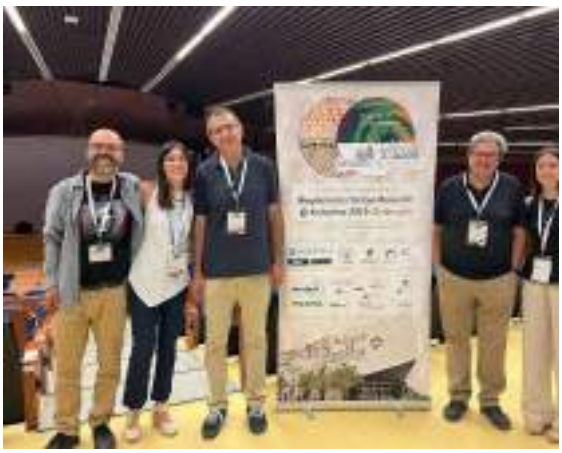


The Institute of Optics
Visual Optics: An eye into the future
Susana Marcos, PhD

THURSDAY, 5TH JUNE 2025










Live imaging of
retinal cell dynamics
with FFOCT


(TPEF) microscopy
as an emergent and alternative
tool for imaging

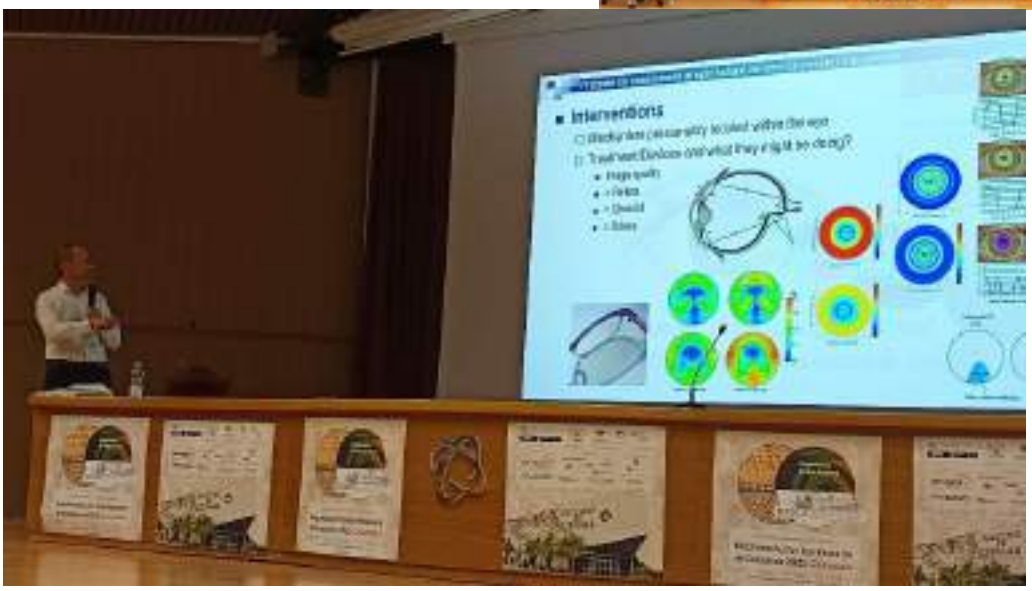
Interventions


ICTER


Computational
Approaches for
Biological Imaging


Eye tracking parameters as biomarkers of cognitive performance in the Stroop Color Word Test


Accommodation parameters in two-photon vision–application in Augmented Reality technology

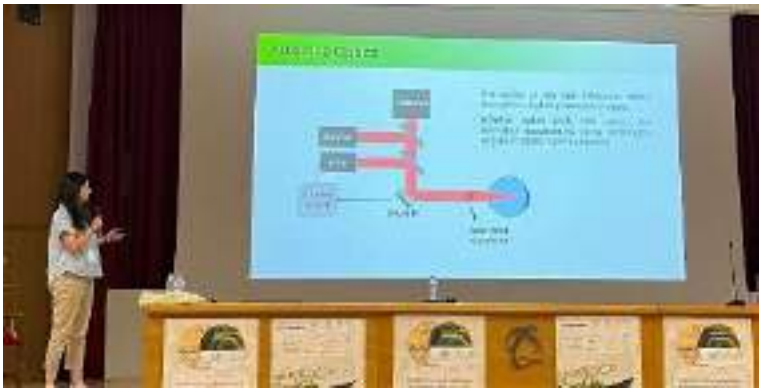

FRIDAY, 6TH JUNE 2025

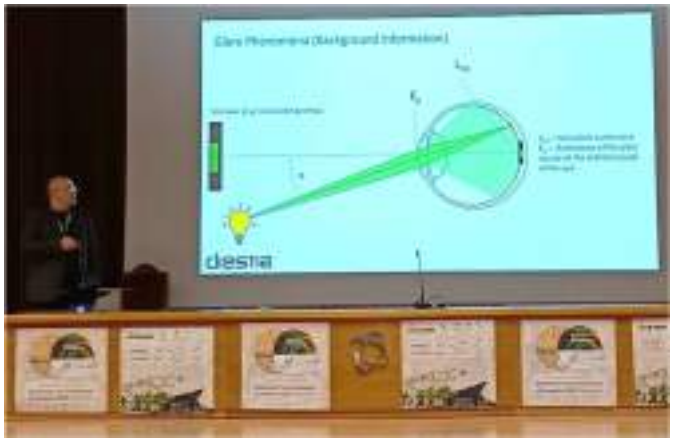
desha


Optoelectronic glasses for
the automatic correction of
presbyopia


30 years of lo·um

slack

Join BER2025 **SLACK channel!!**
https://shorturl.at/7Jvgo

GOLD SPONSORS

servilens fit&cover™ a contact lens company

INDO

UNIVERSIDAD DE GRANADA

Escuela Internacional de Posgrado

Facultad de Ciencias

OPTICA
Advancing Optics and Photonics Worldwide

SILVER SPONSORS

Johnson&Johnson

phaseform

WOOPTIX

NKT Photonics LASING

tobii

fotónica21
Plataforma Tecnológica Española de Fotónica

2EyesVision

COLLABORATORS

essilor

iberOptics sistemas ópticos

SmarThings4Vision

imagine eyes